UNIVERSITY OF OKLAHOMA

GRADUATE COLLEGE

SYNTHESIS AND CHARACTERIZATION OF BIOBASED BIODEGRADABLE POLYESTERS TO REPLACE LDPE/LLDPE IN FLEXIBLE FILM PACKAGING

A DISSERTATION

SUBMITTED TO THE GRADUATE FACULTY

in partial fulfillment of the requirements for the

Degree of

DOCTOR OF PHILOSOPHY

By

HESHAM ABOUKEILA

Norman, Oklahoma

2024

SYNTHESIS AND CHARACTERIZATION OF BIOBASED BIODEGRADABLE POLYESTERS TO REPLACE LDPE/LLDPE IN FLEXIBLE FILM PACKAGING

A DISSERTATION APPROVED FOR THE

SCHOOL OF SUSTAINABLE CHEMICAL, BIOLOGICAL, AND MATERIALS ENGINEERING

BY THE COMMITTEE CONSISTING OF

Dr. Brian P. Grady, Chair

Dr. John Klier, Co-Chair

Dr. Reza Foudazi

Dr. Michele Galizia

Dr. Yingtao Liu

Acknowledgment

I would like to express my deepest gratitude to Professor Brian P. Grady and Dean John Klier for their exceptional supervision and for welcoming me into their esteemed groups. Their patient guidance, enthusiastic encouragement, and constructive criticism have been invaluable to this research. I am particularly thankful to Prof. Grady for his unwavering support and open-door policy throughout the past three and half years. His meticulous reviews of several papers, patent, and my thesis, along with his critical suggestions and challenging questions, have been instrumental to my work.

I extend my sincere thanks to my dissertation committee members, Prof. Reza Foudazi, Prof. Michele Galizia, and Prof. Yingtao Liu, for their ongoing assistance and support, as well as for taking time from their busy schedules to participate in my general exam and dissertation defense.

I am especially grateful to Dr. Onkar Singh for his assistance with polymer synthesis, and for the countless hours spent in the lab to provide the necessary polymers for my experiments. I would also like to thank Mason Rhue, Lucas Condes, and Mathew Webb for their help with various aspects of the experimental work.

I wish to acknowledge Dr. Javen Weston from the University of Tulsa for his help with SAXS, and Prof. Andy Madden and Dr. Preston Larson from the Samuel Roberts Noble Microscopy Laboratory for their assistance with WAXS. I would like to thank the Argonne National Laboratory and, in particular, Dr. Shu Xu for biodegradation measurements.

Finally, and most importantly, I would like to thank my wife, Leena, my parents, and my brother for their unconditional love and endless support, which sustained me through the most challenging moments.

I would like to acknowledge the financial support from the Department of Energy (DOE) under grant DE-EE0009305, which funded this work, the Strategic Investment Equipment Program sponsored by the VPRP Office at the University of Oklahoma for funds related to the purchase of the TGA as well as the National Science Foundation (CMMI-2216074) and the University of Tulsa for funds contributing to the purchase of the SAXS.

Table of Contents

List of Tables

List of Figures

Abstract

This dissertation investigates the recent advancements in the development of biobased and biodegradable polyesters have shown significant promise for replacing conventional petrochemical-based plastics, particularly in flexible film packaging applications. Poly (pentylene adipate-co-terephthalate) (PPeAT) and poly (dodecamethylene furandicarboxylate) (PDDF) were synthesized using direct esterification and polycondensation methods, incorporating various branching agents and nucleating agents to the former to enhance their thermal, mechanical, and rheological properties. Chapter 1 serves as the introduction to this dissertation, providing an overview of the project's motivation, rationale, and the current possible alternative polymers in the field. This chapter outlines the driving forces behind the research, detailing the pressing need for advancements in the area and the potential impact of the project. Chapter 1 dives into the reasons for undertaking the study, highlighting the gaps in existing knowledge and the anticipated contributions to the field. Chapter 2 reviews the latest technologies and methodologies that form the foundation of the research, setting the stage for the detailed exploration and innovative solutions presented in the subsequent chapters. The preliminary results for the pentanediol – furandicarboxylic acid-based polyesters are reported in Chapter 3. None of these polymers were suitable for flexible-film applications because the glass transition temperature was too high, or the melting temperature was too low. Chapter 4 explores the synthesis and characterization of PPeAT, a polymer synthesized with a 40/60 adipic acid/terephthalic acid mole ratio; a mole ratio chosen to best match the glass and melting temperatures of commercial flexible-film packaging resins. PPeAT exhibits high thermal stability and molecular weight, making it a promising candidate for film-blowing applications, despite its inherently slow crystallization rate. Chapter 5 examines the impact of incorporating nucleating agents, such as Li, Mg and Na-neutralized ethylene-methacrylic

acid copolymer-based ionomers and un-neutralized ethylene-methacrylic acid copolymer. These nucleating agents significantly decreased the crystallization half-time, thereby enhancing PPeAT's potential as a biodegradable alternative to linear low-density polyethylene (LLDPE). Chapter 6 investigates the compression molded and film blowing of PPeAT. The blown polyester films were compared with film blown with commercially available polymers such as LLDPE and PBAT. PPeAT showed lower oxygen and carbon dioxide permeability compared with PBAT and LLDPE and lower water vapor transmission rate than PBAT. Film blown PPeAT showed promising results and eventually could be used as a drop-in replacement for LLDE in flexible film packaging Chapter 7 discuss the synthesis and characterization of another possible polymer useful for flexible-film: PDDF, a polymer derived from furandicarboxylic acid and a 12-carbon diol. This polymer demonstrates exceptional gas barrier properties, surpassing those of linear low-density polyethylene (LLDPE) and poly (butylene adipate-co-terephthalate) (PBAT). PDDF's reduced oxygen and carbon dioxide permeability, combined with its robust mechanical properties, makes it an excellent candidate for packaging applications. These developments underline the potential of biobased polyesters to address environmental concerns associated with plastic waste while meeting the demands of global packaging needs.

Chapter 1: Introduction

1.1. Motivation

Since the mid-20th century, plastics have transformed modern life, becoming an indispensable material across countless industries, from healthcare to packaging. More than 400 million metric tons plastic was produced in 2022 globally [1]. Annual plastic production is expected to reach approximately 590 million metric tons globally by 2050 as shown in Figure (1) [2].

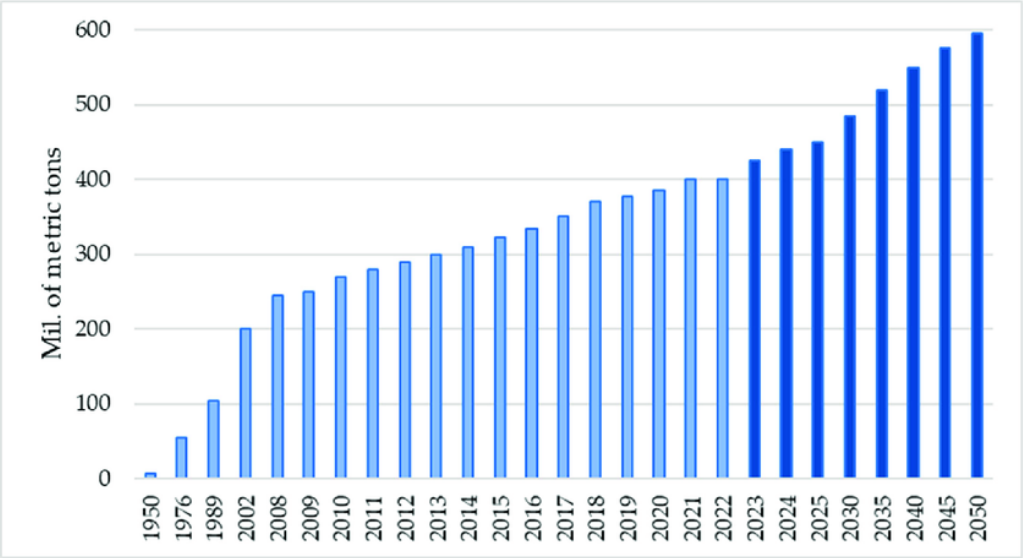

***Figure 1**: Production forecast of plastics worldwide from 1950 to 2050 in millions tons [2].*

Packaging represents the largest end-use market for plastics, accounting for over 36% of total plastic consumption [1]. In 2022, more than 140 million metric tons of plastic packaging were produced, and according to Figure (1), the production rate is projected to rise to 210 million metric tons by 2050 [2]. Furthermore, as shown in Figure (2), flexible packaging holds the second-largest market share among all packaging types, at 19% [3]. Polyolefins, particularly polyethylene, are the most widely used plastics in flexible packaging, making up nearly 90% of the total [4]. Polyethylene is widely used in flexible packaging because of its excellent moisture resistance,

durability, and other suitable properties. Low-density polyethylene (LDPE) and linear low-density polyethylene (LLDPE) serve various roles, such as sealants, structural components, bonding layers or adhesives [5].

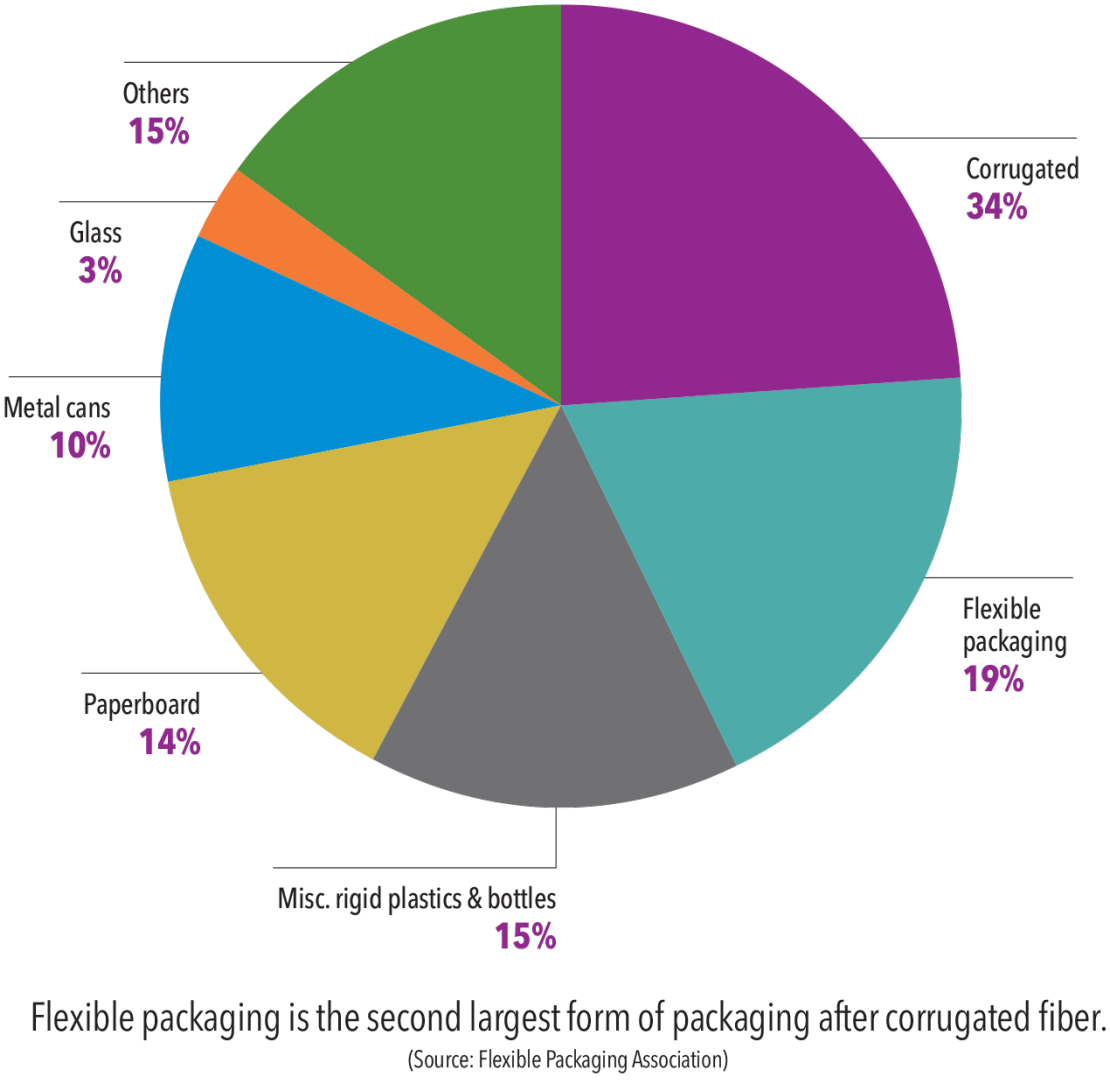

***Figure 2**: Market share of leading packaging material [3].*

However, polyethylene is neither biodegradable nor compostable and takes many decades, if not centuries, to decompose. Polyethylene often accumulates in landfills, posing potential harm to the environment. More than 85% of packaging end up in landfills [1]. Flexible film is a

particularly difficult material environmentally, as this material is difficult to mechanically recycle and because of that, very little mechanical recycling is performed on flexible films. As a result, there is a strong need to develop biodegradable polymers that can match the thermal, mechanical, rheological, and barrier properties of LLDPE and LDPE for use in flexible film applications. Achieving similar performance characteristics in biodegradable alternatives is essential to creating environmentally friendly materials without compromising the functionality and durability required for these applications.

1.2. Classification of plastics

In this work, the term plastics refers to polymeric materials that can be melted into a high viscosity liquid, as opposed to thermosets or rubbers. Plastics, as illustrated in Figure (3), can be broadly categorized into two main groups: conventional plastics and bioplastics. First group is conventional plastics, also known as fossil-fuel plastics, are synthetic materials made from fossil-based feedstock like petroleum, coal, or natural gas [6]. Almost all conventional plastics are not biodegradable. Polyethylene, polypropylene, polyethylene terephthalate, polymethyl methacrylate and polyvinyl chloride are some examples of conventional plastics. 98% of single use plastics packaging are made from fossil-based conventional plastics [1]. Second group is bioplastics which can then be further classified into three distinct subcategories: bio-based bioplastics, biodegradable bioplastics, and those that are both biodegradable and bio-based. Bioplastics are a type of plastic derived from renewable resources like vegetable oils and corn starch, that are biodegradable, produced through biological processes, or a combination of these factors [7]. Biobased polyethylene, biobased polyethylene furanoate, biobased polyethylene terephthalate and biobased polytrimethylene terephthalate are commercial examples of bio-based bioplastics that are not biodegradable. While polylactic acid, polyhydroxyalkanoates,

polyhydroxybutyrate, and starch blends are typical examples of bio-based and biodegradable bioplastics. Finally, polybutylene adipate-co-terephthalate, polybutylene succinate and polycaprolactone are commercial examples of biodegradable bioplastics that are synthesized using fossil-based feedstocks. Biopolymers offer significant advantages over conventional plastics due to their biocompatibility and ability to degrade within a relatively short period of time. This rapid biodegradability helps to minimize environmental pollution and reduces the accumulation of waste in landfills, thus contributing to the preservation of ecosystems. Additionally, biopolymers are considered healthier for humans because they often lack the harmful chemicals and additives commonly found in traditional plastics. By reducing the long-term environmental impact and promoting human health, biopolymers present a more sustainable and eco-friendlier alternative to conventional plastics [8].

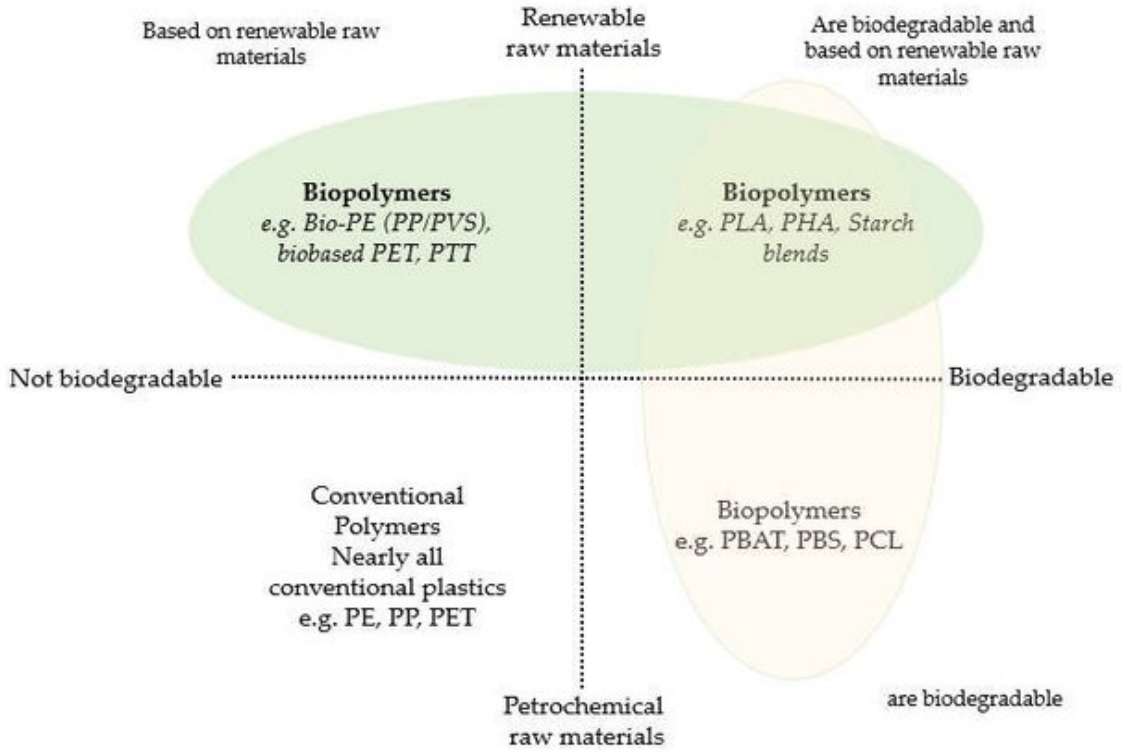

***Figure 3**: Classification of polymers[9].*

1.3. Biodegradable polymers

Biodegradable polymers are materials designed to naturally break down in the environment through the action of microorganisms such as bacteria and fungi or by exposure to natural conditions like sunlight, water, or temperature fluctuations. Unlike conventional plastics, which persist for hundreds of years and contribute to pollution, biodegradable polymers decompose into natural byproducts such as carbon dioxide, water, and biomass within a much shorter time frame. These polymers can be derived from renewable resources, such as plants, or synthesized through chemical processes, making them critical for reducing plastic waste, lowering carbon footprints, and promoting sustainability across industries [10]. A polymer is considered biodegradable when it contains functional groups in its backbone chain that undergo hydrolysis and oxidation reactions, breaking down into smaller compounds. The biodegradation process is facilitated by enzymes or in combination with microbial organisms that deteriorate organic substances. Biodegradable polymers are classified based on their synthesis, which includes biomass products, polymers from microorganisms, bio-derived monomers, and synthetic monomers from petrochemicals as discussed previously. These polymers can originate from plants, animals, or synthetic sources, with widely recognized examples including poly(glycolic acid) (PGA), polylactic acid (PLA), poly(vinyl alcohol) (PVA), polyethylene oxide (PEO), polyacrylic acid (PAA), poly(lactide-co-glycolide) (PLGA), poly(ε-caprolactone) (PCL), polyhydroxyalkanoates (PHAs), and many others, each contributing to diverse applications from packaging and agricultural films to medical devices like sutures and drug delivery systems [11]. The biodegradation of these polymers can occur in various environments, including freshwater, soil, and compost. Freshwater biodegradation occurs in aquatic systems like rivers and lakes, while soil biodegradation involves microbial activity in the earth. Compost biodegradation, which is the most controlled environment, happens

in compost facilities where elevated temperatures and moisture accelerate the breakdown process. Biodegradation testing follows ASTM (American Society for Testing and Materials) guidelines, such as ASTM D6400 and ASTM D6868 for compostable plastics, ASTM D5988 for soil biodegradation, and ASTM D6691 for aquatic biodegradation, to ensure the materials meet specific standards for environmentally safe degradation [12].

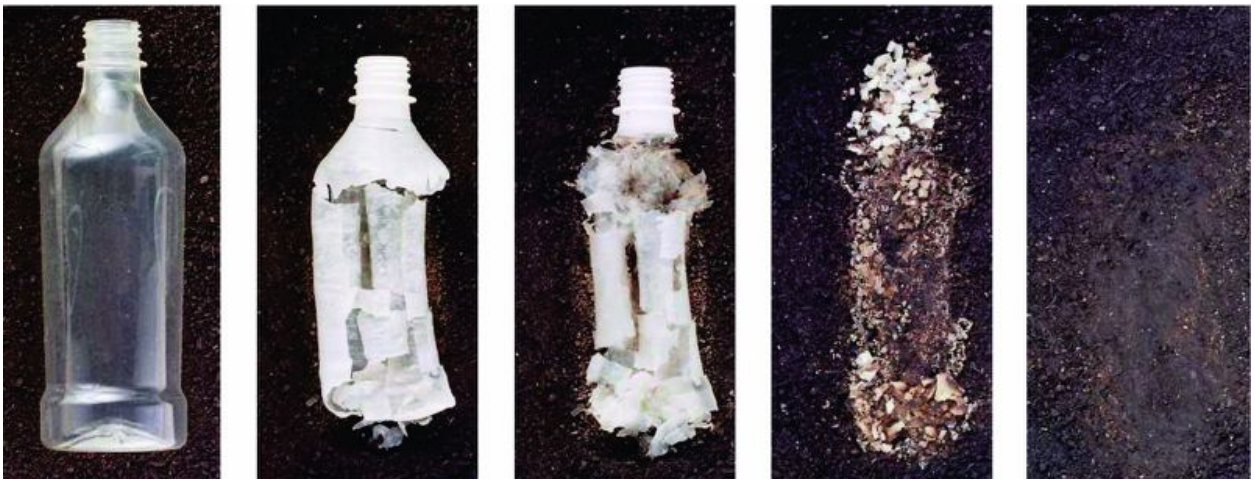

***Figure 4**: Biodegradation process of a polyester bottle.*

1.4. Petroleum based monomers

Petroleum-based monomers can serve as key components in the synthesis of biodegradable polyesters, offering a balance between traditional fossil fuel-derived materials and environmental sustainability. Monomers such as adipic acid, succinic acid, terephthalic acid, and 1,4-butanediol are derived from petroleum sources and are used to create biodegradable polyesters like polybutylene succinate, polycaprolactone and polybutylene adipate-co-terephthalate [13]. These polyesters, while sourced from fossil fuels, are engineered to degrade more readily in natural environments such as soil, freshwater, or compost as previously mentioned. Although petroleum-based, these biodegradable polymers offer a potential solution to reducing plastic waste while still utilizing existing petrochemical resources. However, the environmental trade-offs of relying on

fossil fuels remain, and there is ongoing research into creating similar biodegradable polyesters from bio-based sources to further improve sustainability [14, 15].

1.4.1. Butanediol

1,4-Butanediol as shown in Figure (5) is a versatile chemical compound derived mainly from petroleum-based and serves as an important monomer in the production of biodegradable polyesters. 1,4-Butanediol contains two hydroxyl groups, which enable it to react with dicarboxylic acids or dimethyl esters to form long-chain polyester structures. 1,4-Butanediol is primarily used in the synthesis of polyesters due to its ability to impart flexibility, durability, and biodegradability to the resulting polymers. 1,4-Butanediol is particularly important in the production of biodegradable polyesters because its chemical structure allows for the creation of ester bonds that can degrade in environmental conditions such as soil and compost [16]. Notable examples of polyesters synthesized using 1,4-butanediol include polybutylene succinate, a widely studied biodegradable polymer known for its good mechanical properties and composability; polybutylene adipate-co-terephthalate, which is flexible and often used in packaging applications such as mulch films [13]; and polybutylene carbonate, which combines biodegradability with gas barrier properties, making it suitable for drug delivery and carbon capture [17, 18]. These polyesters, created using 1,4-butanediol, are part of a growing class of materials that offer both functional performance and environmental benefits.

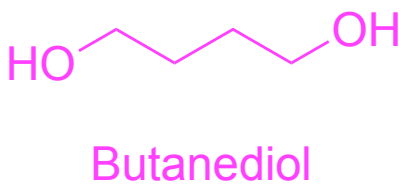

Figure 5*: Chemical structure of 1,4 Butanediol*

1.4.2. Terephthalic acid

Terephthalic acid is a key aromatic dicarboxylic acid derived primarily from petroleum and is widely used in the production of polyesters. Terephthalic acid as shown in Figure (6) has two carboxyl groups (-COOH) that enable it to react with diols, such as ethylene glycol or 1,4-butanediol, to form ester linkages and create long-chain polyester molecules. Terephthalic acid is known for imparting excellent mechanical strength, thermal stability, and chemical resistance to the polymers it helps form [19]. Although terephthalic acid itself is petroleum-based, the polyesters synthesized from it can sometimes be biodegradable when paired with specific diols. Examples of polyesters synthesized using terephthalic acid include polyethylene terephthalate, a widely used material for fibers, bottles, and packaging [20]; polybutylene terephthalate, which is valued for its durability and electrical insulation properties [21]; and polybutylene adipate-co-terephthalate, a flexible and biodegradable polyester often used in compostable films and mulch films applications [22]. The versatility of terephthalic acid-based polyesters makes them integral to numerous industries, while ongoing research focuses on enhancing their environmental profile.

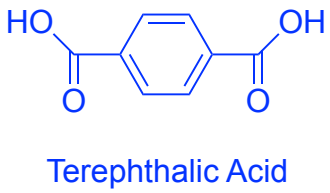

***Figure 6**: Chemical structure of Terephthalic acid*

1.4.3. Adipic acid

Adipic acid is a widely used aliphatic dicarboxylic acid, primarily derived from petroleum, that plays a crucial role in the production of various polyesters and polyamides. As shown in Figure (7), Adipic acid two carboxyl groups (-COOH) allow it to react with diols or diamines to form

polymers, contributing to flexibility, toughness, and biodegradability in the resulting materials. Adipic acid is particularly important in the synthesis of biodegradable polyesters because its linear structure helps create polymers with ester linkages that can break down under environmental conditions [23]. Examples of polyesters synthesized using adipic acid include polybutylene adipate, known for its biodegradability and used in flexible packaging [24]; polybutylene adipate-co-terephthalate, a biodegradable and flexible polyester used in compostable plastic films [23]; and polyethylene adipate, which is often used in applications requiring low melting points and good elasticity [25]. Adipic acid is also a key component in nylon production, highlighting its versatility in both polyester and polyamide synthesis, contributing to materials with varied industrial and environmental applications [26].

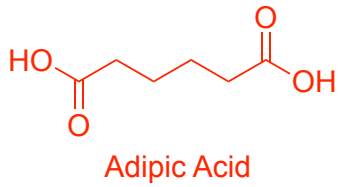

***Figure** 7: Chemical structure of Adipic Acid*

1.5. Biobased monomers

Bio-based monomers are chemical building blocks derived from renewable biological sources, such as plants, sugars, and agricultural waste, and are increasingly used in the production of biodegradable polyesters. These monomers offer a sustainable alternative to petroleum-based counterparts by utilizing renewable feedstocks, thereby reducing reliance on fossil fuels and lowering the carbon footprint of polymer production [27]. When used in the synthesis of biodegradable polyesters, bio-based monomers, such as polylactic acid derived from corn starch or sugarcane, and bio-based succinic acid, create polymers that not only degrade more easily in the environment but also have a smaller environmental impact throughout their lifecycle [28].

Examples of biodegradable polyesters synthesized from bio-based monomers include polylactic acid, which is widely used in packaging and disposable products [29], and polybutylene succinate when synthesized from bio-based succinic acid, offering flexibility and biodegradability for packaging and agricultural films [30]. The development of bio-based monomers for biodegradable polyesters is crucial for advancing green chemistry and creating materials that are both high-performing and environmentally friendly.

1.5.1. Pentanediol

1,5-Pentanediol is a linear diol with two hydroxyl groups (-OH) at both ends of its five-carbon chain, as shown in Figure (8), making it an important monomer for the synthesis of polyesters. Derived from both petrochemical and bio-based sources, 1,5-pentanediol contributes to the flexibility, durability, and thermal stability of the polyesters it forms [31]. Its structure allows it to react with dicarboxylic acids or dimethyl esters, creating long-chain polymers with ester linkages that can offer biodegradability depending on the other components used in the synthesis. Polyesters synthesized using pentanediol include poly(pentylene adipate) which is known for its flexibility and potential for biodegradability, and poly(pentylene succinate), which combines bio-based components with degradable properties for applications like packaging and agricultural films [32]. The use of 1,5-pentanediol in polyester synthesis aligns with the growing demand for sustainable materials that balance performance with environmental responsibility [32].

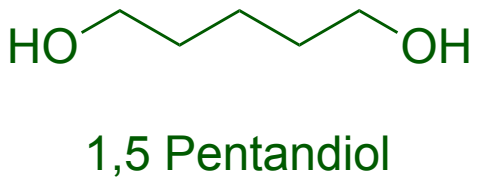

***Figure 8**: Chemical structure of 1,5 Pentanediol*

1.5.2. Furandicarboxlic acid

2,5 Furandicarboxylic acid, shown in Figure (9), is a bio-based dicarboxylic acid derived from renewable resources like plant sugars, and has gained significant attention as a sustainable alternative to petroleum-derived terephthalic acid in the production of polyesters [33]. Furandicarboxylic acid is a key building block for creating bio-based and potentially biodegradable polymers, as its structure contains two carboxyl groups (-COOH) attached to a furan ring, which offers enhanced thermal and mechanical properties compared to non-aromatic monomers. The use of furandicarboxylic acid allows for the production of polymers with excellent barrier properties, making it ideal for packaging applications [34]. Examples of polyesters synthesized using furandicarboxylic acid include poly(ethylene furanoate) (PEF), which is seen as a bio-based alternative to poly(ethylene terephthalate) (PET) and offers superior gas barrier properties [35], and poly(butylene furanoate) (PBF), which is valued for its flexibility and strength [36]. These bio-based polyesters, derived from furandicarboxylic acid, are part of a broader effort to create high-performance, eco-friendly materials that reduce reliance on fossil fuels and improve the sustainability of polymer production [34].

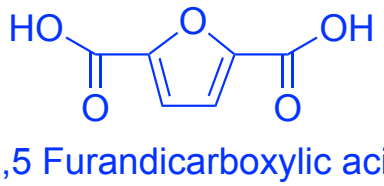

***Figure 9**: Chemical structure of 2,5 Furandicarboxylic Acid*

1.5.3. Dodecanediol

1,12-Dodecanediol, shown in Figure 10, is a long-chain aliphatic diol with two hydroxyl groups (-OH) at both ends of a 12-carbon chain. Its extended carbon backbone imparts flexibility, hydrophobicity, and thermal stability to the polymers synthesized from it, making the polymer

particularly useful for applications requiring durability and flexibility. [37]. Dodecanediol can be derived from both petrochemical and bio-based sources, aligning with the growing interest in renewable materials [38]. Polyesters synthesized using 1,12-dodecanediol include poly(butylene succinate-co-dodecylene succinate), known for its good thermal stability, good mechanical properties, making it suitable for making films [39] and poly(dodecylene adipate) (PDA), which combines flexibility with biodegradation properties, making it suitable for applications such as films and coatings [37]. The use of dodecanediol in polyester synthesis contributes to creating materials that balance performance with environmental benefits, particularly when bio-based dodecanediol is used.

***Figure 10**: Chemical structure of 1,12 Dodecanediol*

1.6. Nucleating agents

To increase the rate of crystallization for polymers, nucleating agents are usually added. Typically, nucleating agents lower the free energy associated with polymer nucleation and increase the rate of the primary nucleation, allowing the growth of crystallites on heterogeneous nuclei. Consequently, polymers experience a noticeable enhancement in crystallization rate and sometimes an increase in total crystallinity [40-42]. Nucleating agents for polyesters can be divided into 3 main categories: inorganic nucleating agents, organic nucleating agents, and polymeric nucleating agents [43, 44]. The first category, inorganic nucleating agents, are mainly inorganic fillers. Talc was used in polyethylene terephthalate (PET) [45, 46], polylactic acid (PLA)

[47, 48], PBAT [49, 50], and polybutylene succinate (PBS) [51, 52]; halloysite was used for PLA [53] and PBAT [54] and silica was used for PLA [55], PET [56], and PBS [57]. Finally, titanium oxide, mica, and calcium carbonate were used for polyesters such as PLA [58-60] and PET [61-63]. The second category, organic nucleating agents, are nucleating agents that undergo chemical reactions with the polyesters at elevated temperatures during melt-mixing to help induce crystallization. Na, Li and K salts of monocarboxylic acids and dicarboxylic acids, ester compounds, amide compounds, hydrazide compounds, and organic salts are examples of organic nucleating agents used for PET [64-68] and PLA [69-73]. The third category is polymeric nucleating agents such as polyoxymethylene, hyperbranched polymers, polyvinyl alcohol, polyvinyl butyral, polycaprolactone, poly (butylene succinate-co-butylene fumarate), and ionomers. This category has been used for polyesters such as PET [67, 74, 75], PLA [76-80], and PBS [81, 82]. The rheological properties of the polymer required to blow a film are critical, and the latter of these three categories of nucleating agents would be most desirable since the rheological properties are expected to be least affected. Also, the transparency of the films is also expected to be least affected.

Ionomers are ion-containing polymers with a small number (typically less than 10 mole percent) of polar ionic groups attached to the non-ionic polymer backbone [83]. Ionomers are mainly used both as neat resins and in polymer blends due to their high impact resistance, transparency, excellent toughness, high impact resistance, and high melt viscosity [84]. The most common ionomers are based on random copolymers of ethylene with methacrylic, or acrylic acid (E-MAA or E-AA respectively) with some of the acid groups neutralized with a metal cation. Un-neutralized acid copolymers are copolymers where all acid groups are neutralized by hydrogen; acid copolymers are not considered ionomers [85].

1.7. Film blowing

Film blowing is favored over compression molding for the production of films due to its ability to create thin, uniform, and continuous films with superior mechanical properties [86]. In film blowing, the polymer is melted and extruded through a circular die to form a thin tube, which is then inflated to produce a film. This process allows for precise control over film thickness, crystal size and chain orientation by adjusting parameters such as extrusion speed, blow-up ratio, and blow-up air temperature [87, 88]. Film blowing is particularly advantageous for producing large quantities of film with consistent quality, making it ideal for applications like packaging [89] and agricultural [90] films. Polymers than can be processed by film blowing include LLDPE [91], LDPE [92, 93], ethylene vinyl alcohol[94], polystyrene [95], polyethylene terephthalate [96], PBAT [97], PLA [98] and polyhydroxyalkanoate [99]. In contrast, compression molding involves placing a polymer in a heated mold, applying pressure, and then cooling it to form a solid part. While compression molding is effective for creating thicker and more complex shapes [100], it is less efficient and more limited in producing the continuous, thin films required for flexible packaging. The ability to achieve high production rates, combined with the excellent film properties, makes film blowing the preferred technique for manufacturing flexible films [86].

1.8. Gap in research

As previously noted, polyolefins, particularly LDPE and LLDPE, dominate the flexible film packaging market, primarily due to their exceptional thermal and mechanical properties. LDPE exhibits a melting temperature (T_m) in the range of 105 - 115°C, a glass transition temperature (T_g) of approximately -110°C and a decomposition temperature (T_d) around 350°C [101]. Moreover, LDPE has a tensile strength around 8 – 12 MPa, an elongation at break up to 500% and a Young's modulus in the range between 150 – 300 MPa [102, 103]. LLDPE exhibits

a T_m in the range of 120 - 125°C, a T_g of approximately -120°C and a T_d typically between 425 - 450°C [104, 105]. Furthermore, LLDPE has a tensile strength around 10 – 25 MPa, an elongation at break between 600 - 800% and a Young's modulus in the range between 150 – 300 MPa [106]. LLDPE has greater tensile strength and puncture resistance than LDPE, making it suitable for film applications such as packaging. However, LDPE is mixed with LLDPE to improve the rheological properties of LLDPE [107]. To replace LDPE and LLDPE, we need to identify biodegradable, bio-based polyesters that offer comparable thermal and mechanical properties, ensuring a seamless drop-in replacement without compromising performance. Aliphatic polybutylene succinate (PBS) and aliphatic-aromatic PBAT were proposed as alternative to LDPE and LLDPE in flexible film packaging. PBS exhibits a T_m in the range of 110 - 120°C, a T_g between -30 and -35°C and a T_d above 300°C [30, 108]. Moreover, PBS has a tensile strength around 30 – 45 MPa, an elongation at break in the range of 200 to 500% and a Young's modulus of approximately 500 – 600 MPa[108]. PBAT (50/50 A:T ratio) exhibits a T_m in the range of 115 - 125°C, a T_g around -30°C and a T_d above 350°C [109]. Furthermore, PBAT has a tensile strength around 20 – 35 MPa, an elongation at break reaching 800% and a Young's modulus in the range between 30 – 100 MPa [110]. Although, commercial aliphatic and aliphatic-aromatic polyesters such as PBS and PBAT have similar melt points to LDPE and LLDPE, but they have not replaced LLDPE and LDPE film for several reasons, even though both have been commercial materials for ~20 years. PBS has a relatively low elongation at break while PBAT has 1/3 the Young's modulus of LDPE and LLDPE. In addition, PBS and PBAT monomers are produced from non-renewable petroleum sources. Polylactic acid and polyhydroxyalkanoates biopolymers emerged as possible candidates for flexible film packaging. Polylactic acid has a T_m in the range of 160 - 170°C, a T_g between 55 and 60°C and a T_d above 300°C [111, 112]. Moreover, polylactic acid has a tensile strength around 50

– 70 MPa, an elongation at break in the range of 2 to 10% and a Young's modulus of approximately 3 – 4 GPa [111, 112]. Polylactic acid's high T_g and extremely low elongation at break have hindered its application in flexible film packaging, making it unsuitable for this purpose. PHAs are a group of natural biodegradable polyesters that are synthesized by microorganisms [113]. poly(3-hydroxybutyrate) (PHB), poly(3-hydroxybutyrate-co-3-hydroxyvalerate) (PHBV), poly(3-hydroxyhexanoate) (P3HH) and poly(3-hydroxyoctanoate) (P3HO) are examples of polyhydroxyalkanoates [113]. PHB has a T_m between 160°C and 175°C, with a T_g ranging from 0°C to 5°C, and it decomposes at temperatures above 290°C [114]. Additionally, its tensile strength is approximately 30–40 MPa, with an elongation at break of 5% to 10%, and a Young's modulus around 3–4 GPa [114, 115]. PHBV exhibits a T_m between 145°C and 175°C, a T_g from -5°C to 0°C, and a T_d exceeding 280°C [116, 117]. Its tensile strength ranges from 20 to 30 MPa, with an elongation at break of 1% to 5%, and a Young's modulus of approximately 1 to 2 GPa [116, 117]. P3HH has a T_m between 50°C and 60°C, a T_g around -35°C, and decomposes above 230°C [118]. Additionally, it possesses a tensile strength ranging from 10 to 20 MPa, an elongation at break of 200% to 300%, and a Young's modulus of approximately 0.1 to 0.3 GPa [118]. P3HO has a T_m ranging from 40°C to 50°C, a T_g of approximately -35°C, and decomposes at temperatures above 350°C [119]. Additionally, it exhibits a tensile strength between 10 and 15 MPa, an elongation at break exceeding 400%, and a Young's modulus of around 50 to 200 MPa [119]. The use of PHB, PHBV, and P3HH in flexible film packaging has been limited due to several factors: the low elongation at break of all three polymers, the high T_g of PHB and PHBV, and the low T_m of PHBV, P3HH and P3HO. These characteristics hinder their suitability for such applications.

This aim of this dissertation is to develop innovative biomass-based polyesters that can serve as alternatives to current packaging polymers. These polyesters will be biodegradable,

chemically recyclable, and engineered with enhanced mechanical and thermal properties. The new polymers will closely resemble aliphatic-aromatic polyesters, such as polybutylene adipate-co-terephthalate, as well as purely aliphatic polyesters like polybutylene succinate. Target properties of the biobased polyesters for this research are as follows:

- The polyester needs to have a biomass content of 50 to 100 wt%.
- Biodegradability of more than 60% in 180 days.
- T_m of more than 100°C and a T_g of less than -10°C,
- Modulus of elasticity and elongation at break of more than 200 MPa and 350%, respectively.
- Zero shear viscosity of approximately 10,000 Pa.s. (required for film blowing)
- Oxygen transmission rate lower than 8000 $cm^3/ (m^2$ day).

Chapter 2: Materials and Methods

2.1. Materials

The chemicals used to synthesis poly (pentylene adipate-co-terephthalate) (PPeAT60) were adipic acid (A, Sigma-Aldrich), terephthalic acid (T, Sigma-Aldrich), chloroform with ethanol as stabilizer (Sigma-Aldrich), 1,5-pentanediol (PeD, Acros Organics), phosphoric acid (Acros Organics) and titanium (IV) isopropoxide (Acros Organics). For the branching agents, glycerol (Gly, Sigma-Aldrich) and hexane-1,2,5,6-tetrol (HTeO) were used. HTeO was synthesized from levoglucosone (Circa Group) using a bifunctional catalyst [120, 121]. Branching agents were added in the beginning of polycondensation process with the original monomers. Li, Mg, and Na-based ionomers were graciously provided by DuPont (now Dow). The list of ionomers, having different neutralization levels and viscosities, can be found in the supplementary material Table (S1). Acid copolymer preparation process from these ionomers is reported elsewhere [85]. The chemicals used to synthesis poly (dodecamethylene furandicarboxylate) (PDDF) were 1,12 dodecanediol (DD, thermos scientific) 2,5-furandicarboxylic acid (FA, Accela), chloroform with amylenes as a stabilizer (Sigma-Aldrich), and titanium (IV) isopropoxide (Acros Organics). All chemicals were used as received. For the sake of comparison, film grade LLDPE with an MFI 0.7 g/10min (LyondellBasell), Film grade LLDPE with an MFI of 2 g/10 min (ExxonMobil LL1002.YB) and Ecoflex® (PBAT, BASF SE) were also tested. LLDPE was kindly provided by Amcor plc and PBAT was purchased from Azelis Americas. The chemical structures of PBAT, PPeAT60, PDDF, Gly, HTeO and E-MAA are shown in Figure (11).

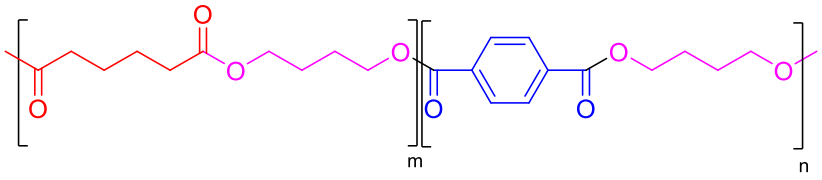

PBAT

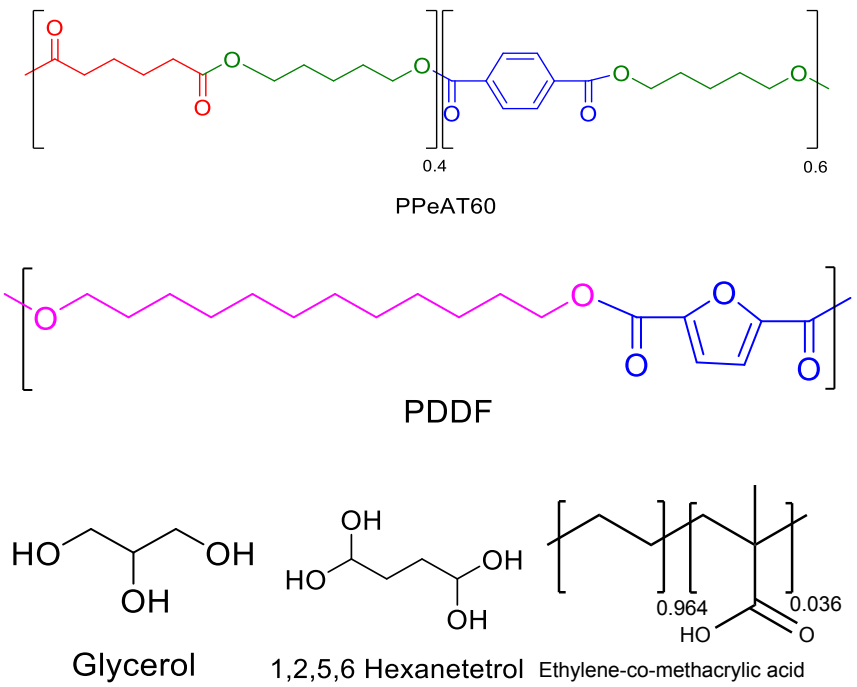

***Figure 11**: Chemical structure for PBAT, PPeAT60, PDDF, Glycerol, 1,2,5,6 Hexaanetrtrol and Ethylene-co-methacrylic acid*

2.2. Polymer Synthesis

Syntheses of polyesters were performed by a two-step procedure, esterification followed by polycondensation as shown in Figure (12) [122]. Except for those esters that contained dodecanediol, the diacids/diol molar ratio was 1:1.77; for dodecanediol a stoichiometric amount was used. The esterification reaction was started by adding over the course of 20 minutes a phosphoric acid-water (0.1 mol % of acid) mix at 170℃ into 60% of the diol under N_2 atmosphere at atmospheric pressure. The in-situ reaction was allowed to proceed for the next 40 mins under an N_2 blanket. The purpose of adding phosphoric acid is to reduce discoloration of the resultant product [122]. Then, 50 ml PeD, and the appropriate amount of FDCA and linear diacid were added, and temperature was increased to 200 ℃ at a rate of 5℃/30 min; for dodecanediol polyesters the temperature was not raised. The esterification reaction was carried out until 90% of the theoretical amount of water was collected using a condenser attached to a receiving flask. After

esterification, the temperature increased to 240 °C (230°C for dodecandiol polyesters) slowly and polycondensation was performed under vacuum (<0.2 mbar). The reaction time varied depending on whether high or low molecular weight products were desired.

All polymer synthesis was conducted by Dr. Onkar Singh.

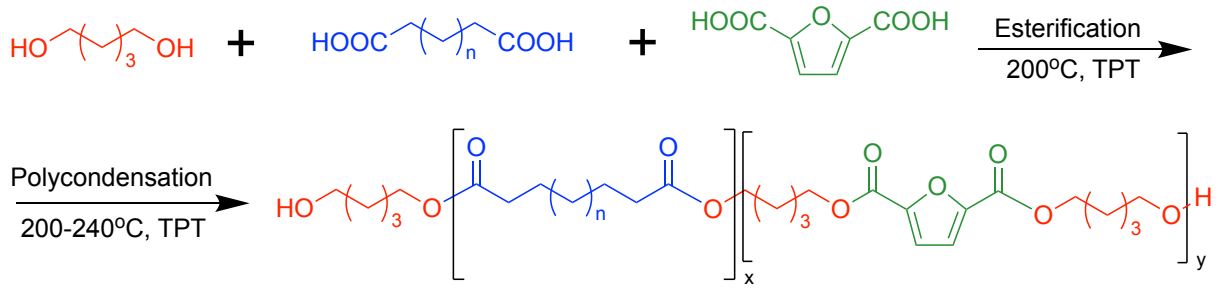

***Figure 12**: Schematic diagram of synthesis of Pentanediol – Furandicarboxylic acid- based polyesters*

2.3. Sample Preparation

2.3.1. Nucleator addition

All materials were dried in a vacuum oven at room temperature for 24 hours prior to melt-mixing. For the crystallization kinetics study, PPeAT/ionomer and PPeAT/acid mixtures were prepared by melt-mixing the required weight percent of nucleating agent with PPeAT in a DSM Xplore 5 micro compounder at 150°C for 2 minutes with a mixing rate of 200 RPM. The extruded strand was then dried in a vacuum oven overnight before further characterization.

For the film blowing application, PPeAT was melt-mixed with 0.5% weight percent ionomer using a 1″ Killion single screw extruder with 24/1 L/D ratio. The 3-barrel heating zones were set to 135/135/135°C and the die heating zone was 120°C while the screw speed was 60 rpm. The extruded strand was cooled using a water/ice bath and fed to a pelletizer to pelletize the nucleated PPeAT.

2.3.2. Compression Molding

PPeAT60 and PDDF samples were compression molded using a Carver laboratory press at a temperature of 190°C and a compression load of 5 metric tons. PPeAT60 solid samples were left for at least 2 hours at room temperature after compression molding prior to measurement; crystallinity was ~complete after this annealing time. While PPDF were left only for 30 minutes. All materials were dried in a vacuum oven at room temperature for 24 hours prior to any processing. For the PDDF samples, drying was conducted at 80°C under vacuum to eliminate any residual moisture.

For tensile properties, WAXS, SAXS, and DMA measurements, a rectangular copper mold measuring 92 x 62 mm with a thickness of approximately 0.4 mm was used, requiring about 3.7 grams of polymer per sample. For shear rheology, a circular stainless-steel mold with a diameter of 25 mm and a thickness of 1 mm was utilized, with each disk sample needing around 0.7 grams of polymer. For elongational viscosity, a TA Instruments EVF stainless-steel mold consisting of 20 rectangles, each measuring 18 x 10 x 0.78 mm, was employed, with approximately 0.13 grams of polymer required per sample.

2.3.3. Film Blowing

Pellets were fed to a LE8-30/C conical single screw extruder (30/1 L/D ratio) fitted with a LUMF-150 ultra microfilm blowing tower from Labtech engineering. The heating barrel temperature was set to 210°C while the die heating temperature was set to 200°C. The annular die was 20 mm in diameter and the blow-up ratio (BUR) was set to 3.5. The other parameters were adjusted so as to produce an average bubble thickness of 0.05 mm for all samples as seen in Figure (13). Hence, the screw speed, air blower, haul-off speed and pull roll and winder speed were set

to 300 RPM, 1020 RPM, 4.9 ft/min and 29.4 ft/min, respectively for LLDPE and 100 RPM, 2000 RPM, 2 ft/min and 15 ft/min, respectively for the PPeAT and PBAT. Compression molded sheets were compression molded in a Carver laboratory press at 5 metric tons and a temperature of 180°C to a thickness between 0.4 and 0.5 mm.

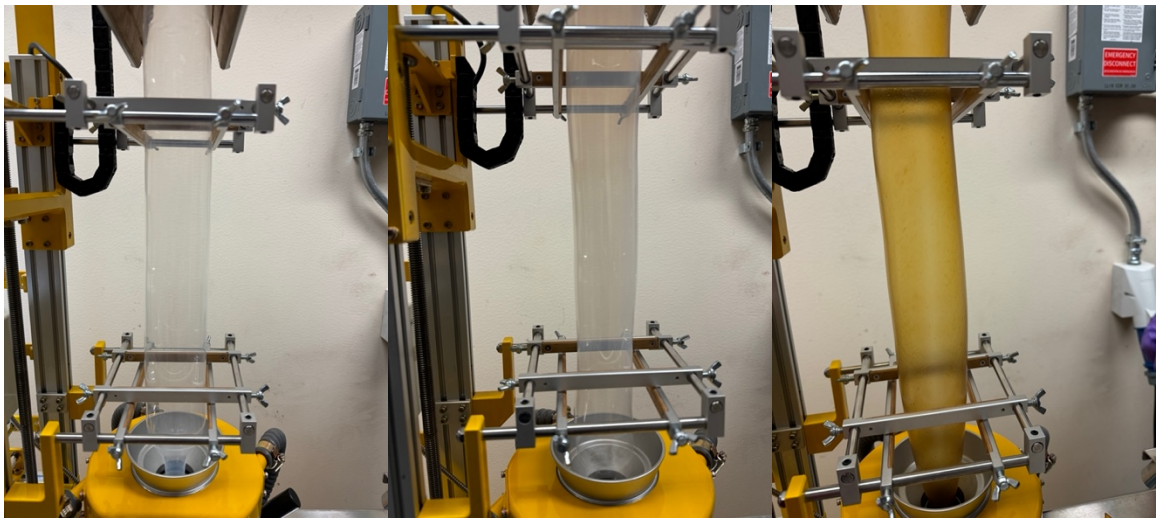

Figure 13: *Stable film bubble from LUMF-150 for LLDPE, PBAT and PPeAT*

2.4. Polymer Characterization

Two different size exclusion chromatography systems were used to measure the weight average molecular weight (M_w), number-average molecular weight (M_n) and dispersity indices (Đ = Mw/Mn). The first system was Waters 590 with Agilent Polypore 7.5 × 300 mm, 5μm column and a UV detector was used to measure, with PDI=M_w/M_n. Chloroform was used as the carrier solvent with a flowrate of 1 mL/min and oven temperature of 40°C. Eight different polystyrene standards at eight different molecular weights were used to obtain the calibration curve. The second system, located at Colorado State University, was an Agilent HPLC equipped with a guard column and two or three PLgel 5 µm mixed-C gel permeation columns, coupled with a Wyatt DAWN HELEOS II multi-angle (18) light scattering detector and a Wyatt Optilab TrEX dRI detector. The analysis was conducted at 40°C with chloroform as the eluent, flowing at 1.0

mL/min, and molecular weight data were processed using Wyatt ASTRA 7.1.2 software. The samples were analyzed using the "assume 100% mass recovery" option, where dn/dc (0.0282 mg/mL) was calculated internally based on the known polymer concentration of 2.00–4.00 mg/mL prior to injection.

^{1}H nuclear magnetic resonance (NMR) spectra were obtained using a Varian VNMRS 400 MHz spectrometer with deuterated chloroform as the solvent. To prepare the samples for NMR analysis, they were initially dissolved in chloroform and then recrystallized in cold methanol to eliminate minor impurities. Afterward, samples were vacuum dried for 24 hours before being dissolved in deuterated chloroform at a concentration of 3-4 mg/ml for analysis. Each measurement was based on an average of 16 scans.

Thermogravimetric analysis (TGA) for the copolyesters was performed using a TA Instruments TGA55. Polymer samples were heated from 40°C to 700°C at a heating rate of 10°C/min under nitrogen gas as a protective blanket. 100 μL platinum pans were used with a sample size ranging from 10 to 20 mg.

Wide-angle X-ray scattering (WAXS) analyses were conducted on a Rigaku SmartLab diffractometer with Cu-K-alpha radiation (40 kV, 200 mA) and a Bragg-Brentano geometry was used as a detector. Scans were taken in the 2θ range with a step size of 0.01° from 5° to 50°. To calculate fractional crystallinity, a program was used to fit a baseline followed by a Gaussian curve to each peak and the amorphous halo. Small-angle X-ray scattering (SAXS) measurements were performed using a Xenocs XEUSS 3.0 with Cu-K-alpha (1.54 Å). The apparatus was operated at 50 kV and 0.6 mA with a q-range of 0.01 to 0.3 $Å^{-1}$ and an exposure time of 120 mins was used.

Differential scanning calorimetry (DSC) measurements were carried out using a TA Instruments DSC 2500 with indium metal, tin, and biphenyl used for calibration. Aluminum pans

were used with a sample size ranging from 5 to 15 mg. Polymers were first heated from -85°C to 180°C with a heating rate of 10°C/min. The sample was maintained at 180°C for 5 minutes to erase the thermal history. The sample was then cooled down to -85°C at a cooling rate of 10°C/min and finally heated again to 180°C at a heating rate of 10°C/min. For isothermal crystallization experiments, samples were initially heated to 180°C and then quenched at 80°C/min to the required crystallization temperature and held for 2 hours.

A 2000 lb. SSTM tester from United Testing Systems was used to measure tensile properties at room temperature. A dog-bone shaped sample according to the ASTM D-1708 standard was cut from compression molded samples. The thickness of the samples varied from 0.4 to 0.5 mm. An average of 5 samples were used to calculate the final properties of each polymer.

Rheological properties were investigated using a TA instruments ARES G2 constant strain rheometer. Storage modulus, loss modulus, and complex viscosity were studied using 25 mm parallel stainless-steel plates and a 1 mm gap. Each sample was examined at a constant temperature of 190°C and a frequency range from 600 rad/s to 0.01 rad/s. This temperature was chosen to mimic the film blowing temperature for LLDPE [123]. Extensional viscosity was measured using the Extensional Viscosity Fixture of the Ares G2 rheometer at 130°C at an extensional rate of 0.3 s^{-1}. The former value was chosen because to be slightly above the melting temperature to avoid any sagging. The latter value was chosen because a Hencky strain of 2.5 at an elongational rate of 0.3 s^{-1} were found to be representative values for film blowing [124]. Dynamic mechanical analysis (DMA) for the polymers was performed using a linear tension fixture geometry on the Ares G2. The test was conducted at a temperature range of -75°C to the sample melting temperature, a frequency of 1 Hz, and a temperature step of 3°C.

The Student's t-test was employed for every set of measurement to measure the null hypnosis. The statistical significance was considered at $p < .05$. The built in Excel function (t.test) was implemented to obtain the results and reported in Tables (S2) - (S5).

CO_2 and O_2 permeability of the films was measured at 1 bar and 25°C in a constant volume, variable pressure barometric device with a 47 mm HP filter holder. Prior to the experiment, the system was left under vacuum for 24 hours to remove any humidity and previously absorbed gases. Upstream pressure was monitored using a PX-409-USHB pressure transducer with a full-scale of 1000 psi while the downstream pressure was monitored using another PX-409-USHB with a full scale of 260 torr. The change in downstream pressure over time was recorded and the permeability (P) at steady state can be calculated using equation. (16):

$$\mathrm{P} = \frac{lV_{down}}{ART\Delta p}.\frac{dp}{dt}_{down} \tag{16}$$

Where, l and A are the thickness and the area of the film, respectively, R is the universal gas constant, T is the absolute temperature, V_{down} is the downstream volume, Δp is the pressure difference across the film, and $\frac{dp}{dt}_{down}$ is the steady state slope of pressure versus time in the downstream.

Water vapor transmission rate (WVTR) was measured according to ASTM E96 (dry cup method) by first fixing a dry sample (of mass m_0) on a vail filled with desiccant ($CaSO_4$) in a desiccator saturated with water vapor and then monitoring the increase in mass (m_g) as a function of exposure time. The vials covered with the film were weighed at certain times until 21 days. Weight changes of the vial were plotted vs. times and then slopes of the plot of each sample were obtained. The thickness and area of each sample were measured prior to testing. WVTR was calculated using equation (17):

$$WVTR = \frac{dm_g}{dt}\Big|_{s.s} . \frac{l}{A} \quad (17)$$

Where, $\frac{dm_g}{dt}\Big|_{s.s}$ is the steady state slope of mass gained versus time and l and A are the thickness and the area of the film, respectively.

The freshwater biodegradability study of the polyesters followed the guidelines of ISO 14851. Each polyester underwent testing in triplicate using 300 mL biological oxygen demand (BOD) glass bottles from VWR International. In each bottle, 200 mL of an aqueous medium containing KH_2PO_4 (85 mg/L), K_2HPO_4 (217.5 mg/L), Na_2HPO_4 (334 mg/L), NH_4Cl (15 mg/L), $MgSO_4 \cdot 7H2O$ (22.5 mg/L), $CaCl_2 \cdot 2H_2O$ (36.4 mg/L), and $FeCl_3 \cdot 6H2O$ (0.25 mg/L) from Fisher Scientific was mixed with activated sludge obtained from a wastewater treatment plant in Lemont, IL, resulting in a total solid concentration of 60 mg/L in the BOD bottle. Polyester samples (PDDF or PBAT) in film form (2 mm × 2 mm × 0.5 mm) were added to each BOD bottle, with a total organic carbon content of 9.0 mg. Triplicate sets of negative controls (without additional carbon) and positive controls (with 9.0 mg total organic carbon from d-glucose and cellulose) were also prepared. Incubation of all bottles occurred in a New Brunswick Scientific incubator shaker (Eppendorf, model I-24) at 25 °C and 150 rpm. Oxygen consumption, indicative of BOD, was measured using a pH/RDO/DO meter (Thermo Fisher Scientific, model Orion Star A216) according to ISO 14851 standards as well. The biodegradability percentage was calculated using equation (18).

$$Biodegradation\ \% = \frac{BOD_{sample} - BOD_{blank}}{C\ \times Th_{OD}} \quad (18)$$

BOD_{sample} and BOD_{blank} represent the recorded measurements from the sample and blank bioreactor, respectively. C denotes the amount of sample added, while Th_{OD} stands for the theoretical oxygen demand value of the sample, derived from its chemical formula under the

assumption of full oxidation to CO_2 and H_2O. The procedure mandates that the positive control (glucose and microcrystalline cellulose) achieve a 60% biodegradation level by the test's conclusion, with the standard deviation of each sample being under 20% of the mean.

Biodegradability tests in the soil environment (soil respiration tests) were conducted according to ASTM D5988-18. The soil respiration tests were set up in 1 L Kimble bottles (with Wheaton Black Phenolic Cap and Gray Butyl Septa and Flange, DWK Life Sciences) in triplicate. Each test bottle contained 150 g of soil (a mixture of soil samples taken from local forests in Illinois). To each test bottle, additional water was added to reach 70% of the field capacity (water holding capacity) of the soil sample. The field capacity of the soil was measured using the ASTM D2980-17E01. Each of the polymer sample (10 mm × 10 mm × 0.5 mm size) containing 0.30 g of total organic carbon was added to the BOD bottles and well mixed with the soil. A negative control with no additional content and two positive controls with glucose and cellulose containing 0.30 g total organic carbon were also set up in triplicate. The degradation of the polymers, glucose, and starch was monitored by measuring the CO_2 volume released into the headspace of the bottles. Samples collected from the headspace were analyzed by gas chromatography (Shimadzu, model GC-2014). The biodegradation of polymers in percentage is calculated as shown in equation (19)

$$Biodegradation\ \% = \frac{V_{CO_2,sample} - V_{CO_2,Blank}}{ThV_{CO_2,sample}} \quad (19)$$

The $V_{CO2,\ sample}$ is the theoretical production volume of CO_2 calculated from the carbon mass in polymer samples.

End-of-life tests in industrial composting environments were conducted according to ASTM D5338-15 method [125]. The AER-800 Research Respirometer (Challenge Technology, USA) was used to quantify the CO_2 production rate in aerobic mode. The compost was acquired

from a local compost facility (Land-and-Lakes Company, Romeoville, IL, USA) and screened through a 10 mm sieve. Microcrystalline cellulose (particle size 0.05 mm, Acros Organics) was used as positive control. Each chamber was loaded with compost of 40 g total solid and 1.5 g of microcrystalline cellulose or PDDF polymer film samples (cut to 10 mm× 10 mm× 0.5 mm pieces). Additional three chambers were set up only with compost as the negative control. Each positive control or polymer was also run in triplicate (three test chambers). The biodegradation test chambers were maintained in a 58 ± 2 °C water bath, with a built-in KOH trap to absorb the produced CO_2. The KOH solution (45% in water, Sigma-Aldrich) was changed periodically. Continuous flow of ultra-high purity O_2 was maintained at 5 psi to compensate for the trapped CO_2 and the flow rate of O_2 into each chamber in mg was recorded by the respirometer as the CO_2 production rate. Milli-Q water was periodically added to each chamber to maintain the relative humidity at approximately 55%. The percentage biodegradation of polymers was calculated using:

$$\%Biodegradation = \frac{m_{CO2,sample} - m_{CO2,blank}}{Thm_{CO2,sample}} \times 100\% \quad (20)$$

$Thm_{CO2,\ sample}$ was the theoretical production mass of CO_2 calculated from the mass of carbon in polymer samples.

Chapter 3: Pentanediol - Furandicarboxylic acid-based polyesters

3.1. Abstract

This study focuses on the synthesis and characterization of high molecular weight copolyesters derived from PeD and FDCA, both bio-based components, to develop sustainable polymer systems for use in flexible film packaging. PeD, derived from bio-based feedstocks, was selected for its flexible, hydrophobic chain while FDCA, an aromatic diacid derived from plant-based carbohydrates, was selected for its ability to enhance the mechanical strength and thermal stability of the copolyesters. By varying the chain length of the aliphatic diacids, we tried to tailor T_g and T_m to meet the requirements for a flexible packaging application. This application requires ΔT (T_m-T_g) of over 110°C. A biomass content exceeding 50% highlights the sustainability of these copolyesters. Our results show that increasing the FDCA content increased T_m, while the length of the aliphatic diacid chain influenced T_g and flexibility. However, our findings show that ΔT over 110°C of PeD and FDCA based copolyesters is not possible.

3.2. Results and Discussion

The primary aim of this work was to synthesize and characterize of high molecular weight copolyesters for flexible packaging applications. PeD was selected as the diol because it can be synthesized from bio-based feedstocks, making it a key component in our efforts to develop a more sustainable polymer system [126]. FDCA was selected as the aromatic diacid. FDCA has gained significant attention in the realm of sustainable polymer chemistry, as it can be synthesized from plant-derived carbohydrates, thus contributing to the overall biomass content of the copolyester [127]. The third component of the copolyester system was the aliphatic diacid, which we varied in chain length from the 4-carbon succinic acid to 14-carbon tetradecanoic acid to tailor the final properties of the polymer. The full list of aliphatic linear diacids used is found in Table (1).

By varying the chain length of the aliphatic diacid and the ratio of aliphatic to aromatic diacids, we aimed to precisely control the T_m and T_g of the copolyesters, which are critical parameters for determining the suitability of the material for flexible packaging. A T_m from about 100°C to 120°C is essential for flexible film packaging for proper performance during sealing and use, while a lower T_g improves flexibility and ease of handling. This tunability makes the copolyester system ideal for film packaging applications, where the combination of high performance, processability, and sustainability is critical.

Importantly, the biomass content of these copolyesters exceeds 50%, as both the PeD and FDCA can be derived from renewable biomass sources. By creating materials that are both high-performing and environmentally friendly, we contribute to a growing body of research aimed at minimizing the environmental impact of polymer production while still meeting the demands of modern industry.

Thirty-four PeD-FDCA acid-based polyesters were successfully synthesized. T_m, T_g, M_w and M_n of selected polyesters are shown in Table (2). Polyesters that contain succinic acid, glutaric acid and azelaic acid only showed a T_g. No T_m was observed even after X months of room temperature annealing. For the succinic acid, T_m is expected to be near room temperature, preventing the sample from crystallizing under those conditions. The other two acids have an odd-number of carbons, and an even-odd effect could be manifested here.

***Table 1**: List of linear diacids used. the number of carbons refers to the total carbon atoms in the diacid, while n represents the number of internal carbons, excluding the two terminal carbons at each end*

Abbreviation	Name	Number of Carbon	n
S	Succinic Acid	4	0
G	Glutaric Acid	5	1
A	Adipic Acid	6	2
Su	Suberic Acid	8	4
Az	Azelaic Acid	9	5
Se	Sebacic Acid	10	6
D	Dodecanedioic Acid	12	8
TD	Tetradecanoic Acid	14	10

Polyesters containing adipic acid, sebacic acid and dodecanedioic acid with 50% FDCA by mole have an acceptable T_g (below -20°C). However, T_m for all 3 polyesters is extremely low. As the mole percentage of FDCA increased from 50% to 70%, the T_m rose accordingly, but this also resulted in an increase in T_g. For polyesters containing tetradecanoic acid, T_m was observed, but no T_g was detected likely because the presence of the long-chain linear diacid lowered the T_g below the detection limit of our DSC. The difference between the T_m and T_g, referred to as ΔT, was calculated. ΔT remained nearly constant across all PeD-FDCA acid-based polyesters, regardless of the identity or amount of aliphatic diacid. To achieve the desired T_m and T_g ($T_m >$

100°C and T_g < -10°C), the ΔT needs to be more than 110°C. Therefore, ΔT is insufficient for these materials to be suitable for flexible film applications.

***Table 2**: Pentanediol-Furandicarboxylic acid-based polyesters results.*

No. of Carbon	Sample	T_g (°C)	T_m (°C)	T_m-T_g (°C)	Mw	Mn
4	PPeSF50	-28.4	-	-	17,996	9,087
5	PPeGF50	-31.5	-	-	288,339	74,718
6	PPeAF50	-20.9	46.0	66.1	22,681	19,866
6	PPeAF70	-21.5	44.8	66.3	49,167	24,900
8	PPeSuF50	-39.3	-	-	191,727	66,612
8	PPeSuF70	-33.0	44.8	77.8	8,056	754
9	PPeAzF50	-37.7	-	-	194,725	61,433
10	PPeSeF50	-40.2	14.2	54.4	20,291	14,839
10	PPeSeF70	-29.3	46.4	70.3	19,797	13,021
12	PPeDF50	-34.8	34.3	69.1	57,080	31,829
12	PPeDF70	-25.1	38.0	60.2	198,371	79,111
12	PPeDF90	-4.2	56.0	66.3	50,105	27,991
14	PPeTDF60	-	32.5	-	269,780	99,555

Poly (pentylene dodecanoate-co-furandicarboxylate) (PPeDF) copolyesters were synthesized at various dodecanedioic acid/ furandicarboxylic acid ratios (D/F) across the full composition range. The copolymers PPeDF are abbreviated as PPeDF$_{\chi}$ where (100-χ)/χ represents the D/F mole ratio. The Mw, Mn, PDI, T_g, T_m and X_c results for the PPeDF, PPeD and PPeF copolyester are reported in Table (3). The properties tend to have a minimum fractional crystallinity, melting temperature and glass transition temperature at intermediate molar ratios of the two diacids. Polymers made at roughly equimolar acid ratios are particularly intriguing given their low glass transition temperatures and high elongation at breaks with moduli 50-100 MPa [128]. The crystallization kinetics of the PPeF crystals were quite slow likely due to the odd

number of carbon atoms in pentanediol vs. polyesters made with butanediol, as well as furan-based polyesters having slow crystallization kinetics relative to terephthalic-based polyesters [128].

***Table 3**: Results for poly (pentylene dodecanoate-co-furandicarboxylate).*

Sample	Mw	Mn	PDI	T_g (°C)	T_m (°C)	X_c (%)
PPeD		-	-	–	67.2	64.0
PPeDF10	81700	66600	1.23	–	60.2	53.5
PPeDF20	65900	46500	1.42	–	54.8	47.6
PPeDF30	167900	76200	2.2	-19	45.5	35.4
PPeDF40	112600	77000	1.46	-22.1	26.3/43.5	46.2
PPeDF50	57100	31800	1.79	-32.3	25.4/41.8	35.3
PPeDF60	70500	48100	1.46	-31.5	16.7/42.1	32.0
PPeDF70	198400	79100	2.45	-25.1	38.1	29.0
PPeDF80	34600	23700	1.46	-18.7	42.3	27.8
PPeDF90	50100	28000	1.79	-4.2	56	15.4
PPeF	57300	31300	1.82	9.9	65.2	26.3

3.3. Conclusion

High molecular weight copolyesters incorporating bio-based PeD, FDCA, and various aliphatic diacids. The flexible design of the polymer backbone, achieved by adjusting the chain length and composition of the aliphatic diacids, allowed for precise control over thermal properties, such as T_g and T_m. Despite achieving a high degree of sustainability with a biomass content exceeding 50%, the materials exhibited challenges in terms of their crystallization kinetics, particularly with polyesters containing shorter aliphatic diacids. For applications like flexible film packaging, T_m-T_g greater than 110°C is essential. Unfortunately, this difference is not large enough for PeD-FDCA based materials to be suitable for flexible film applications.

Chapter 4: Poly (pentylene adipate-co-terephthalate) *

4.1. Abstract

Traditionally, most flexible food packaging is made of linear-low density polyethylene (LLDPE) which cannot easily be recycled, nor will it degrade in a reasonable timescale. In this work, a biobased biodegradable polyester alternative was investigated as a possible replacement for LLDPE. High molecular weight poly (pentylene adipate-co-terephthalate) with a 40/60 adipic acid/terephthalic acid mole ratio was synthesized using direct esterification and polycondensation. Glycerol and hexane-1,2,5,6-tetrol were added as branching agents to better match the structure of the LLDPE which in turn might help the ability of these materials in film-blowing. Thermal, mechanical, and rheological properties of the copolyesters were thoroughly investigated. All copolyesters had a weight-average molecular weight of over 140,000 g/mol, which is necessary for proper rheology, and were thermally stable up to 350°C. The addition of branching agents led to a slight decrease in crystallinity, d-spacing, melting temperature, enthalpy of melting, stress at break, and elongation at break. However, an increase in Young's Modulus and complex viscosity at high frequency were observed compared to PPeAT60 without branching agent added. Although the improved crystallinity and mechanical properties of the copolyesters made them viable for film-blowing, the slow crystallization rate creates a major challenge.

**Adapted with permission from Aboukeila et al. [129]*

4.2. Results and Discussion

Average molecular weight and PDI, relative to polystyrene standards, are reported in Table (4) along with commercial PBAT. The average molecular weights of PBAT and PPeAT60 are similar thus allowing meaningful comparison of mechanical and rheological properties.

***Table 4**: GPC results for PBAT, PPeAT60, PPeAT60+0.5% Gly and PPeAT60+0.1% HTeO.*

Sample	M_w	M_n	Đ
	g/mol	g/mol	-
PBAT	148,800	97,800	2
PPeAT60	188,600	106,450	1.8
PPeAT60 + 0.5% Gly	156,600	99,600	1.6
PPeAT60 + 0.1% HTeO	141,300	88,400	1.6

4.2.1. Thermal Properties

The temperature at which decomposition reached 5% ($T_{d,5\%}$), the temperature at maximum decomposition rate ($T_{d,\,max}$) and residual mass at 600°C ($R_{600°C}$) from TGA are shown in Table (5). Figure (14) shows that PPeAT60 has a slightly improved $T_{d,5\%}$ when compared to PBAT, which might be due to the longer aliphatic chain of PeD. The addition of branching agents did not affect the thermal stability of the copolyesters as shown in Figure (14). All copolyesters yield a residue of 4% at 600°C due to the pyrolysis of the aromatic fraction leading to the formation of stable char. LLDPE shows a better thermal stability with a $T_{d,\,max}$ of 453°C and an $R_{600°C}$ of 0%. The reduced thermal stability of the polyesters is due to the ester linkage. Regardless, all synthesized copolyesters have good thermal stability, allowing for processing at temperatures above their respective T_m without experiencing thermal degradation. Of bigger concern of course regarding processing is hydrolysis, which is why the samples should be dried prior to processing.

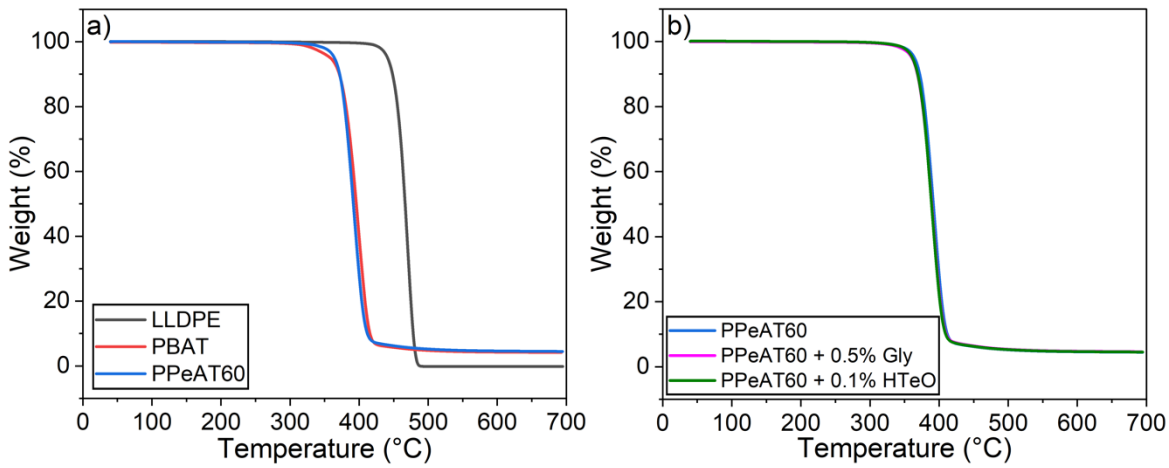

***Figure 14**: TGA results for a) LLDPE, PBAT, and PPeAT60 and b) PPeAT60, PPeAT60+0.1% HTeO and PPeAT60+0.5% Gly.*

***Table 5**: Thermal properties from TGA and DSC for PBAT, PPeAT60, PPeAT60+0.5% Gly and PPeAT60+0.1% HTeO.*

Sample	First Heating		First Cooling	Second Heating			TGA		
	T_m	ΔH_m	T_c	T_g	T_m	ΔH_m	$T_{d,5\%}$	$T_{d,max}$	$R_{600℃}$
	℃	J/g	℃	℃	℃	J/g	℃	℃	%
LLDPE	116	131	106	-	116	127	441	453	0
PBAT	115	34	38	-30	118	20	358	376	4.3
PPeAT60	101	35	-	-9	-	-	364	373	4.6
PPeAT60 + 0.5% Gly	88	31	-	-13	-	-	361	371	4.8
PPeAT60 + 0.1% HTeO	99	29	-	-11	-	-	361	371	4.7

Figure (15) and Figure (16) show DSC curves. The first heating cycle of LLDPE and the copolyesters shows a clear endothermic peak due to the melting temperature of the polymer. However, for the first cooling cycle an exothermic peak can only be observed for LLDPE and PBAT which indicates that PeD-based polyesters had a slower crystallization rate. The commercial PBAT could have had crystal nucleator added; however, laboratory synthesized PBAT without crystal nucleator shows kinetics similar to what is shown here [130]. The absence of an

endothermic melting peak in the second heating cycle for the PeD-based polyesters validated the slow crystallization rate assumption. The melting temperature (T_m), enthalpy of melting (ΔH_m), crystallization temperature (T_c) and glass transition temperature (T_g) are summarized in Table (5). The results show that PBAT has a higher T_m (118°C) and a lower T_g (-30°C) than PPeAT60 (T_m=101°C and T_g=-9°C). Unpublished work from our lab shows that T_m and T_g can both be shifted up or down with more terephthalic acid or more adipic acid respectively, but the difference T_m-T_g is nearly constant. The fact that the difference was smaller with pentanediol instead of butanediol is attributed to the odd-even effect of the two diols [131]. T_m of PPeAT60 + 0.5% Gly branched material is 13°C lower than the linear material with only a 4°C drop in T_g. At high enough levels, the addition of branching agents to polyester will decrease the T_m and ΔH_m because branches act as defects in the crystal which reduces the long spacing [132]. Boyer concluded that the ΔT between T_m and T_g does not change drastically thus the T_m decrease due to branching will consequently lead to a decrease in T_g [133]. Hence, PPeAT60 + 0.1% HTeO follows the Boyer conclusion while PPeAT60 + 0.5% Gly does not. For sake of comparison, film grade LLDPE was also measured and reported in Figure (15) and Table (5). T_g could not be detected by DSC for LLDPE.

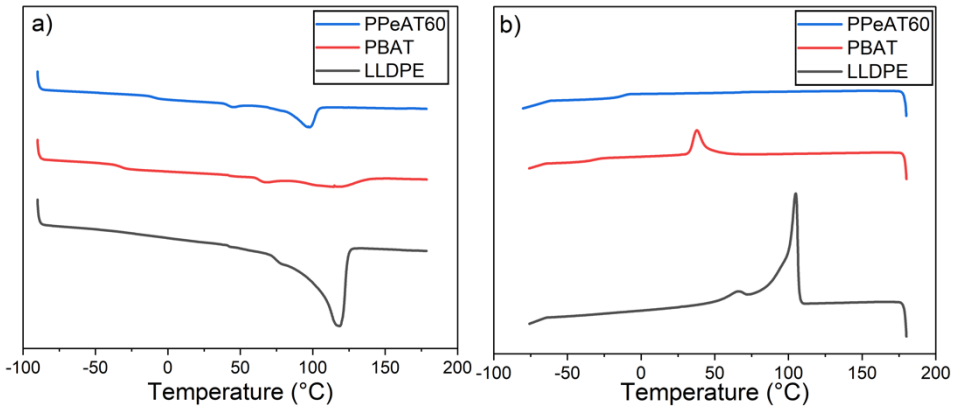

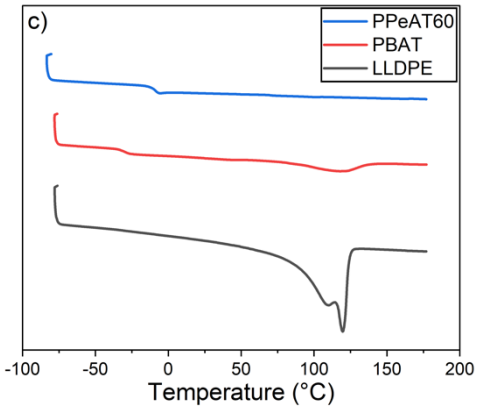

***Figure 15**: DSC curves for a) first heating cycle, b) first cooling cycle, and c) second heating cycle for LLDPE, PBAT, and PPeAT60. Results have been shifted vertically for clarity.*

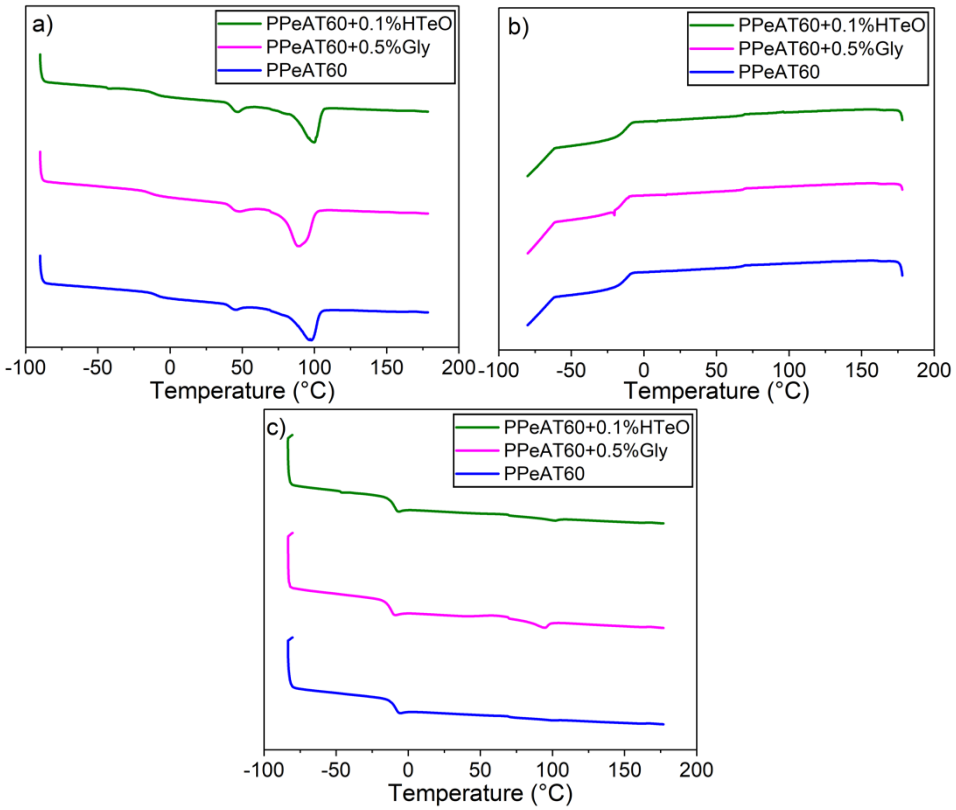

***Figure 16**: DSC curves for a) first heating cycle, b) first cooling cycle, and c) second heating cycle for PPeAT60, PPeAT60+0.1% HTeO and PPeAT60+0.5% Gly. Results have been shifted vertically for clarity.*

Isothermal crystallization kinetics of the copolyesters were investigated by DSC at different temperatures and are shown in Figure (17). The maximum crystallization rate was found at 40°C for PPeAT60 which matched that of the commercial PBAT (data not shown). The

maximum crystallization rate dropped to lower temperature (30°C) for PPeAT60 + 0.5% Gly and PPeAT60 + 0.1% HTeO as shown in Figure (S2).

The well-known Avrami model was employed to better understand the isothermal crystallization process. The Avrami model describes the relative crystallinity (X_t) in terms of time at a constant temperature as shown in equation (21):

$$X_t = 1 - \exp(-kt^n) \quad (21)$$

***Table 6**: Avrami model for PPeAT60, PPeAT60+0.5% Gly and PPeAT60+0.1% HTeO.*

Sample	T_c	$t_{1/2}$	$k * 10^{-5}$	n
	℃	min	min^{-n}	-
PPeAT60	20	67.5	0.2	3.05
	30	30.7	3.6	2.88
	40	27.5	5.3	2.86
	50	38.1	1.6	2.94
	60	63.5	0.8	2.74
PPeAt60+0.5% Gly	20	52.6	0.56	2.96
	30	33.9	3.85	2.78
	40	37.6	2.23	2.85
	50	69.3	0.38	2.86
PPeAT60+0.1% HTeO	10	36.3	4.89	2.66
	20	9.5	73.7	3.03
	30	8.2	1730	1.73
	40	16.8	43.9	2.6
	50	27.4	12.2	2.61
	60	63.4	0.82	2.74

k is the rate constant for crystallization which is a function of nucleation and growth rates, and n is the Avrami exponent. The results for the Avrami model as well as the half time for 100%

relative crystallization ($t_{1/2}$) are shown in Table (6). The experimental data and the Avrami model were in agreement hence secondary crystallization is insignificant [134]. For all copolyesters, Avrami exponent varies from a minimum of 2.6 to a maximum of 3 except for one test temperature; PPeAT60 + 0.1% HTeO had an Avrami exponent of 1.7 at 30°C. Therefore, according to the Avrami exponent, the growth mechanism is a combination of 1D and 2D growth. The addition of glycerol slowed the crystallite growth rate slightly while HTeO increased the crystallite growth rate, especially at the temperature corresponding to the maximum rate. PBAT had a $t_{1/2}$ of 0.5 min at 40°C (data not shown).

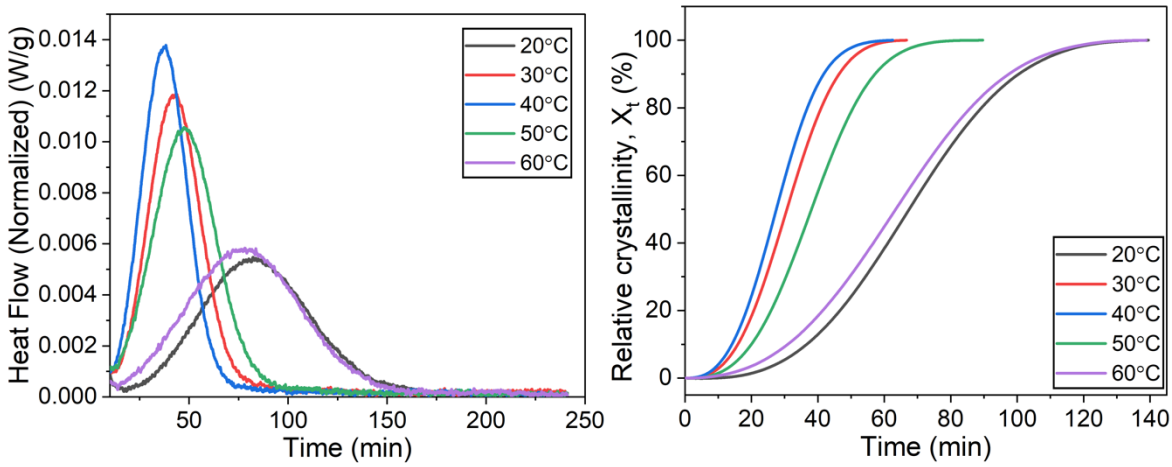

***Figure 17**: Isothermal crystallization and Avrami model results for PPeAT60*

4.2.2. Crystal Properties

WAXS patterns for the copolyesters and LLDPE are shown in Figure (18), while the percent crystallinity for the copolyesters and LLDPE are given in Table (7). For PBAT, scattering angles ($2\theta°$) observed are 16.2°, 17.3°, 20.4°, 23.2° and 24.8 corresponding to the planes (011), (010), (102), (100) and (111) respectively [135]. For PPeAT60, $2\theta°$ are 15.9°, 17.4°, 21.8°, 23.5° and 25.5° with all peaks presumably corresponding to the same planes as for PBAT. The diol swap from butanediol to pentanediol provided a slight decrease in the percent crystallinity from 19.4% to 18.5% as shown in Table (7); the ratio of these two values is roughly consistent with the ΔH_ms

shown in Table (5). The crystal fraction of PBAT and PPeAT60 are formed by BT and PeT units, respectively [135]; therefore the drop in crystallinity could be attributed to the odd-even effect; that is pentanediol with an odd number of carbons in the diol is expected to have lower crystallinity than butanediol with an even number of carbons.

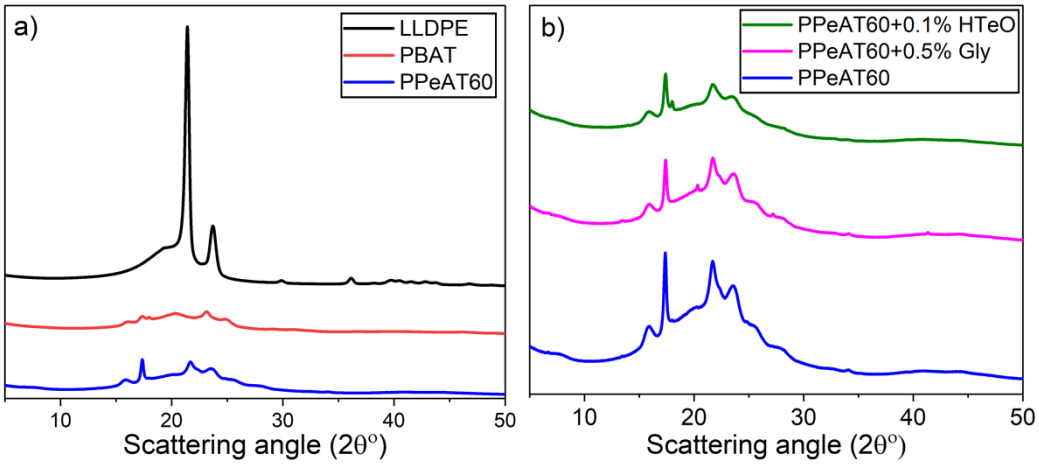

***Figure 18**: WAXS results for a) LLDPE, PBAT and PPeAT60 and b) PPeAT60, PPeAT60+0.1% HTeO and PPeAT60+0.5% Gly.*

The addition of branching agents such as Gly and HTeO did not affect peak locations but led to a slight decrease in percent crystallinity to 15.7% and 18.4% respectively; the former qualitatively ~agrees with the drop in ΔH_m shown in Table (5) while the ΔH_m drop for the latter is much more than the WAXS result indicates. The addition of branching agent generally reduces crystallinity of semi-crystalline polymers [136]. These measurements do not conclusively indicate a statistically significant difference in crystallinity because of the error in calculating ΔH_m or crystallinity from WAXS for these samples. LLDPE shows two sharp crystalline peaks at the $2\theta°$ value 21.4° and 23.6° assigned to (110) and (200) planes. The percent crystallinity was calculated to be 50.4%. LLDPE results are in approximate agreement with the literature [137].

SAXS results for LLDPE and the copolyesters are shown in Figure (19) and Table (7). Since the shape of the crystallites are expected to be lamellar, the maximum provided by $q^2I(q)$ vs

q is the characteristic long spacing from Bragg's Law. The long period (d-spacing) is calculated using equation (22) where q_{max} is the value where $q^2I(q)$ vs q.

$$d = \frac{2\pi}{q_{max}} \tag{22}$$

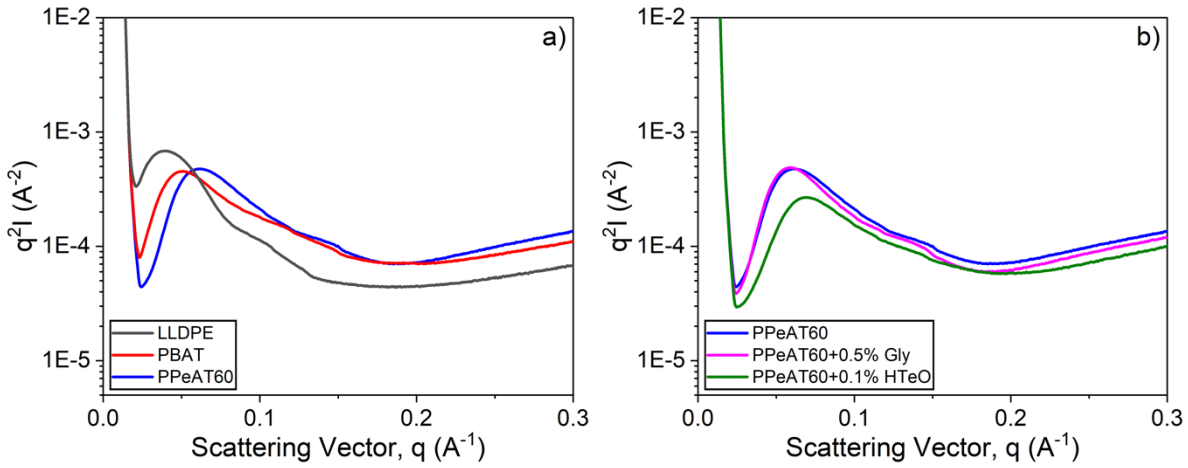

***Figure 19**: SAXS results for a) LLDPE, PBAT, and PPeAT60 and b) PPeAT60, PPeAT60+0.1% HTeO and PPeAT60+0.5% Gly.*

***Table 7**: Crystallinity properties for LLDPE, PBAT, PPeAT60, PPeAT60+0.5% Gly and PPeAT60+0.1% HTeO.*

Sample	WAXS	SAXS		
	χ_c	q_{max}	d-Spacing	Lamellar thickness
	%	$Å^{-1}$	Å	Å
LLDPE	50.4	0.039	160	80.8
PBAT	19.4	0.051	124	24.1
PPeAT60	18.5	0.061	102	18.9
PPeAT60 + 0.5% Gly	15.7	0.060	105	16.5
PPeAT60 + 0.1% HTeO	18.4	0.069	91	16.9

Lamellar thickness was obtained by multiplying the fractional crystallinity by the d-Spacing. As mentioned earlier, adding branch points adds crystal defects which in turn causes the lamellar thickness for the samples with added multifunctional alcohol to be lower. For LLDPE,

the d-spacing and lamellar thickness were calculated to be 160 Å and 80.8 Å, respectively which are in agreement with the literature [138].

4.2.3. Mechanical Properties

Figure (20) shows stress strain curves for LLDPE, PBAT and the PPeAT60 copolyesters. Young's modulus (E), yield stress (δ_y), yield strain (ε_y), stress at break (δ_b), elongation at break (ε_b) and tensile toughness (U_t) are presented in Table (8). PBAT exhibits ductile behavior with values of E, δ_y, ε_y, δ_b and ε_b in agreement with literature results [110]. For PPeAT60, the stress at break, elongation at break and tensile toughness are similar to PBAT. However, the diol swap from butanediol to pentanediol led to a doubling of E of PPeAT60 to 138 MPa with an elongation at break and tensile toughness decreasing only slightly.

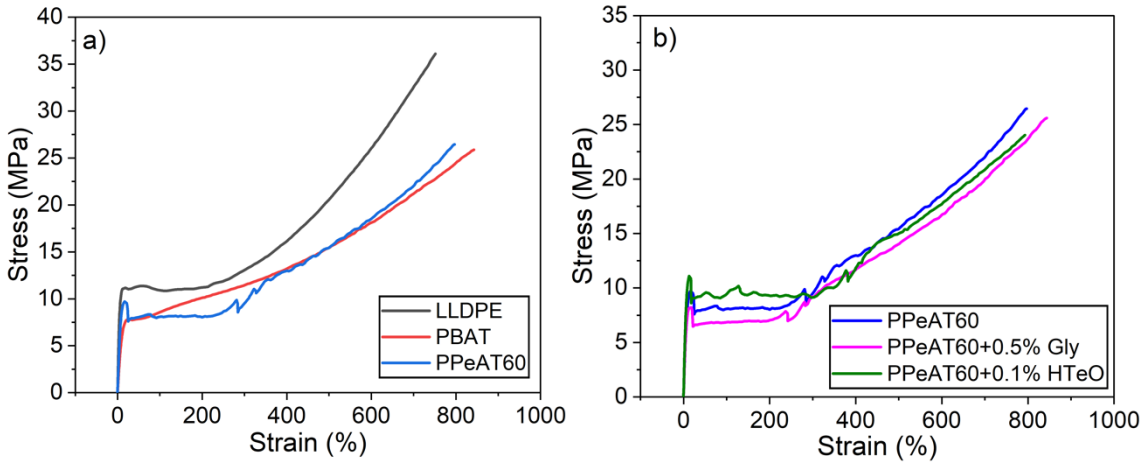

***Figure 20**: Stress-strain curves for a) LLDPE, PBAT, and PPeAT60 and b) PPeAT60, PPeAT60+0.1% HTeO and PPeAT60+0.5% Gly*

The larger lamellar thickness for PBAT is likely the source of this difference; given the same fractional crystallinity PBAT will have a lower density of stiff crystalline regions that can reinforce the polymer. Another possibility is that the rigid amorphous fraction (RAF) for the PPeAT60 was larger; we did not try to isolate the RAF in DSC measurements. The addition of branching agents to PPeAT60 led to a decrease in stress and elongation at break with PPeAT60 +

0.1% HTeO exhibiting a more significant decrease than PPeAT60 + 0.5% Gly. However, Young's modulus increased upon the addition of HTeO to PPeAT60 by ~20% due likely due to more efficient crosslinking. Furthermore, the reduced stress and elongation at break resulted in a lower tensile toughness for branched polyesters compared to non-branched PPeAT60. For the sake of completeness, the mechanical properties of were measured and reported in Table (8). The values for LLDPE were in approximate agreement with literature values [106].

***Table 8**: Mechanical properties for LLDPE, PBAT, PPeAT60, PPeAT60+0.5% Gly and PPeAT60+0.1% HTeO.*

Sample	E	δ_y	ε_y	δ_b	ε_b	U_t
	MPa	MPa	%	MPa	%	MJ/m^3
LLDPE	251 ± 46	12 ± 0.6	49 ± 14	29 ± 6	637 ± 110	105 ± 25
PBAT	78 ± 10	-	-	26 ± 3	815 ± 67	127 ± 19
PPeAT60	138 ± 5	10 ± 0.5	16 ± 2	27 ± 2	784 ± 22	113 ± 9
PPeAT60 + 0.5% Gly	137 ± 14	9 ± 1.2	15 ± 2	23 ± 4	748 ± 107	98 ± 21
PPeAT60 + 0.1% HTeO	165 ± 18	11 ± 0.9	13 ± 1	21 ± 3	711 ± 93	92 ± 17

4.2.4. Rheological Properties

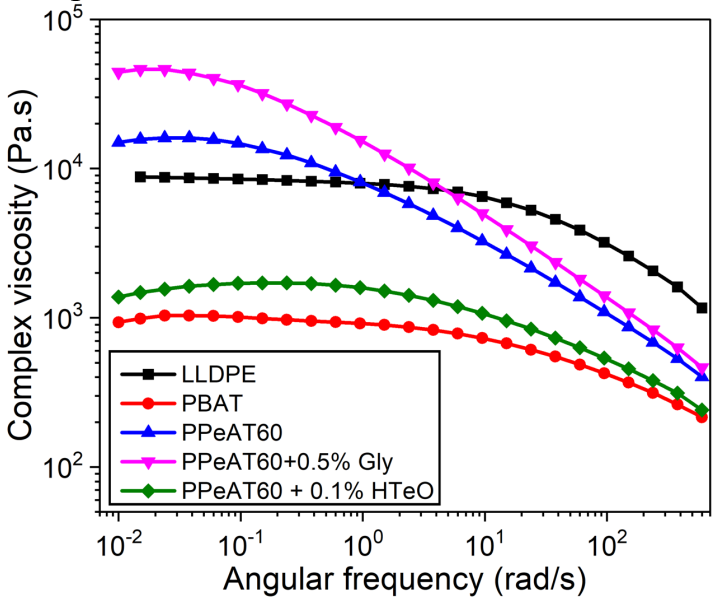

***Figure 21**: Complex viscosity results for LLDPE, PBAT, PPeAT60, PPeAT60+0.1% HTeO and PPeAT60+0.5% Gly*

Complex shear viscosities were studied using 25mm parallel plates at 190°C and are shown in Figure (21). All copolyesters and LLDPE exhibit shear-thinning behavior at high frequency and a Newtonian plateau at low frequencies. At high frequencies, all copolyesters had a similar complex viscosity which was lower than LLDPE at the same frequency. The shear rate in the extruder during film blowing is around 45 s^{-1} [124]. Since the shear viscosity result as a function of shear rate is equivalent to the complex viscosity result as a function of angular frequency hence, if Cox-Merz applies to these polymers as seen in Figure (S6). Therefore, the energy needed to extrude the copolyesters is much lower than the energy needed to extrude LLDPE. The addition of branching agents led to an increase in complex viscosity at low frequencies compared to PPeAT60 synthesized without branching agent. The zero-shear viscosity mainly depends on temperature, the average molecular weight and the additives used. The addition of Gly caused an increase in the zero-shear viscosity by about a factor of compared to PPeAT60 synthesized without branching agent. The complex viscosity curve was lower for PPeAT60 + 0.1% HTeO than PPeAT60 and PPeAT60 + 0.5% Gly likely due to the lower molecular weight of PPeAT60 + 0.1% HTeO.

Complex viscosities were modeled using the five-parameter Carreau-Yasuda model shown in equation (23), the results of which are reported in Table (9).

$$\frac{\eta(\omega) - \eta_\infty}{\eta_0 - \eta_\infty} = [1 + (\omega\lambda)^a]^{\frac{n-1}{a}} \tag{23}$$

η_∞ is the infinite shear viscosity in (Pa.s), η_0 is the zero-shear viscosity in (Pa.s), ω is the angular frequency in (rad/s), λ is the characteristic relaxation time in (s), a is the transition parameter and n is the flow index in Carreau-Yasuda model. For polymer melts, the infinite shear viscosity (η_∞) is zero. This model was chosen because it can accurately predict both the Newtonian plateau and

the shear thinning behavior. Fitted data show good agreement with the experimental results. The addition of Gly to PPeAT60 led to a decrease in the flow index and increase in the characteristic relaxation time which is evidence of a decrease in the shear thinning behavior and a narrower Newtonian plateau region, respectively. However, the branching agent did not affect the transition parameter. A decrease in flow index and increase in relaxation time due to branching has been reported in the literature [139, 140].

***Table 9**: Rheological properties for LLDPE, PBAT, PPeAT60, PPeAT60+0.5% Gly and PPeAT60+0.1% HTeO.*

Samples	**Shear viscosity**				**Elongational viscosity at Hencky strain of 2.5 and 0.3 s^{-1}**
	η_o	n	a	λ	η_E
	Pa.s	-	-	s	Pa.s
LLDPE	8711	0.12	0.62	0.01	47,000
PBAT	1006	0.67	0.76	0.12	350,000
PPeAT60	15873	0.59	1.54	5.21	562,000
PPeAT60 + 0.5% Gly	46628	0.53	1.54	11.42	350,000
PPeAT60 + 0.1% HTeO	1620	0.68	1.68	0.37	78,000

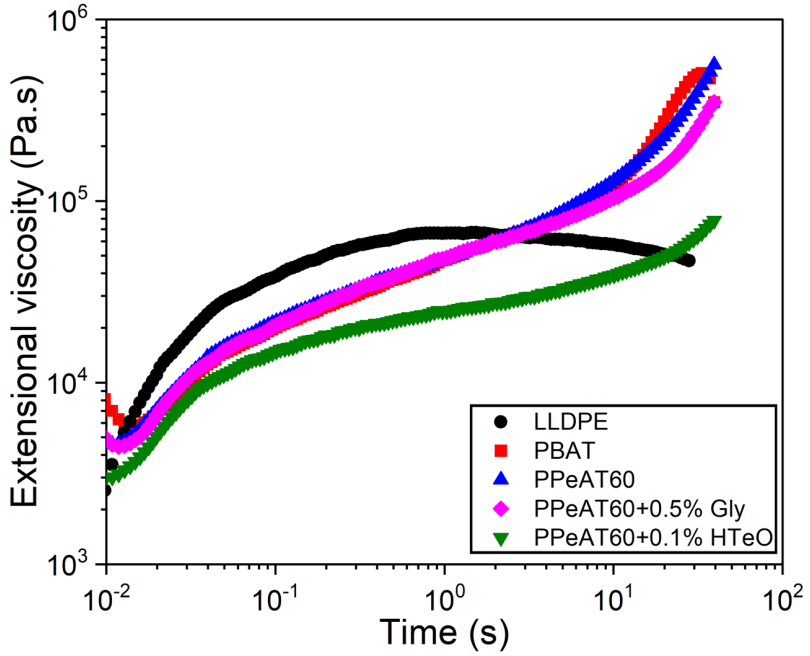

***Figure 22**: Elongational viscosity results for LLDPE, PBAT, PPeAT60, PPeAT60+0.1% HTeO and PPeAT60+0.5% Gly*

The time-dependent elongational viscosities of LLDPE and copolyesters at 130°C and 0.3 s^{-1} are plotted in Figure (22). A lower temperature was used relative to the temperature used for shear viscosity because sagging of the sample occurs at high temperature. Also, as noted previously, a Hencky strain of 2.5 at an elongational rate of 0.3 s^{-1} were found to be representative values for film blowing [124] and these values are found in Table 9. A high elongational viscosity is an indication of a high melt strength and hence a more stable bubble during film blowing. The addition of branching agents led to a decrease in the elongation viscosity at a given Hencky strain and elongational rate. Strain hardening is described as the rise in elongation flow above the linear viscoelastic curve [141]. All copolyesters exhibit strain hardening while LLDPE show no strain hardening due to the narrow molecular weight distribution and no long-chain branches. Micic et al. reported that strain hardening is correlated with better bubble stability in film blowing [142]. Therefore, the absence of strain hardening in LLDPE is one of the main reasons for the instability of the bubble [143]. Although strain hardening is a characteristic of long-chain branches, the strain hardening of the copolyesters may be due to some of the longest chains remaining stretched before sample failure [141]. Strain hardening behavior shown by the copolyesters is a good indication for stable bubbles during film blowing.

4.3. Conclusions

Direct esterification and polycondensation were used to synthesize a high molecular weight poly (pentylene adipate-co-terephthalate) with a 40/60 adipic acid/terephthalic acid mole percent (PPeAT60). As branching agents, Gly and HTeO with three and four hydroxyl groups, respectively, were used. The weight-average and number-average molecular weight of all copolyesters were above 140,000 g/mol and 85,000 g/mol respectively. PPeAT60 has a lower T_m

and higher T_g than a commercial PBAT, which is likely to be a result of the odd-even effect of B vs Pe; the odd-even effect is also likely the cause of a very slow rate of crystallization for PPeAT60 relative to PBAT. Importantly, PPeAT60 has a Young's modulus that is almost double that vs PBAT, with only small decreases in elongation at break. Changes in modulus were likely a result of the odd-even effect. The tensile strength and elongation at break slightly decreased for the branched polyesters while the Young's modulus increased which could be due to the decrease in the flexibility of the structure since the crystallinities were actually slightly lower for the branched structures. SAXS showed that the addition of branching agents led to a slight reduction in d-spacing and lamellar thickness. All copolyesters exhibit shear-thinning behavior at high frequencies and a Newtonian plateau at low frequencies. The addition of Gly increased the zero-shear viscosity of the copolyesters. Elongational viscosity on the other hand decreased upon the addition of branching agents. Therefore, PPeAT60 copolyesters could be a viable candidate for film blowing if the crystallization rate can be increased.

Chapter 5: Impact of Nucleating Agents on the Crystallization Behavior of Polyesters **

5.1. Abstract

Various Li, Mg and Na-neutralized ethylene-methacrylic acid copolymer ionomers and an un-neutralized ethylene-methacrylic acid copolymer were used as nucleating agents for PPeAT. The mixtures were tested for isothermal and non-isothermal crystallization in a differential scanning calorimeter. Neat PPeAT showed a minimum crystallization half-time of 28 minutes at 40°C. The addition of 0.05 wt% nucleating agents led to a decrease in crystallization half-time at 40°C to an average of 2.3, 2.4, 1.9 and 0.7 minutes for Li, Mg, and Na-neutralized ionomers and the unneutralized acid copolymer respectively. The only difference found in nucleating ability was for cation type, e.g. resin molecular weight and neutralization level for a given cation showed no difference in nucleation ability. Further investigations with the Na ionomer showed that a minimum in crystallization half-time of 0.6 minutes at 40°C was found at 0.5 wt% ionomer content; an increase in the acid copolymer to 0.5 wt% caused a slight increase in crystallization half-time to 0.76 minutes. Fully crystallized PPeAT without added ionomer nucleating agent had statistically significantly higher elongation at break and nearly double the tensile strength than fully crystallized PPeAT with 0.05 wt% ionomer nucleating agent; the former did have ~20% higher fractional crystallinity. Moduli for the ionomer nucleated PPeATs were about 15% higher than the unnucleated PPeAT. With 0.5 wt% nucleating agent however, mechanical property and crystallinity values were about the same as for unnucleated PPeAT. This reduction in crystallization half-time allows PPeAT to possibly be a viable biobased biodegradable alternative to linear low-density polyethylene for flexible film packaging applications.

** *Being prepared for publication.*

5.2. Results and Discussion

Ionomer samples were grouped by neutralizing ion type; the results for each sample are also shown in Table (S1). For unnucleated PPeAT and PPEAT nucleated with the acid copolymer, five different samples cut from the same material were measured. Inspection of Table (10) shows that the relative error obtained with different ionomers having a single cation was similar to the relative error obtained from a single sample run five consecutive times; Table (11) and Table (12) shows the same, but for the absolute error.

5.2.1. Isothermal Study

***Table 10**: Half-time crystallization and Avrami model parameters for different ionomers added at 0.05 wt%.*

Sample	**$t_{1/2}$**	**k**	**n**
	min	min^{-n}	-
Neat PPeAT	31.5 ± 2.2	$3.7 \pm 0.6 * 10^{-6}$	3.53 ± 0.1
PPeAT + Acid	0.62 ± 0.03	2.34 ± 0.1	2.54 ± 0.2
PPeAT + Li	2.3 ± 0.2	0.08 ± 0.02	2.74 ± 0.1
PPeAT + Na	1.9 ± 0.2	0.12 ± 0.03	2.77 ± 0.2
PPeAT + Mg	2.4 ± 0.1	0.06 ± 0.02	2.84 ± 0.2

For the first part of the study, a constant weight percent of each ionomer or acid copolymer was used to study the effect of different ionomers on the crystallization kinetics. Lower levels were chosen to show more differences; 0.05 wt% addition was chosen because this value represents the minimum amount we could accurately mix with one pass in the extruder. Relative crystallinity X_t was derived by integrating the exothermal isothermal crystallization curve during the crystallization process and then normalizing it using Equation (24).

$$X_t = \frac{\int_0^t \left(\frac{dH_c}{dt}\right) dt}{\int_0^\infty \left(\frac{dH_c}{dt}\right) dt} \times 100\% \tag{24}$$

According to Student's t-test (Table S3) and Figure (24), PPeAT nucleated with the acid copolymer has a significantly faster crystallization rate compared with the PPeAT nucleated with ionomer. For ionomer-based mixtures, PPeAT nucleated with Na ionomer has a faster crystallization rate than the other two ionomer nucleating agents, while the PPeAT nucleated with Mg ionomer has statistically the same crystallization rate as PPeAT nucleated with Li ionomer. The effect of neutralizing cation on nucleation of polyesters using ionomers has been noticed previously; PET nucleated with Na E-AA ionomers have faster crystallization rates vs. those nucleated with Zn E-AA ionomers [144].

The Avrami model was employed to better understand the isothermal crystallization process. The Avrami model is used to acquire numerical parameters for the crystallization kinetics. The model describes the relative crystallinity (X_t) in terms of time at a constant temperature as shown in Equation (25) and the linear form of the equation in Equation (26):

$$X_t = 1 - \exp(-kt^n) \tag{25}$$

$$\ln[-\ln(1 - X_t)] = \ln(k) + nln(t) \tag{26}$$

The half-time for 100% relative crystallization ($t_{1/2}$) was calculated using Equation (27):

$$t_{\frac{1}{2}} = \left(\frac{\ln 2}{k}\right)^{\frac{1}{n}} \tag{27}$$

k is the rate constant for crystallization which is a function of nucleation and growth rates, and n is the Avrami exponent. The results for the Avrami model parameters are reported in Table (10) and Avrami model plots are shown in Figure (25). The experimental data and the Avrami model fit agree hence secondary crystallization is insignificant. The half-time for 100% relative crystallization ($t_{1/2}$) for neat PPeAT and nucleated PPeAT are also reported in Table (10). Error bars in this table and all subsequent error bars represent one standard deviation calculated from the

different ionomers for a given cation. For the PPeAT nucleated with acid copolymer and the neat PPeAT, variability was calculated using 5 different samples cut from the same polymer sample.

PPeAT + Acid has about a 2 order of magnitude increase in Avrami constant and about 3 times shorter $t_{1/2}$ compared with the PPeAT + ionomer. For all nucleated PPeAT, the Avrami exponent falls in between 2.7 and 2.8. Therefore, according to the Avrami exponent, the growth geometry is a combination of crystal growth and disk-like growth geometry with the geometry being closer to crystal growth geometry. The efficacy of the acid copolymer and ionomer as a nucleating agent are substantial; the rate constant crystallization (k) for nucleated PPeAT increased by 3 and 5 orders of magnitude compared to the k of neat PPeAT, while the half-time for crystallization dropped by nearly 1.5 and 2 orders of magnitude for ionomers and acid copolymer.

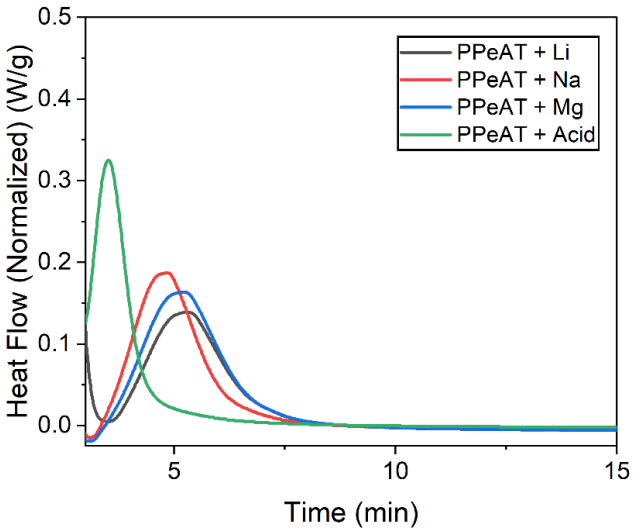

***Figure 23**: Representative isothermal crystallization results for different ionomers and the acid with same starting MW. For the ionomers, samples represent ~the same neutralization level.*

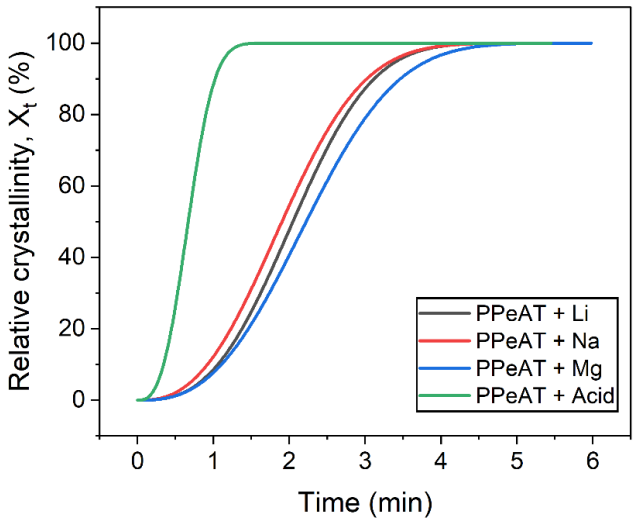

***Figure 24**: Change in relative crystallization (X_t) with respect to time for different ionomers for ionomers corresponding to Figure 2.*

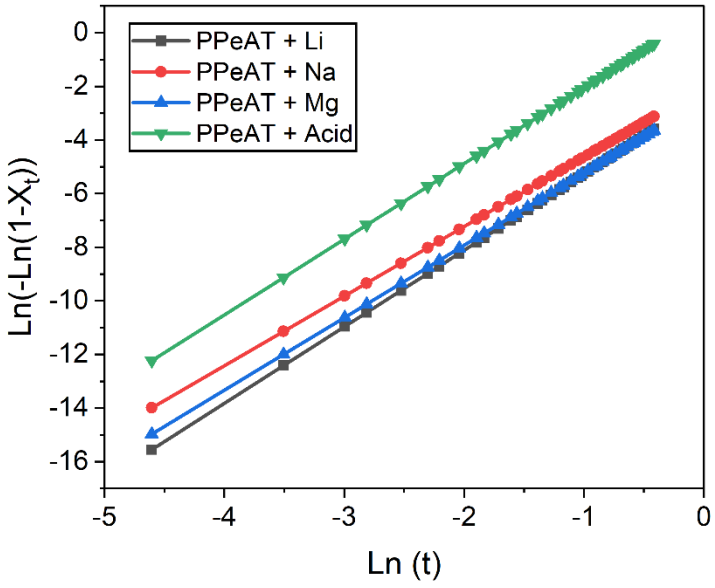

***Figure 25**: Avrami model results for acid and different ionomers for ionomers corresponding to Figure 2.*

5.2.2. Non-Isothermal Study

***Table 11**: Non-isothermal crystallization results for different ionomers (0.05 wt% addition except where noted).*

Sample	T_g	T_c	ΔH_C	$T_{m,1}$	$\Delta H_{m,1}$	$T_{m,2}$
	°C	°C	J/g	°C	J/g	°C
Neat PPeAT	-6.6 ± 0.6	-	-	101 ± 0.4	32.4 ± 1.4	-
PPeAT + Acid	-12.9 ± 0.2	51.7 ± 0.1	18.8 ± 0.2	96.0 ± 0.6	30.3 ± 0.8	97.7 ± 0.2
PPeAT + Li	-15.8 ± 0.4	32.3 ± 2.2	14.2 ± 1.8	90.6 ± 0.9	26.5 ± 1.9	91.3 ± 0.4
PPeAT + Na	-16.1 ± 0.7	33.8 ± 2.7	13.2 ± 2.8	90.3 ± 1.0	27.0 ± 1.2	91.2 ± 0.2
PPeAT + Mg	-16.1 ± 0.3	33.8 ± 0.9	14.4 ± 1.2	90.1 ± 0.9	26.8 ± 0.6	91.3 ± 0.8
PPeAT + 0.5 wt% Acid	-12.8 ± 0.3	50.0 ± 0.2	17.0 ± 0.2	96.3 ± 0.5	27.8 ± 0.6	97.8 ± 0.3
PPeAT + 0.5 wt% Na	-12.3 ± 0.1	44.6 ± 0.2	16.8 ± 0.4	97.2 ± 0.1	31.6 ± 0.4	97.0 ± 0.5

DSC curves for the first heating cycle, cooling cycle, and second heating cycle for neat PPeAT and nucleated PPeAT are shown in Figure (26), Figure (27), and Figure (28), respectively. The first heating cycle, which represents the result after many days of aging at room temperature and is believed to represent ~complete crystallization for all samples, shows a clear endothermic peak for all samples due to melting of the copolyesters. Not surprisingly, the melting temperature is significantly higher for the unnucleated sample indicating thicker crystals. The fractional crystallinity of the unnucleated sample is also significantly higher. As expected for the first cooling cycle, neat PPeAT does not show an exothermic crystallization peak due to slow crystallization. The addition of ionomers or acid copolymer as a nucleating agent led to the appearance of an exothermic crystallization peak for all nucleated PPeAT as shown in Figure (27). Subsequently, an endothermic melting peak can be seen for the second heating cycle for all the nucleated PPeAT while for the neat PPeAT, the endothermic peak is absent. The non-isothermal crystallization

temperature (T_c), second heating cycle glass transition temperature (T_g), first heating cycle enthalpy of melting ($\Delta H_{m,1}$), enthalpy of crystallization (ΔH_c), first heating cycle melting temperature ($T_{m,1}$), and second heating cycle melting temperature ($T_{m,2}$) are summarized in Table (11). The addition of acid copolymer or ionomers led to a drop in $T_{m,1}$, $\Delta H_{m,1}$ and $T_{g.}$ vs the neat PPeAT, which are all statistically significant differences according to the Student's t-test (Table S2). Thinner crystals with nucleated samples leading to a smaller melting temperature is expected; however, we have no explanation for the lower $\Delta H_{m,1}$ and hence lower crystallinity for the samples with 0.05 wt% nucleating agent. Since T_g was determined on the reheat immediately after cooling at 10°C/min causing the neat sample to show no crystallites, higher T_g for the unnucleated samples was expected since the aromatic content in the amorphous phase was higher for the neat sample. Ionomer PPeAT nucleated have statistically significant lower T_c, T_g, ΔH_c, $T_{m,1,}$ $\Delta H_{m,1}$ and $T_{m,2}$

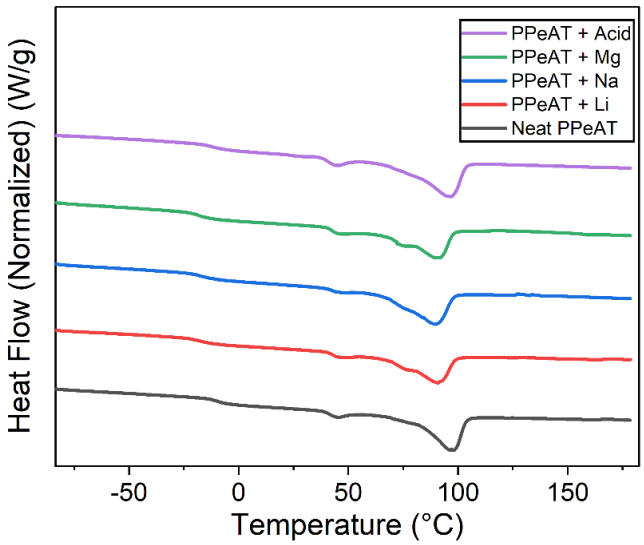

***Figure 26**: Representative DSC 1st heating cycle curves for the PPeATs for different ionomers and acid for ionomers and acid corresponding to Figure 2. Results have been shifted vertically for clarity.*

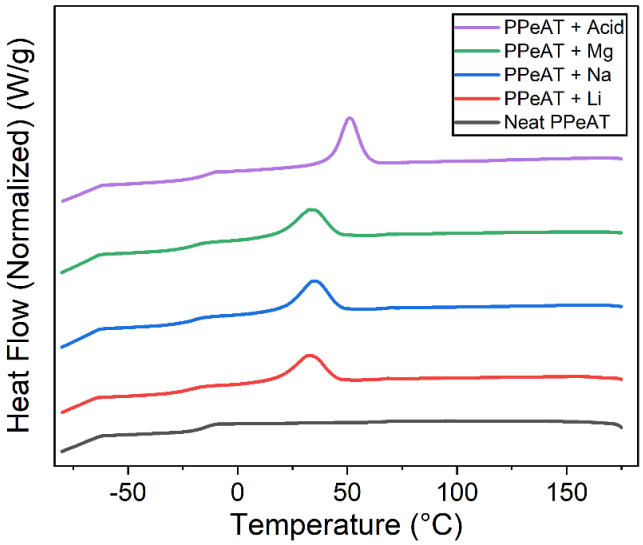

***Figure 27**: Representative DSC cooling curves for the non-isothermal crystallization for different ionomers and acid for ionomers and acid corresponding to Figure 2. Results have been shifted vertically for clarity.*

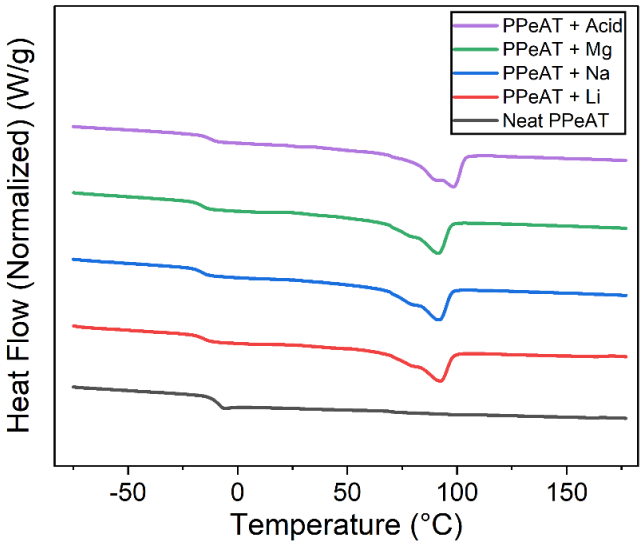

***Figure 28**: DSC curves for the 2nd heating cycle for different ionomer for ionomers corresponding to Figure 2. Results have been shifted vertically for clarity.*

compared to acid nucleated PPeAT (Table S2). The reason for these differences is not clear. Cation type did not lead statistically significant differences in T_c, T_g, ΔH_c, $T_{m,1}$, $\Delta H_{m,1}$ or $T_{m,2}$ for the PPeAT with added ionomer. The faster crystallization rate found in isothermal studies for PPeAT

with added Na ionomer should have translated to a higher Tc as well; perhaps the difference was not enough to be outside statistical error for the number of samples that were run. Different metallic salts of phenylmalonic acid were used to successfully nucleate PLA; T_c, ΔH_c, $T_{m,1}$, $\Delta H_{m,1}$ or $T_{m,2}$ results for Na, Li, Mg salts were similar as well [145].

5.2.3. Different ionomer concentration

Because Na ionomer was the most effective at nucleating crystallinity for the ionomers, Na ionomer with 78.4% neutralization and melt index of 1.26 was mixed in with PPeAT at different weight percentages to study the effect of different ionomer concentrations on the crystallization kinetics. Isothermal crystallization kinetics of the different nucleated PPeAT are shown in Figure (30).

***Table 12**: Half-time crystallization and Avrami model parameters for different blend compositions.*

Sample	$t_{1/2}$	k	n
	min	min^{-n}	-
PPeAT + 0.05 wt%	1.9	0.12	2.77
PPeAT + 0.1 wt%	0.96	0.76	2.46
PPeAT + 0.3 wt%	0.73	1.50	2.45
PPeAT + 0.5 wt%	0.57	3.15	2.75
PPeAT + 1 wt%	0.70	1.87	2.85
PPeAT + 2.5 wt%	0.79	1.36	2.72

Because Na ionomer was the most effective at nucleating crystallinity for the ionomers, Na ionomer with 78.4% neutralization and melt index of 1.26 was mixed in with PPeAT at different weight percentages to study the effect of different ionomer concentrations on the crystallization kinetics. Isothermal crystallization kinetics of the different nucleated PPeAT are shown in Figure (29). A maximum crystallization rate was obtained at 0.5 wt%. The results for the Avrami model parameters obtained from Equation (26) and $t_{1/2}$ for nucleated polyesters obtained from Equation

(27) are reported in Table (12). Again, the experimental data and the Avrami model fit agreed hence secondary crystallization is insignificant and the Avrami exponent falls in between 2.7 and 2.9. Using 0.5 wt% instead of 0.05 wt% acid copolymer led to the decrease in the crystallization rate and Avrami's constant to 1.43 min^{-n} and 2.63 respectively and an increase in $t_{1/2}$ to 0.76 min. Obviously, the maximum crystallization rate occurred at a lower amount than 0.5 wt% for the acid copolymer.

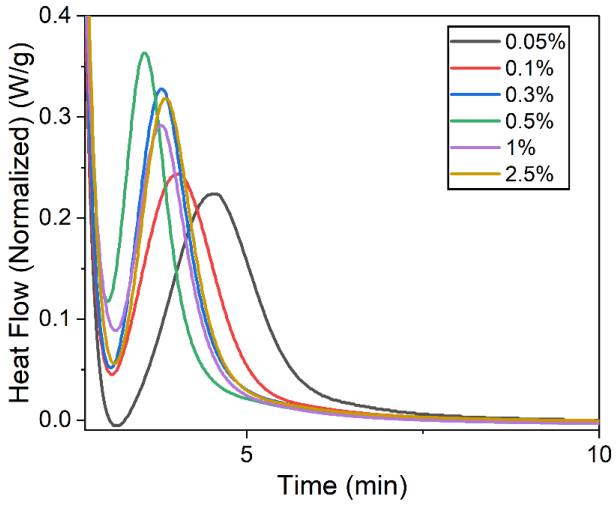

***Figure 29**: Isothermal Crystallization and Avrami model results for different Na ionomer concentrations.*

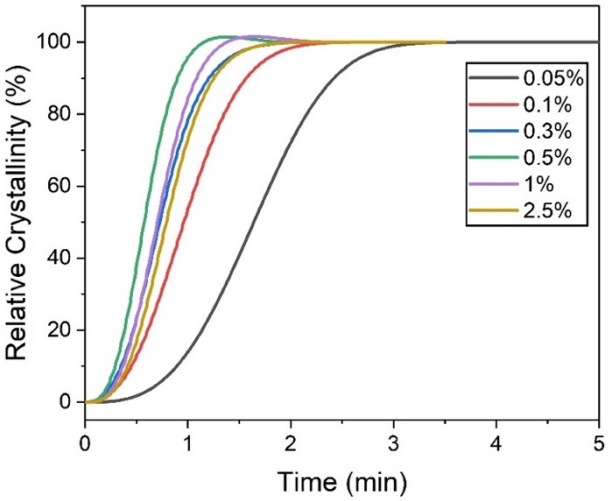

***Figure 30**: Change in relative crystallization (X_t) with respect to time for different Na ionomer concentrations.*

5.2.4. Mechanical properties

Young's modulus (E), yield stress (δ_y), yield strain (ε_y), stress at break (δ_b), elongation at break (ε_b) and tensile toughness (U_t) for neat PPeAT and 0.05 wt% ionomer nucleated PPeAT are presented in Table (13). We did not have enough PPeAT for mechanical property tests for acid nucleated samples. As with samples that yielded $\Delta H_{m,1}$ and $T_{m,1}$, these samples were aged for many days at room temperature prior to measurement and should represent the properties when crystallization was ~complete. The addition of 0.05 wt% ionomer led to a statistically significant increase in E and a statistically significant decrease in δ_b and ε_b. Smaller, more numerous crystallites for the nucleated samples should yield a higher E while the higher fractional crystallinity of the non-nucleated samples apparently corresponds to a higher stress and elongation at break. According to the Student's t-test in Table (S4), there is no statistical difference between nucleated samples for E, δ_y, ε_y, δ_b and U_t. However, for the sample nucleated with 0.5 wt% Na ionomer, the modulus, stress at break and elongation at break recovered to neat PPeAT according to Student's t-test in Table S5. This result is consistent with $\Delta H_{m,1}$ data in Table (12).

***Table 13**: Mechanical Properties for different ionomers (Ionomer concentration is 0.05 wt% addition except where noted)*

Sample	**E**	**δ_y**	**ε_y**	**δ_b**	**ε_b**	**U_t**
	MPa	MPa	%	MPa	%	MJ/m^3
Neat PPeAT	138 ± 5	10 ± 0.5	16 ± 2	27 ± 2	784 ± 22	113 ± 9
PPeAT + Li	160 ± 12	11 ± 0.5	14 ± 1	15 ± 2	654 ± 66	75 ± 12
PPeAT + Na	168 ± 13	12 ± 1.2	14 ± 3	15 ± 2	557 ± 76	71 ± 13
PPeAT + Mg	159 ± 9	11 ± 0.8	13 ± 2	16 ±23	626 ± 114	70 ± 14
PPeAT + 0.5 wt% Na	148 ± 8	11.5 ± 0.4	18 ± 2	29 ± 2	780 ± 26	119 ± 17

5.2.5. Rheological properties

The effect of Na ionomer on the shear storage modulus (G′) and the shear loss modulus (G″) studied using 25mm parallel plates at 190°C are shown in Figure (31) and Figure (32). The complex viscosity is shown in Figure (S6). The addition of 0.5 wt% Na ionomer to PPeAT didn't affect G′ and G″ at high angular frequency. However, at low angular frequency PPeAT + 0.5 wt% Na ionomer has lower G′ and G″ than PPeAT. A similar trend can be observed for polypropylene upon the addition of dibenzylidene sorbitol and N_1, N_1′-(propane-1,3-diyl) bis (N_2-hexyloxalamide) as nucleators [146, 147]. The shear rate in the extruder during film blowing is around 45 s^{-1} [96], hence, assuming Cox-Merz applies to these polyesters, then the addition of nucleating agent should not affect the melt viscosity during the film blowing process.

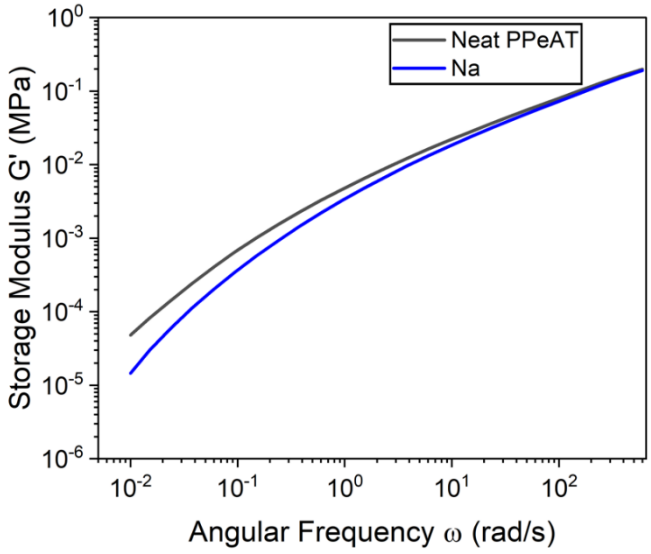

***Figure 31**: Storage modulus results for neat PPeAT and PPeAT+0.5 wt% Na ionomer*

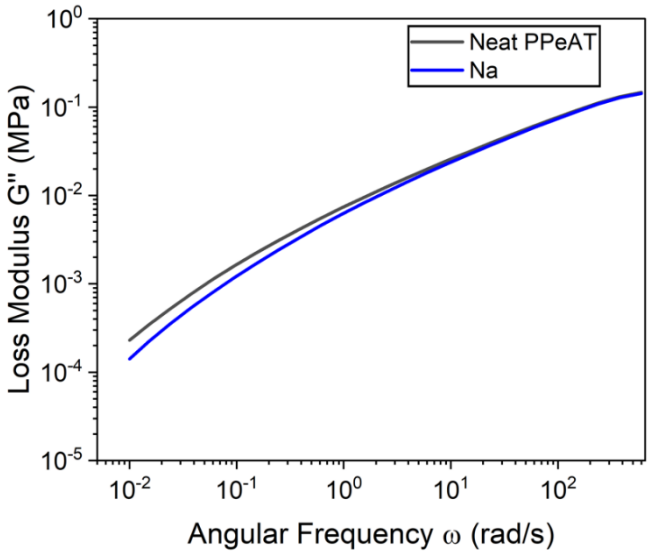

***Figure 32**: Loss modulus results for neat PPeAT and PPeAT+0.5 wt% Na*

5.3. Conclusions

Different Li, Mg, and Na E-MAA ionomers or E-MAA acid copolymer were melt-mixed with PPeAT to increase the crystallization rate. The addition of ionomers and acid copolymer led to a ~1.5 and 2 order-of-magnitude decrease in half-time crystallization and a ~three and five-order-of-magnitude increase in the Avrami rate constant, respectively. Also, the acid copolymer was the most efficient nucleator in that smaller amounts were required to achieve this crystallization rate improvement. We cannot explain why differences in nucleation efficiency occur between the different nucleating agents. Increasing the ionomer concentration from 0.05 wt% to 0.5 wt% led to an additional half-order of magnitude decrease in the crystallization half-time and an additional 1.5 order of magnitude increase in the Avrami rate constant; further increases caused a slowing of crystallization. The addition of ionomers and acid copolymer at 0.05 wt% led to a decrease in melting temperature for materials and reduction of crystalline fraction under conditions where crystallization was presumably complete. At 0.5 wt%, these values were statistically equal to the non-nucleated samples. 0.05 wt% ionomer nucleating agents cause an

increase in Young's modulus, a decrease in the elongation at break and a decrease in the tensile strength; again, these differences disappear with 0.5 wt% ionomer nucleating agent. The addition of 0.5 wt% Na ionomer doesn't affect the viscosity at high angular frequency, with only slight changes at lower frequencies.

Chapter 6: The effect of different processing conditions on the properties of polyesters ***

6.1. Abstract

Film blowing has been widely used to produce flexible films. Poly (pentylene adipate-co-terephthalate) (PPeAT), polybutylene adipate terephthalate (PBAT) and linear low-density polyethylene (LLDPE) films were prepared using film blowing. Machine direction (MD) and transverse direction (TD) properties of the films were compared to the properties compression molded (CM) sheets. PBAT and PPeAT films show a higher storage modulus compared to CM sheets. Wide-angle and small-angle x-ray scattering show that CM sheets have higher percent crystallinity, longer d-spacing and thicker lamellar thickness compared with blown films for LLDPE, PBAT and PPeAT. For the blown films, SAXS measurements have more intensity in the MD vs. the TD while the d-spacing is slightly higher for the TD direction consistent with the WAXS results indicating higher percent crystallinity in the TD. CM sheets exhibit a lower oxygen permeability, carbon dioxide permeability and water vapor transmission rates compared with blown films. PPeAT showed lower carbon dioxide permeability compared with PBAT and LLDPE and lower water vapor transmission rate than PBAT. Film blown PPeAT showed promising results and eventually could be used as a drop-in replacement for LLDE in flexible film packaging.

*** *Being prepared for publication.*

6.2. Results and Discussion

The number average molecular weight, weight average molecular weight and polydispersity index for PPeAT were 69,900 g/mol, 219,000 g/mol and 3.13, respectively. The rheological curves for PPeAT of this work are a bit lower than the rheological curves obtained for PPeAT from chapter (5) due to the reduction in number average molecular weight.

6.2.1. Wide Angle X-ray Scattering (WAXS)

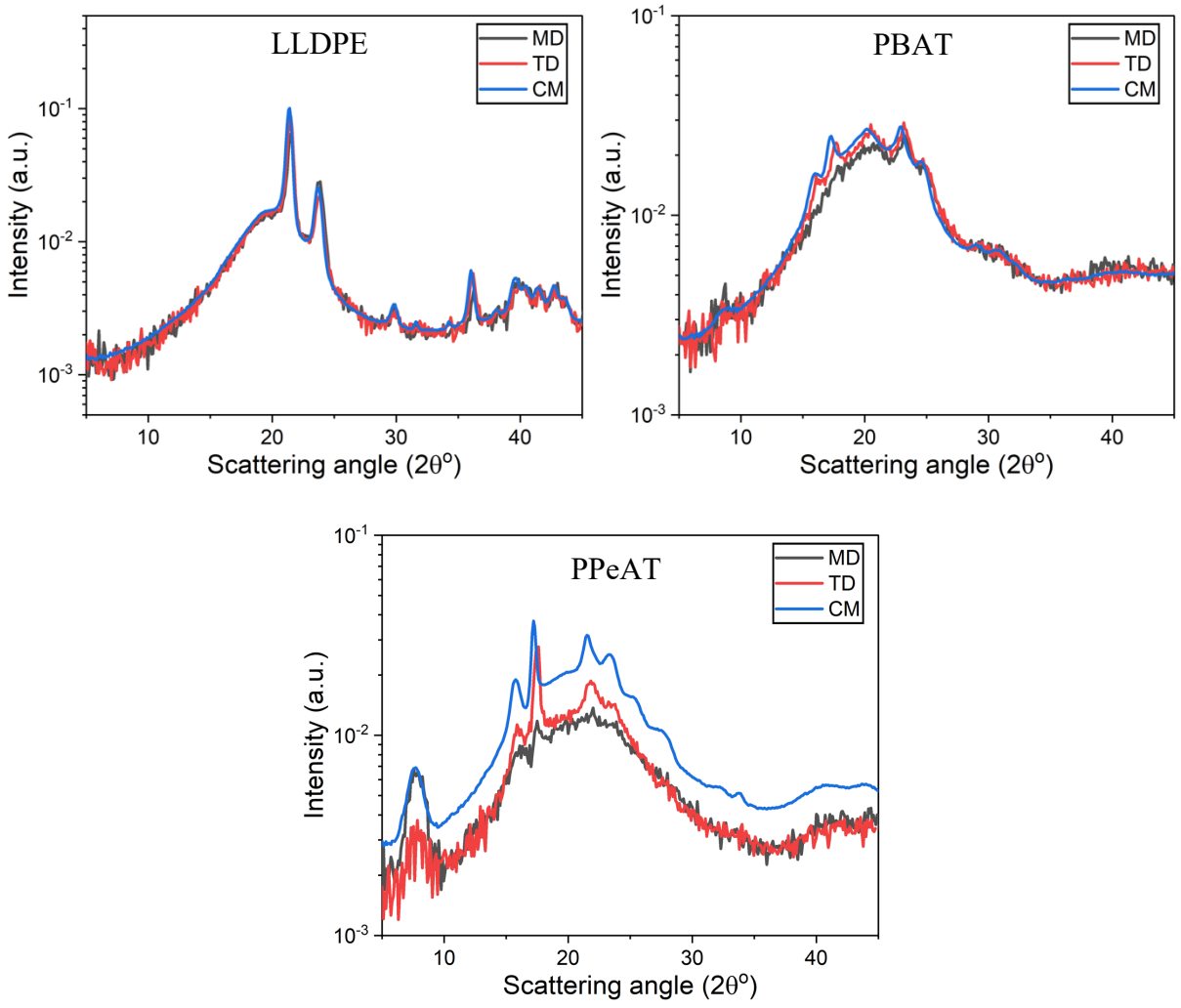

Figure 33:Wide angle x-ray scattering results for LLDPE, PBAT and PPeAT CM sheets and blown films.

Figure (33) shows the WAXS spectra of the CM sheets, MD and TD films of LLDPE, PBAT and PPeAT, while Table (14) reports the percent crystallinity values for these polymers. The film preparation technique didn't affect the peaks' location. CM sheets show higher percent crystallinity than both the MD and TD blown films. Mejia et al. reported that compression molded films have higher percent crystallinity than injected molded films [148]. Moreover, Hedesiu et al. reported that when the films are cooled gradually, the polymer's molecular chains will have the opportunity to arrange into a more structured form, resulting in increased crystallinity [149]. The absolute scattering intensity of CM sheets cannot be compared to the other two films. TD blown films were shown to have a higher percent crystallinity than MD blown films. A possible explanation for the latter could be that in the machine direction, the polymer melt is stretched as the film is drawn upwards. This stretching aligns the polymer chains along the TD, promoting better chain packing and allowing the molecular chains to crystallize more easily, resulting in a higher degree of crystallinity. The reflection at ~17° in both PBAT and PPeAT shows a clear difference in intensity between MD and TD. Because the angle between this peak and the chain direction/normal to the lamellae plane is not known, more quantitation is not possible. PPeAT films have a lower percent crystallinity compared to PBAT films, consistent with results obtained from the CM sheets presented here as well as results on CM sheets presented previously using a different batch of PPeAT [129].

Table 14: Crystallinity properties of LLDPE, PBAT and PPeAT CM sheets and blown films.

Samples		WAXS	SAXS			
		X_c	q_{max}	d-spacing	Lamellar thickness	$\langle \cos^2 \phi \rangle$
		%	$Å^{-1}$	Å	Å	–
LLDPE	**CM**	41.8	0.034	183.86	76.80	0.33
	MD	36.8	0.040	155.96	57.33	0.35
	TD	38.2	0.038	165.07	63.07	0.30
PBAT	**CM**	18.6	0.052	120.93	22.45	0.33
	MD	11.7	0.057	110.31	12.93	0.40
	TD	14.3	0.058	109.25	15.66	0.27
PPeAT	**CM**	16.0	0.063	99.62	15.91	0.33
	MD	5.9	0.076	82.84	4.85	0.45
	TD	14.7	0.080	78.80	11.58	0.21

6.2.2. Small Angle X-ray Scattering (SAXS)

Figure (34) and Table (14) show SAXS results for CM sheets, MD and TD films of LLDPE, PBAT and PPeAT. In this case, the much higher intensity for the CM sheet is real since absolute intensities are presented. The difference looks to be in baseline scattering, which is attributed to either surface topological imperfections, chemical release agent remaining on the surface, or some very different thermal vibrations or density variations in the sample. As the crystallites are anticipated to have a lamellar shape, the peak observed in $q^2I(q)$ vs q represents the characteristic long spacing derived from Bragg's law. The long period (d-spacing) is calculated using equation (21) where q_{max} is the value where $q^2I(q)$ vs q.

The lamellar thickness reported in Table (14) are obtained by multiplication of fractional crystallinity with d spacing values. As expected, blown films have a shorter d-spacing and a thinner lamellar thickness than compression molded sheets due to the fast-cooling rate during film blowing. As previously mentioned, TD films have a higher percent crystallinity than MD films and these results show that the lamellar thickness are also higher. PPeAT films have a shorter d-spacing and smaller lamellar thickness compared to PBAT films, consistent with results obtained from the CM sheets showed earlier.

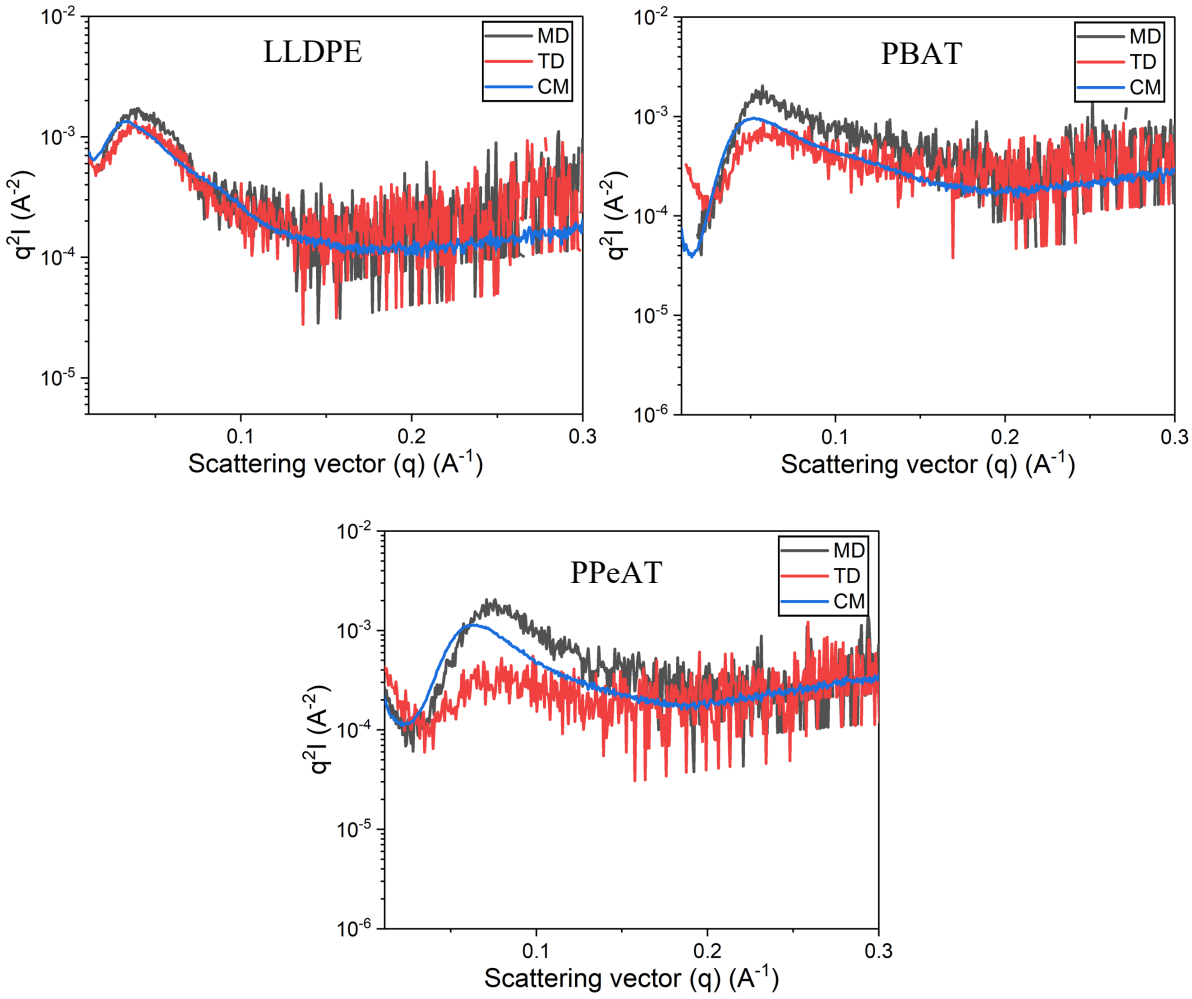

***Figure 34**: Small angle x-ray scattering results for LLDPE, PBAT and PPeAT CM and blown films.*

To observe the change in orientation between the CM sheets and blown films of LLDPE, PBAT and PPeAT, the SAXS patterns were examined for change in the transmissional intensities

as a function of the azimuthal angle along the film line. Results are shown in Figure (37). Scattering vector range used for orientation was 0.015 and 0.1 A^{-1} for LLDPE, 0.02 and 0.015 A^{-1} for PBAT and 0.03 and 0.1 A^{-1} for PPeAT. Intensity for blown films has a sinusoidal shape due change in orientation between MD and TD while for CM sheets, the normalized intensity is almost constant with respect to the azimuthal angle ($\emptyset$). This observation is consistent with result in the literature [150].

The orientation parameter is calculated using equation (28) and reported in Table (2) [151].

$$< \cos^2 \emptyset > \; = \frac{\int_0^{\frac{\pi}{2}} I(\emptyset). \sin \emptyset \,. \cos^2 \emptyset \, d\emptyset}{\int_0^{\frac{\pi}{2}} I(\emptyset). \sin \emptyset \, d\emptyset} \tag{28}$$

$< \cos^2 \emptyset >$ is the average cosine square of the angles between and the oriented molecular chain and the drawing direction and $I(\emptyset)$ is the baseline subtracted intensity distribution around the azimuthal angle. The baseline was assumed to be of the form $A+Bq^{-4}$ where the first term represents incoherent scattering, and the second term is a Porod-type term. Also, the baseline was determined for data below 0.2 $Å^{-1}$ since the slight increase in intensity above this scattering vector is due to the beginning of the amorphous halo.

The value of $< \cos^2 \emptyset >$ approaches 1 as the orientation becomes more aligned with the film drawing direction (MD). Conversely, $< \cos^2 \emptyset >$ approaches 0 as the orientation becomes more perpendicular to the film drawing direction (TD). For random orientation, $< \cos^2 \emptyset >$ is 1/3 [151]. As shown in Table (14), the $< \cos^2 \emptyset >$ values for CM sheets for all 3 polymers is ~0.33, hence CM sheets are considered randomly oriented. For the blown film (BF) samples, MD films have $< \cos^2 \emptyset >$ greater than 0.33 while TD films have $< \cos^2 \emptyset >$ less than 0.33, indicating that the normal of more crystalline lamellae are oriented in the MD than in the TD and/or crystallites are larger in the MD direction.

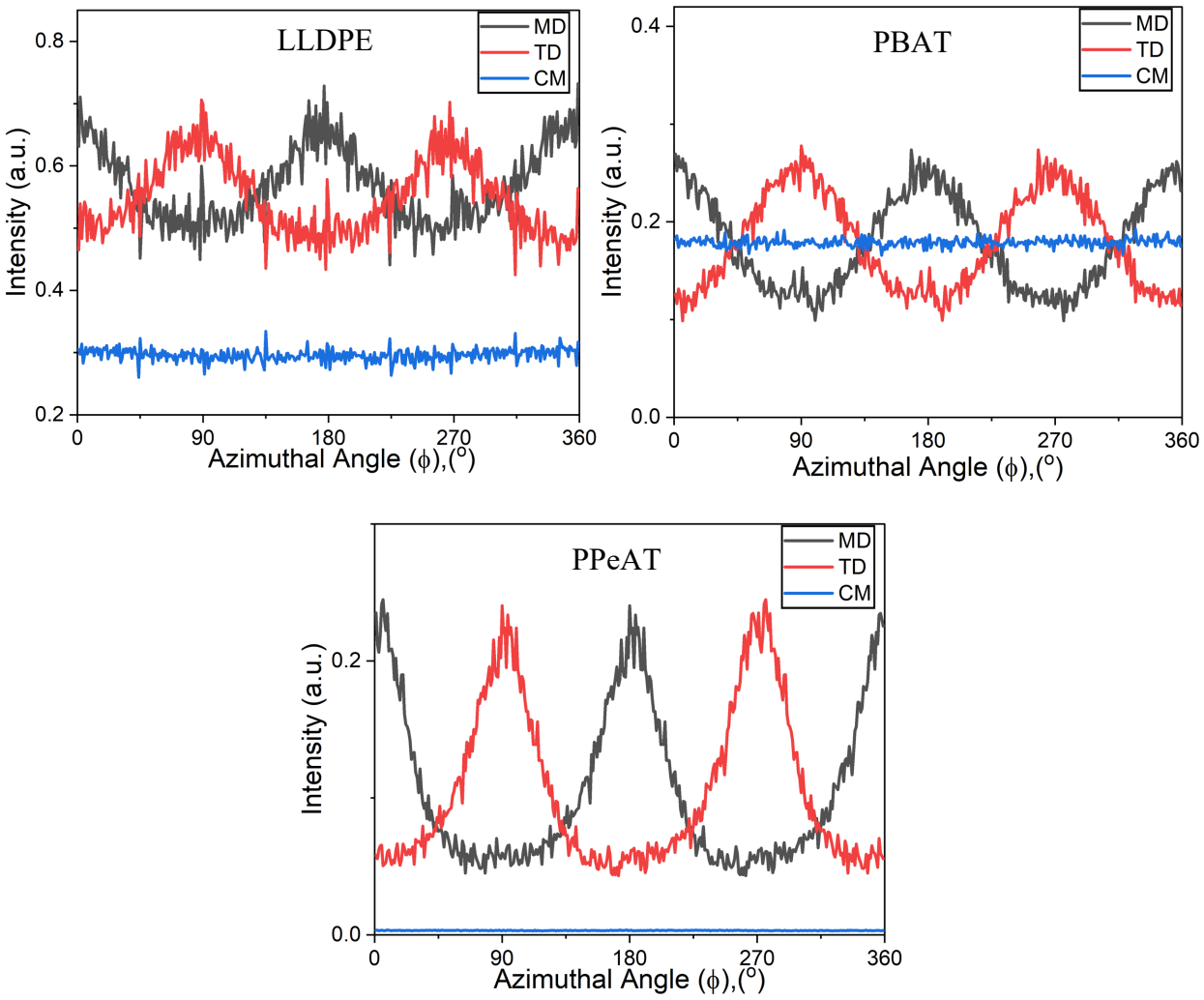

***Figure 35**: Film orientation from single x-ray scattering for LLDPE, PBAT and PPeAT CM sheets and blown films. Normalized intensities represent the following: maximum scattered intensity along the azimuthal angle is one while the minimum is zero.*

6.2.3. Dynamic Mechanical Analysis (DMA)

Storage modulus (E'), loss modulus (E'') and damping factor (tan δ) as a function of temperature for CM, MD and TD films of LLDPE, PBAT and PPeAT are shown in Figure (36). No statistically significant differences exist for TD vs. MD films. For PBAT and PPeAT, E' and E'' plateaus above glass transition temperatures (T_gs) for the blown films (MD and TD) shifted to higher values compared with CM sheets. The opposite is true for LLDPE. The difference between the two is likely related to the fact that the LLDPE is branched while the polyesters are not. The

peak maximum of tan δ for the CM PBAT and PPeAT films shifted to a lower temperature with respect to the blown films (MD and TD) which is an indication in lower T_g. As previously mentioned, CM sheets have a larger d-spacing than BFs. The decrease in d-spacing and lamellar thickness of BFs was reflected in a decrease in T_g as has been reported elsewhere [152, 153]. T_gs from these DMA measurements are consistent with T_gs obtained from DSC measurements for CM and blown films (results not shown).

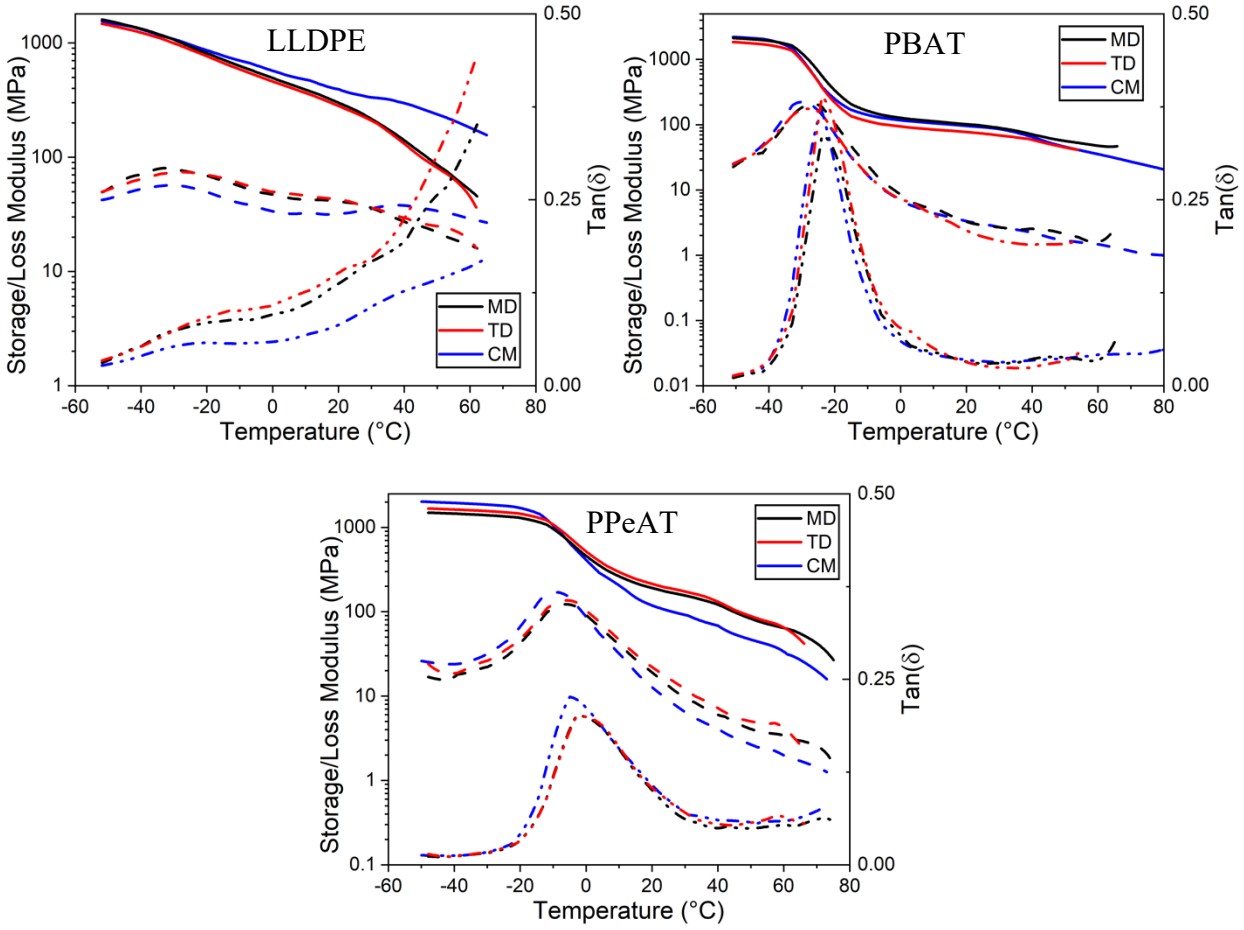

***Figure 36**: Viscoelastic profile form Dynamic Mechanical Analyzer for LLDPE, PBAT and PPeAT CM sheets and blown films. Storage modulus is represented as (- solid lines), loss modulus is represented as (- - dashed lines) and damping factor is represented as (-⋯- dashed lines).*

6.2.4. Barrier Properties

***Table 15**: Oxygen and carbon dioxide permeation and WVTR results for LLDPE, PBAT and PPeAT CM sheets and blown films.*

Samples		P_{O_2}	P_{CO_2}	WVTR
		Barrer	Barrer	g.mm/m^2.d
LLDPE	CM	2.65 ± 0.23	12 ± 1.06	0.099 ± 0.02
	BF	3.56 ± 0.32	14.5 ± 1.28	0.17 ± 0.1
PBAT	CM	1.2 ± 0.20	12.55 ± 1.99	6.95 ± 0.21
	BF	1.3 ± 0.26	14.8 ± 2.98	10.86 ± 0.26
PPeAT	CM	0.25 ± 0.02	2.25 ± 0.21	1.44 ± 0.12
	BF	0.7 ± 0.08	5.9 ± 0.63	1.51 ± 0.20

Oxygen (P_{O_2}) and carbon dioxide (P_{CO_2}) permeabilities are shown in Table (15). P_{O_2} and P_{CO_2} for LLDPE and PBAT agree with the literature [154-156]. Compression molded sheets showed lower P_{O_2} and P_{CO_2} than blown films. Kim et al. reported that blown films exhibit an increase permeability due to the more permeable perpendicular orientation of spherulite lamellae, whereas slowly cooled compression molded sheets develop a higher percentage of parallel-oriented lamellae, resulting in lower permeability [157]. Khanna et al. observed that the stretching of oriented films introduces mechanical defects and stresses, which inhibit the anticipated reduction in permeability that typically results from orientation [158]. Polyesters tend to have a lower P_{O_2} than polyolefins due to the presence of carbonyl and ester bonds which led to a more hydrophilic structure and thus a lower P_{O_2} [159]. As expected, PPeAT and PBAT have a lower P_{O_2}than LLDPE making them good candidates for food packaging. Water vapor transmission rate (WVTR) results for LLDPE, PBAT and PPeAT are shown in Table (15). CM sheets exhibit a lower WVTR compared to the BF, following the same trend as P_{O_2} and P_{CO_2}. PBAT and PPeAT

have a higher WVTR than LLDPE due to the hydrophilic nature of the polar functional groups such as hydroxyl, ester and carboxyl groups which form hydrogen bonds with water vapor molecules [160]. PPeAT exhibits a lower WVTR than PBAT, likely due to its thinner lamellar, which results in a more compact structure. Furthermore, an increase in percent crystallinity leads to a decrease in WVTR due to the fact that the diffusion constant of water through the amorphous polymer will be much larger than the diffusion rate through the crystalline polymer [161].

6.3. Conclusions

PPeAT was successfully film blown using a lab scale film blower and was compared with film blown commercial LLDPE and PBAT and blown films were compared with compression molded sheets. Film blown PBAT and PPeAT shows a higher storage modulus compared to CM sheets which is consistent with the results obtained from the Young's modulus. A strong crystal orientation can be observed for blown films while no crystal orientation can be observed for CM for LLDPE, PBAT and PPeAT. The random orientation of CM sheets can be captured using the orientation parameter as the value for $< \cos^2 \emptyset >$ is 1/3. CM sheets exhibit higher percent crystallinity, longer d-spacing, larger lamellar thickness and lower glass transition temperature compared with blown films for LLDPE, PBAT and PPeAT. CM sheets had a lower oxygen permeability, carbon dioxide permeability and water vapor transmission rates compared with blown films due to the longer d-spacing and larger d-spacing of the CM sheets. PPeAT showed lower oxygen and carbon dioxide permeabilities compared with PBAT and LLDPE and lower water vapor transmission rate than PBAT which is attributed to the difference in lamellar thickness.

Chapter 7: Poly (dodecamethylene furandicarboxylate) ****

7.1. Abstract

Biobased and biodegradable furandicarboxylic acid (FDCA) based polyesters have emerged as promising candidates for substituting conventional petrochemical-based plastics. In this study, an aromatic polyester using FDCA, and a 12-carbon diol (1,12 dodecanediol, DD) was synthesized using direct esterification and polycondensation to produce poly (dodecamethylene furandicarboxylate) (PDDF). Thermal, mechanical, and rheological properties of the polymer were thoroughly investigated using different techniques, including differential scanning calorimetry, thermogravimetric analysis, wide and small-angle x-ray scattering, dynamic mechanical analysis, rheology and biodegradation studies. PDDF has a lower oxygen and carbon dioxide permeability than two commonly used polymers used for flexible film, namely PBAT and LLDPE. However, the biodegradation studies showed that the degradation of PDDF is slower than PBAT. Nevertheless, these gas barrier properties along with its mechanical, thermal, and rheological properties make PDDF a viable candidate for film packaging applications.

**** *Being prepared for publication.*

7.2. Results and Discussion

The average molecular weights and PDI of PDDF, relative polystyrene standards, are compared to commercial PBAT in Table (16). The values for PDDF from the transesterification process were Mn= 39,000 g/mol and Mw=69,000 g/mol [162], i.e. pretty similar to what is reported here.

***Table 16**: GPC results for PBAT and PDDF*

Sample	**Mw**	**Mn**	**Đ**
	g/mol	*g/mol*	-
PBAT	148,800	97,800	2.0
PDDF	52,600	31,600	1.7

7.2.1. Thermal properties

Table (17) shows the temperatures for different decomposition stages: the temperature at which 5% decomposition occurred ($T_{d,5\%}$), the temperature of maximum decomposition rate ($T_{d,\ max}$), and the residual mass at 600°C ($R_{600°C}$) obtained from TGA. PBAT has better thermal stability than PDDF as shown in Figure (37) and a slightly better $T_{d,5\%,}$ and $T_{d,\ max}$ as shown in Table (17). The decrease in thermal stability could be linked to the presence of a high number of methylene units in PDDF [163]. However, PDDF has a lower residue at 600°C vs. PBAT which is attributed to the furan ring compared with the benzene ring present in PBAT. The presence of residue at 600°C is due to the pyrolysis of the aromatic fraction leading to the formation of stable char. LLDPE exhibits better thermal stability than both copolyesters with a $T_{d,5\%}$, $T_{d,\ max,}$ and $R_{600°C}$ of 441°C, 453°C, and 0% respectively. Both polyesters, PBAT and PDDF are thermally stable in nitrogen up to 350°C. However, PDDF does undergo thermal degradation due to hydrolysis of the FDCA Therefore, the samples need to be dried overnight before any processing.

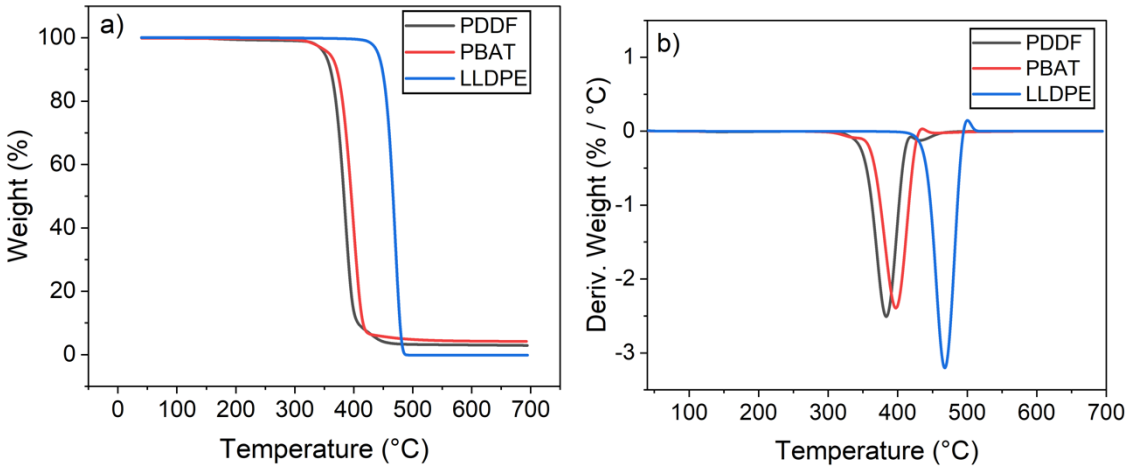

***Figure 37**: TGA and DTGA results for PDDF, PBAT and LLDPE.*

***Table 17**: Thermal properties from DSC and TGA for LLDPE, PBAT and PDDF.*

Sample	First Heating		First Cooling		Second Heating			TGA		
	T_m	ΔH_m	T_c	ΔH_c	T_g	T_m	ΔH_m	$T_{d,5\%}$	$T_{d,max}$	$R_{600℃}$
	℃	J/g	℃	J/g	℃	℃	J/g	℃	℃	%
LLDPE	116	131	106	109	-	116	127	441	453	0
PBAT	115	34	38	20	-30	118	20	358	376	4.3
PDDF	108	75	58	63	-9	102	41	351	366	3.1

A clear endothermic peak due to melting was observed for PDDF and LLDPE while a very broad peak was seen for PBAT during the first and the second heating cycles in DSC thermograms shown in Figure (38). For the first cooling cycle, an exothermic peak was spotted for all polymers which is an indication of a relatively fast crystallization rate. The melting temperature (T_m), enthalpy of melting (ΔH_m), crystallization temperature (T_c), enthalpy of crystallization (ΔH_c), and glass transition temperature (T_g) are reported in Table (17). PDDF has a similar T_m (108°C) and a higher T_g (-9°C) than PBAT (T_m=115°C and T_g=-30°C). However, the ΔH_m of PDDF (75 J/g) was more than double the ΔH_m of PBAT (34 J/g) which could be attributed to the presence of the long-chain diol which led to a higher degree of crystallinity. Furthermore, PDDF has a higher T_c (58°C) and ΔH_c (63 J/g) than PBAT (T_c=38°C and ΔH_c=20 J/g) which could be an indication of a faster

crystallization rate. T_m, ΔH_m and T_c results are consistent with results obtained by Papageorgiou et al (T_m=111°C, ΔH_c=69.6 J/g and T_c=68°C at 10°C/min cooling rate); however, the T_g (-22°C) was different [162]. Grosshardt et al. also found a melting temperature (T_m=109°C) for PDDF consistent with that reported here [164].

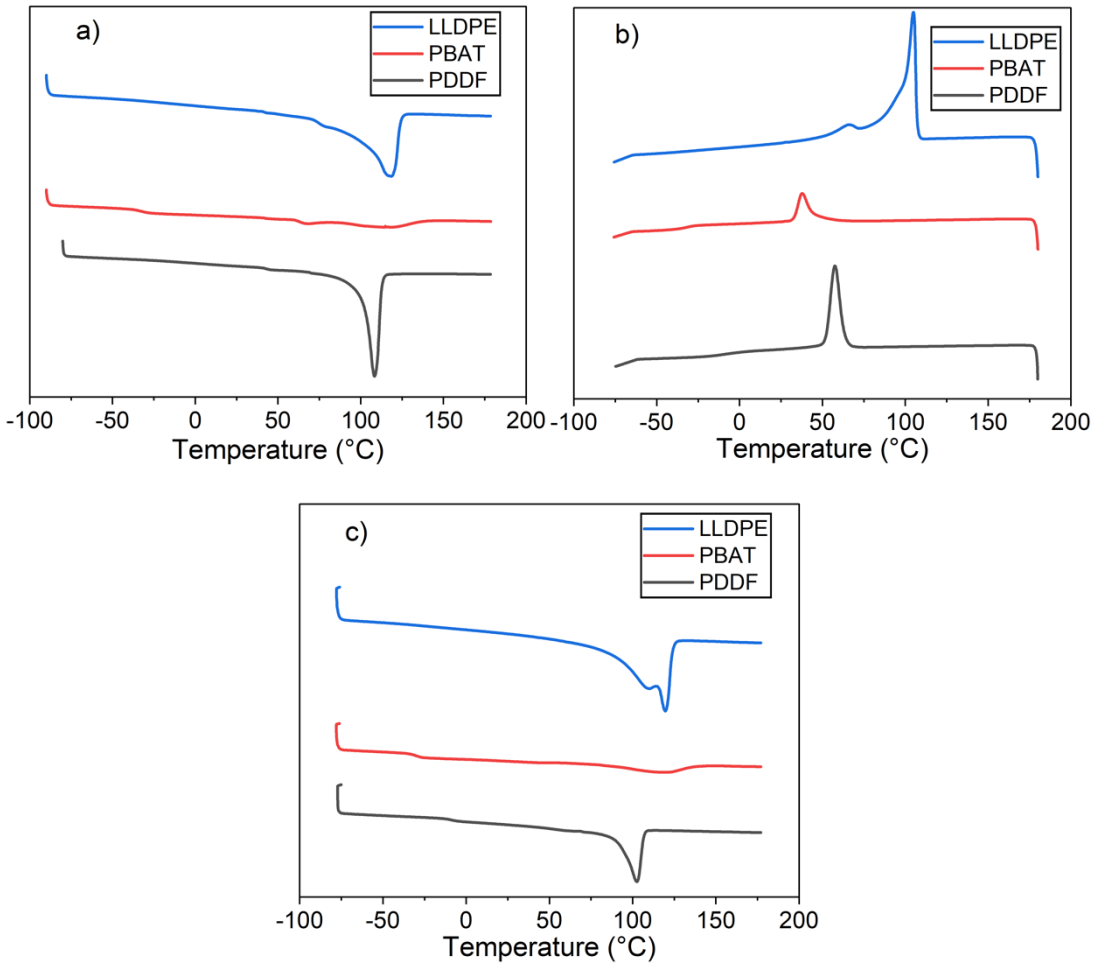

***Figure 38**: DSC results for a) first heating cycle, b) first cooling cycle, and c) second heating cycle for PDDF, PBAT, and LLDPE. Results have been shifted vertically for clarity.*

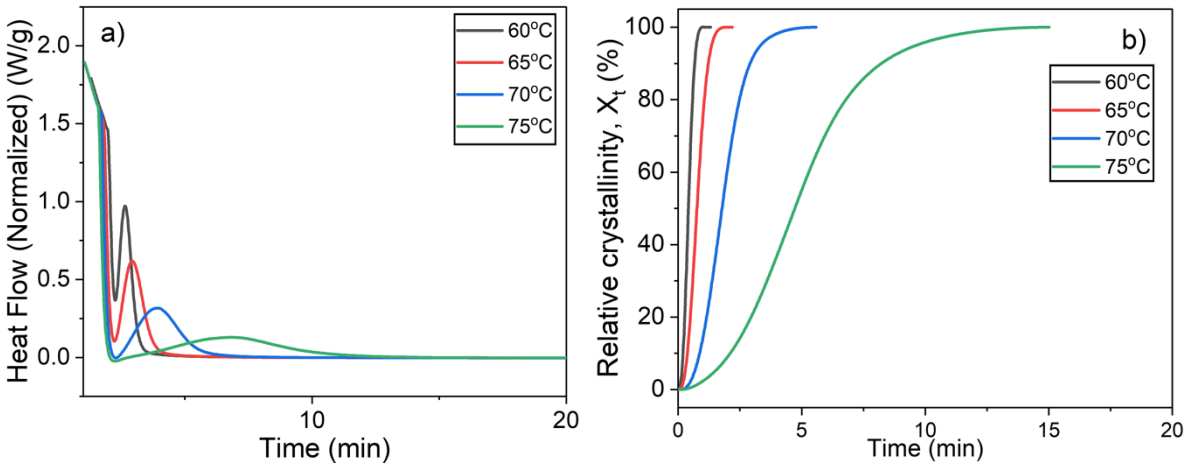

***Figure 39**: Isothermal crystallization and Avrami model results for PDDF.*

Isothermal crystallization kinetics of PDDF were studied at different temperatures using DSC and the results are presented in Figure (39). As expected, the rate of crystallization at 60°C is much faster than the rate of crystallization at 75°C. The well-known Avrami model was utilized to gain deeper insights into the isothermal crystallization process. The Avrami model illustrates the time-dependent relative crystallinity (X_t) at a constant temperature, as presented in equation (29):

$$X_t = 1 - \exp(-kt^n) \tag{29}$$

k is the rate constant for crystallization which is a function of nucleation and growth rates, and n is the Avrami exponent. The crystallization half-time ($t_{1/2}$) and the Avrami model parameter are reported in Table (18). As previously mentioned, the rate of crystallization decreases with the increase in crystallization temperature. Not surprisingly then, an increase in $t_{1/2}$ and a decrease in k can be observed with the increase in crystallization temperature. The Avrami exponent is constant from 60-75°C while the two higher temperatures have a lower exponent. Therefore, the growth mechanism changes from one that is equally distributed between two and one-dimensional growth to one that is more one-dimensional growth [165].

***Table 18**: Avrami model parameters for PDDF*

Sample	T_c	$t_{1/2}$	k	n
	℃	min	min^{-n}	-
PDDF	55	0.31	13.64	2.52
	60	0.42	6.42	2.54
	65	0.77	1.39	2.58
	70	1.78	0.16	2.50
	75	4.72	0.02	2.25
	80	10.64	0.005	2.13

7.2.2. Crystal properties

Figure (40) illustrates the WAXS spectra of the polyesters and LLDPE, while Table (19) provides the percent crystallinity values for these polymers. For PBAT, scattering angles (2θ°) observed are 16.2°, 17.3°, 20.4°, 23.2° and 24.8 corresponding to the planes (011), (010), (102), (100), and (111) respectively which are consistent with the literature. For LLDPE, two sharp crystalline peaks can be observed at the $2\theta°$ value 21.4° and 23.6° which are assigned to (110) and (200) planes. For PDDF, 2θ° are 9.8°, 17.9°, 21.6° and 23.8° with the latter two scattering angles at approximately at the same angles as the planes (110), and (200) of LLDPE. The results for PDDF are consistent with results obtained by Papageorgiou et al. [162]. The percent crystallinity of PDDF (28.6%) is half the percent crystallinity of LLDPE (50.4%) as shown in Table (19); the ratio of these two values is roughly consistent with the ΔH_ms shown in Table (17). Moreover, PDDF has a higher percent crystallinity than PBAT which is due to the presence of a higher number of methylene units in the diacid leading to a more crystalline polyester. Although quantitative data was not presented in the Papageorgiou paper, upon inspection of WAXS patterns the fractional crystallinity looks similar.

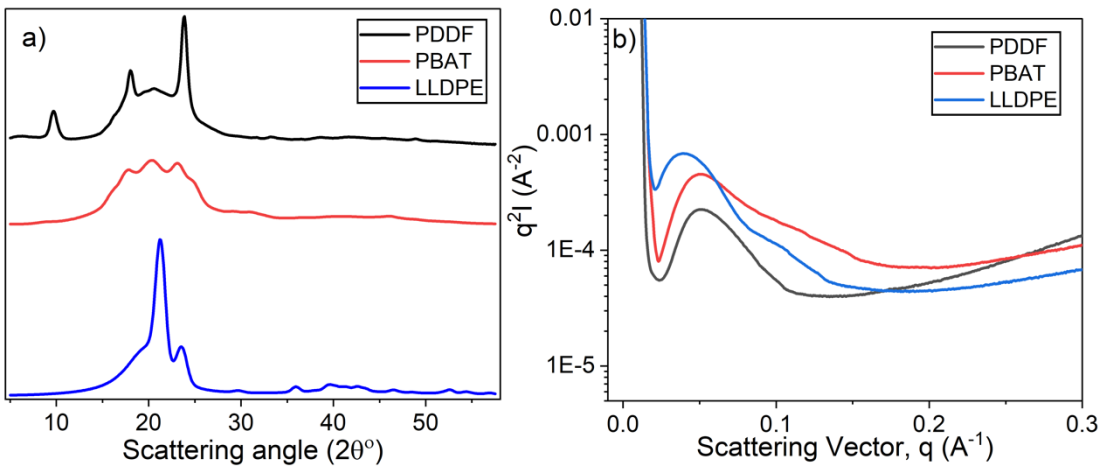

***Figure 40**: WAXS and SAXS results for PDDF, PBAT, and LLDPE*

Figure (40) and Table (19) show SAXS results for PDDF, PBAT and LLDPE. As the crystallites are anticipated to have a lamellar shape, the peak observed in $q^2I(q)$ vs q represents the characteristic long spacing derived from Bragg's law. The long period (d-spacing) is calculated using equation (19) where q_{max} is the value where $q^2I(q)$ vs q.

The values of lamellar thickness reported in Table (19) are derived from the multiplication of fractional crystallinity with d spacing values. The d-spacing is the same so the lamellar thickness of PDDF (35.3Å) is half the lamellar thickness of LLDPE (80.8Å); the ratio of these two values is consistent with the percent crystallinity shown in Table (19).

***Table 19**: Crystallinity properties for LLDPE, PBAT and PDDF.*

Sample	WAXS	SAXS		
	χ_c	q_{max}	d-spacing	Lamellar thickness
	%	$Å^{-1}$	Å	Å
LLDPE	50.4	0.039	160	80.8
PBAT	19.4	0.051	124	24.2
PDDF	28.6	0.051	124	35.3

7.2.3. Mechanical properties

Stress-strain curves for PDDF, PBAT and LDDPE are exhibited in Figure (41). Young's modulus (E), yield stress (δ_y), yield strain (ε_y), stress at break (δ_b). elongation at break (ε_b) and tensile toughness (U_t) are calculated and reported in Table (20). All three polymers exhibit ductile behavior with a high elongation at break. The E, δ_y, ε_y, δ_b and ε_b values for LLDPE and PBAT are in agreement with literature results [110, 166]. PDDF (247 MPa) has a similar Young's modulus as LLDPE (255 MPa) and almost 3 times the Young's modulus of PBAT (78 MPa). This high Young's modulus is accompanied with a decrease in elongation at and break while maintaining a similar stress at break as LLDPE and PBAT. The difference in Young's modulus and elongation at break between PDDF and PBAT is likely due to the higher fractional crystallinity of the former. Furthermore, the reduced elongation at break resulted in a lower tensile toughness for PDDF compared to LLDPE and PBAT. The E, δ_b and ε_b results for our PDDF are inconsistent with results obtained by Papageorgiou et al [162] as shown in Table (20). That discrepancy could be due to the different synthesis (e.g. was transesterification complete) and/or cooling method used after the compression molding step. Regarding the latter, the mold was immersed in cooling water at 20°C to rapidly cool the polyester while here slow cooling in the mold was utilized.

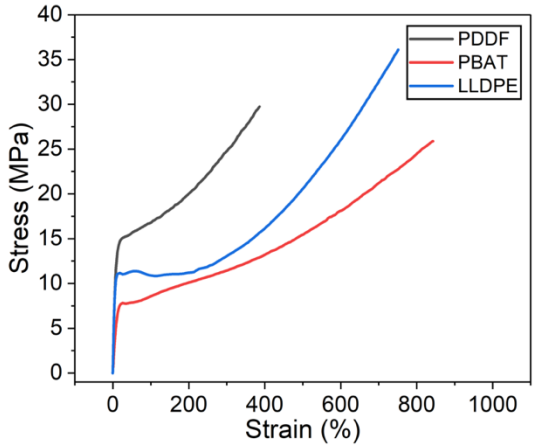

***Figure 41**: Stress-strain curves for PDDF, PBAT, and LLDPE.*

***Table 20**: Mechanical properties for LLDPE, PBAT and PDDF.*

Sample	E	δ_y	ε_y	δ_b	ε_b	U_t
	MPa	MPa	%	MPa	%	MJ/m^3
LLDPE	255 ± 33	11 ± 0.3	19 ± 21	30 ± 4	645 ± 71	105 ± 25
PBAT	78 ± 10	-	-	26 ± 3	815 ± 67	127 ± 19
PDDF	247 ± 7	-	-	21 ± 2	220 ± 60	40 ± 6
PDDF[162]	181 ± 16	9.5 ± 1.1	-	11 ± 0.9	130 ± 10	-

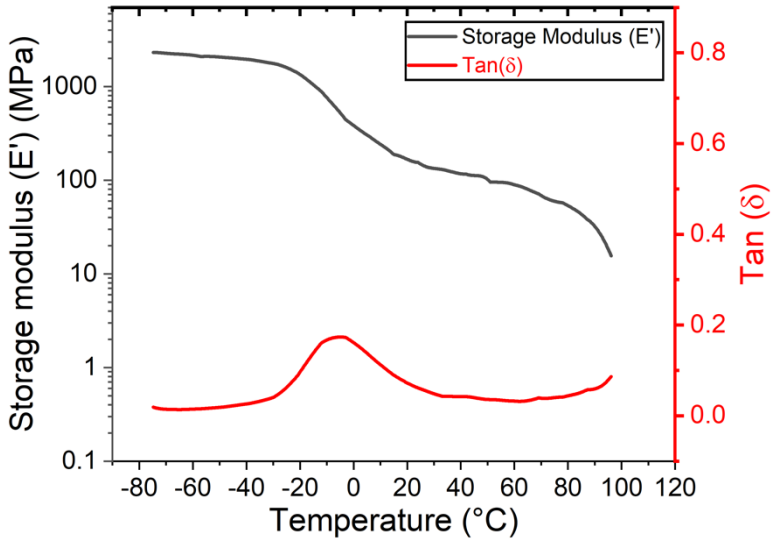

***Figure 42**: DMA results for PDDF.*

Storage modulus (E') and damping factor (tan δ) as a function of temperature for PDDF are shown in Figure (42). T_g was determined by the temperature that corresponded to the peak in tan δ (-9°C). This value obtained from DMA was consistent with the T_g (-9°C) obtained from DSC.

7.2.4. Rheological properties

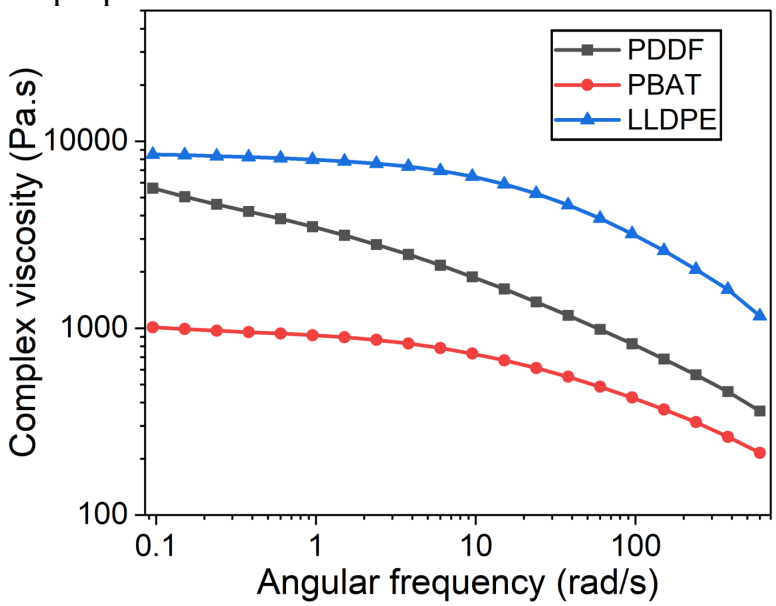

***Figure 43**: Complex viscosity results for PDDF, PBAT, and LLDPE.*

Complex shear viscosities vs angular frequency at 190°C for PDDF, LLDPE and PBAT are shown in Figure (43). Shear-thinning behavior at high frequency and a Newtonian plateau at low frequencies can be observed for PDDF, LLDPE and PBAT. The higher viscosity of the PDDF vs. the PBAT is somewhat surprising given that the molecular weight of the former is ~1/3 the molecular weight of the latter. At high frequencies, PDDF had a lower complex viscosity than LLDPE at the same frequency. The shear rate within the extruder during film blowing is expected to be 45 s^{-1} [124], hence, if the Cox-Merz rule is applicable to these polymers, then the extrusion energy required for PDDF is significantly lower than that needed for LLDPE. We were not able to obtain the complex viscosity of PDDF at low angular frequency due to the thermal degradation of 2,5-furandicarboxylic acid. Thermal degradation of polyesters based on FA has been reported previously in the literature [167, 168].

The five-parameter Carreau-Yasuda was used to model the complex viscosities. The model is shown in equation (30) and the results of which are reported in Table (21).

$$\frac{\eta(\omega)-\eta_{\infty}}{\eta_0-\eta_{\infty}}=[1+(\omega\lambda)^a]^{\frac{n-1}{a}} \quad (30)$$

η_{∞} is the infinite shear viscosity in (Pa.s), η_0 is the zero-shear viscosity in (Pa.s), ω is the angular frequency in (rad/s), λ is the characteristic relaxation time in (s), a is the transition parameter and n is the flow index in Carreau-Yasuda model. The infinite shear viscosity (η_{∞}) for the polymer melt is assumed to be zero. Fitted data show good agreement with the experimental results. PDDF had a lower flow index and a higher characteristic relaxation time than PBAT reflective of a decrease in shear thinning behavior and a narrower Newtonian plateau region, respectively. A low transition parameter is an indication of a broader transition from shear thinning region to a Newtonian region.

***Table 21**: Rheological properties for LLDPE, PBAT and PDDF.*

Sample	**Shear viscosity**				**Elongational viscosity at Hencky strain of 2.5 and 0.3 s^{-1}**
	η_o	n	a	λ	η_E
	Pa.s	-	-	s	Pa.s
LLDPE	8711	0.12	0.62	0.01	47,000
PBAT	1006	0.67	0.76	0.12	350,000
PDDF	9168	0.45	0.29	0.28	225,000

Elongational viscosities vs. time for PDDF, LLDPE and PBAT at 130°C and 0.3 s^{-1} are plotted in Figure (44) A lower temperature was chosen compared to the temperature used for shear viscosity measurements, as high temperatures lead to sample sagging. Also, as mentioned previously, a Hencky strain of 2.5 at an elongational rate of 0.3 s^{-1} were found to be representative values for film blowing [124] and these values are found in Table (21). High elongational viscosity

serves as an indicator of elevated melt strength, consequently contributing to a more stable bubble during the film blowing process. Strain hardening is characterized by an increase in elongation viscosity above the linear viscoelastic plateau [141]. PDDF and PBAT exhibit strain hardening while the absence of strain hardening in LLDPE is attributed to its narrow molecular weight distribution and the absence of long-chain branches. While strain hardening typically arises from long-chain branches, in the case of the polyesters, it could be attributed to certain long chains remaining stretched until the sample's failure [143]. Micic et al. reported that strain hardening is linked to improved stability of the bubble during the film blowing process [142].

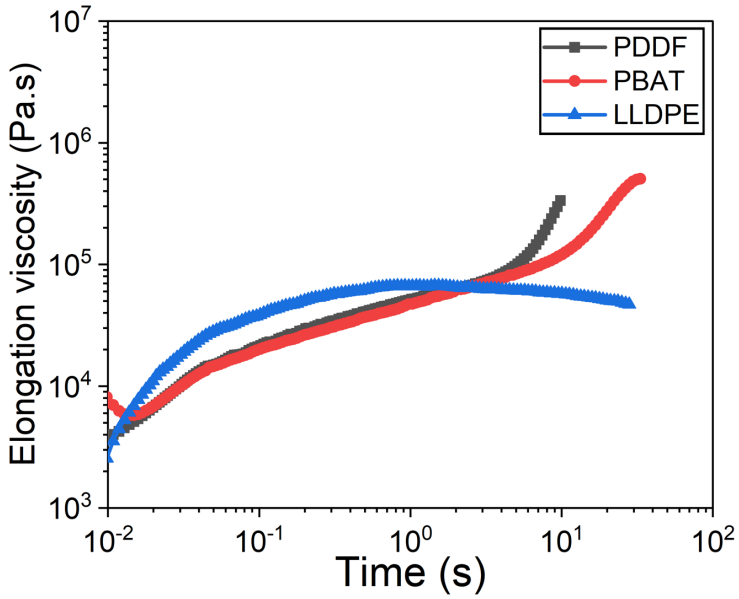

***Figure 44**: Elongational viscosity results for PDDF, PBAT, and LLDPE.*

7.2.5. Barrier properties

Oxygen (P_{O_2}) and carbon dioxide (P_{CO_2}) permeabilities are shown in Figure (45). Permeability measurements were obtained at 25°C and 1 bar. P_{O_2} and P_{CO_2} for LLDPE and PBAT agree with the literature [154, 155]. An increase in percent crystallinity leads to a decrease in gas permeability since permeability occurs almost exclusively through the amorphous regions. Not surprisingly then, PDDF has a lower P_{O_2} and P_{CO_2} than PBAT due to the higher percent crystallinity

of PDDF compared to PBAT [159, 169]. Moreover, polyesters tend to have a lower P_{O_2} than polyolefins due to the presence of carbonyl and ester bonds which led to a more hydrophilic structure and thus a lower P_{O_2} [159]. Therefore, PDDF and PBAT have a lower P_{O_2} than LLDPE making them good candidates for food packaging. Water vapor transmission rate (WTVR) in $g.\mu m.m^{-2}.d^{-1}$ results for PDDF, LLDPE and PBAT are shown in Figure (48). PBAT has a much higher WVTR than LLDPE and PBAT due to the hydrophilic nature of the poler functional groups such as hydroxyl, ester and carboxyl groups which form hydrogen bonds with water vapor molecules [160]. Furthermore, an increase in percent crystallinity leads to a decrease in WVTR due to the increase in rigidity and decrease in allowed space for water vapor. Thus, LLDPE have a lower WVTR than PDDF and PBAT [161].

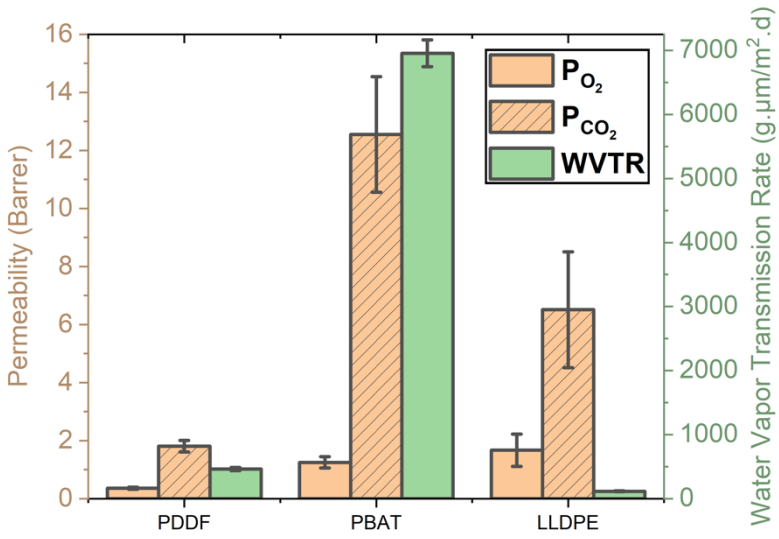

***Figure 45**: Oxygen and carbon dioxide permeation and WVTR results for PDDF, PBAT, and LLDPE.*

7.2.6. Biodegradation Study

The biodegradation of PDDF and PBAT was conducted in both freshwater, soil and compost environments with the results shown in Figure (46). The results for PBAT was reported previously reported by Zheng et al. [170]. In the freshwater environment, PDDF achieved approximately 17% biodegradation in 72 days, while PBAT reached around 35% within the same

period. Therefore, the estimated end of lifetime, based on first-order kinetics, is 395 days for PBAT, whereas for PDDF, it is projected to be 990 days under the same conditions. However, in soil environment, PBAT reach around 20% biodegradation in 96 days but for PDDF no biodegradation was observed after 96 days. The estimated end of lifetime, based on first-order kinetics, is 971 days for PBAT in soil environment. Additionally, in compost environment, PDDF reached around 28% biodegradation in 62 days with an estimated end of lifetime of 475 days based on first order kinetics. The slower biodegradation rate of PDDF compared to PBAT in freshwater environments may be attributed to two key factors. First, PDDF has a higher degree of crystallinity, which makes the polymer structure more rigid and less accessible to microbial attack [171]. Second, the incorporation of a long-chain diol in PDDF results in fewer ester groups per unit length of the polymer chain. Since ester groups are the primary sites for hydrolytic degradation, their lower density in PDDF likely reduces its susceptibility to biodegradation. These structural characteristics collectively contribute to the more prolonged degradation process observed in PDDF [172].

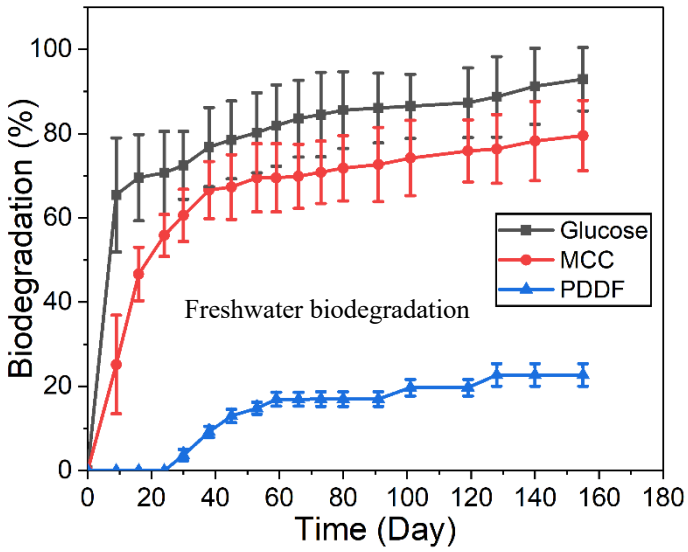

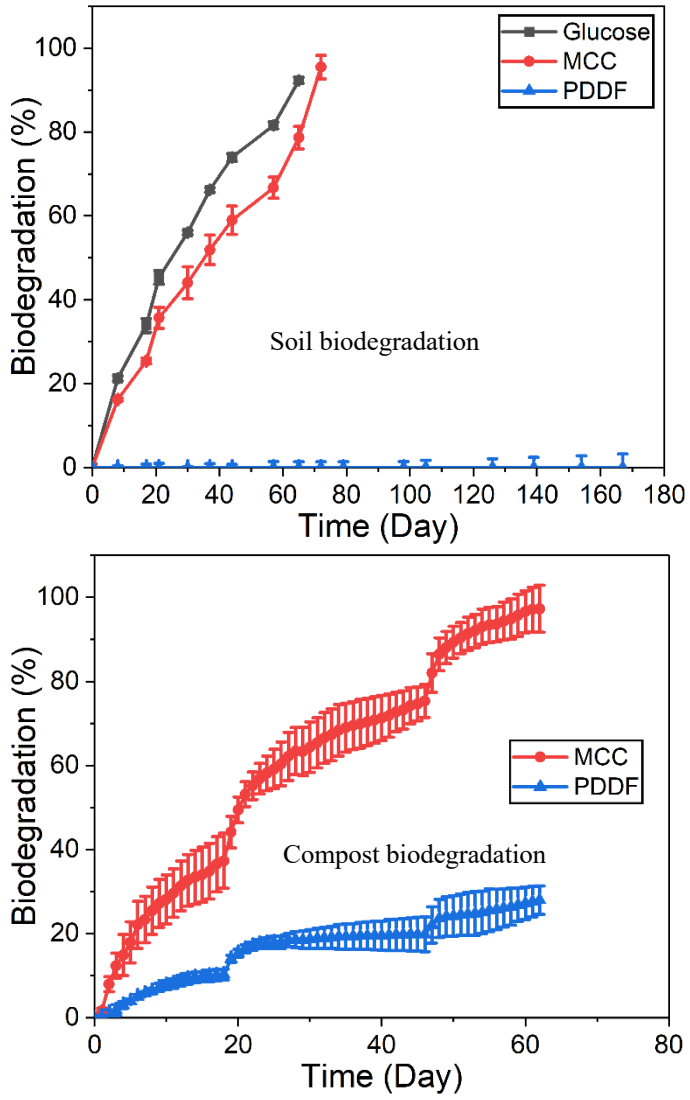

***Figure 46**: Freshwater, soil and compost biodegradation results for PDDF.*

7.3. Conclusions

Direct esterification and polycondensation were used to synthesize a biobased polyester with a DD and FDCA. Both polyesters, PDDF and PBAT, are thermally stable up to 350°C. PDDF has a similar T_m and a higher ΔH_m than PBAT. That increase in ΔH_m was consistent with the higher percent crystallinity measured via WAXS, and the lamellar thickness was larger for PDDF than PBAT. Moreover, the increase in percent crystallinity likely was a primary reason for the increase in Young's modulus and a decrease in elongation at break for PDDF compared to PBAT. PDDF

exhibits shear-thinning behavior at high frequencies, however, at low frequencies the Newtonian plateau couldn't be observed due to the thermal degradation of 2,5-furandicarboxylic acid. PBAT and PDDF both show a strain hardening phenomena in an the elongational viscosity test; however, PDDF has a lower elongational viscosity at a Hencky strain of 2.5 and elongation rate of 0.3 s^{-1}, which is perhaps because the molecular weight of PDDF is ~1/3 that of PBAT. Finally, PDDF has a lower oxygen and carbon dioxide permeability than PBAT. PDDF could be a viable candidate for flexible film packaging. However, the biodegradation properties of PDDF were not as good as PBAT due to the higher percent crystallinity.

Chapter 8: Summary and Recommendation for Future Work

8.1. Summary

This dissertation represents a significant advancement in the development of biobased and biodegradable polyesters, offering a promising alternative to conventional petrochemical-based plastics, especially for use in flexible film packaging applications. The initial objective was to synthesize a polyester using biobased pentanediol as the diol and biobased furandicarboxylic acid as the aromatic diacid, while varying the linear diacid to achieve the desired melting temperature (T_m) and glass transition temperature (T_g). However, the difference between the melting and glass transition temperatures is insufficient for these materials to be suitable for flexible film applications. The next step was synthesizing and characterizing a polyester using pentanediol, adipic acid, and terephthalic acid to replicate the structure of poly (butylene adipate-co-terephthalate) (PBAT), but with biobased content. Poly (pentylene adipate-co-terephthalate) (PPeAT60) with a 40/60 adipic acid/terephthalic acid ratio was synthesized using direct esterification and polycondensation. Branching agents' glycerol and hexane-1,2,5,6-tetrol were used, with copolyesters showing molecular weights above 140,000 g/mol. PPeAT60 had a lower T_m and higher T_g than PBAT, likely due to the odd-even effect, which also slowed crystallization. PPeAT60's Young's modulus nearly doubled PBAT's, with minimal impact on elongation. Branching increased modulus but reduced elongation and flexibility. Small-angle X-ray scattering (SAXS) showed reduced d-spacing and lamellar thickness with branching. The copolyesters displayed shear-thinning behavior. To improve the slow crystallization issue of PPeAT60, a nucleating agent was added. Different Li, Mg, and Na E-MAA ionomers or E-MAA acid copolymer were melt-mixed with PPeAT to increase the crystallization rate. The addition of ionomers and acid copolymer led to a ~1.5 and 2 order-of-magnitude decrease in half-time

crystallization and a ~three and five-order-of-magnitude increase in the Avrami rate constant, respectively. Also, the acid copolymer was the most efficient nucleator in that smaller amounts were required to achieve this crystallization rate improvement. We cannot explain why differences in nucleation efficiency occur between the different nucleating agents. Increasing the ionomer concentration from 0.05 wt% to 0.5 wt% led to an additional half-order of magnitude decrease in the crystallization half-time and an additional 1.5 order of magnitude increase in the Avrami rate constant; further increases caused a slowing of crystallization. The addition of ionomers and acid copolymer at 0.05 wt% led to a decrease in melting temperature for materials and reduction of crystalline fraction under conditions where crystallization was presumably complete. At 0.5 wt%, these values were statistically equal to the non-nucleated samples. 0.05 wt% ionomer nucleating agents cause an increase in Young's modulus, a decrease in the elongation at break and a decrease in the tensile strength; again, these differences disappear with 0.5 wt% ionomer nucleating agent. The addition of 0.5 wt% Na ionomer doesn't affect the viscosity at high angular frequency, with only slight changes at lower frequencies. Moreover, PPeAT60 was successfully film-blown using a lab-scale film blower and compared to commercial linear low-density polyethylene (LLDPE) and PBAT films. The film-blown samples exhibited improved mechanical properties compared to compression-molded (CM) films. Transverse direction (TD) films showed higher Young's modulus, while machine direction (MD) films had greater elongation at break. Both film-blown PBAT and PPeAT60 had higher storage moduli than CM films, indicating stronger crystal orientation in the FB films, which was absent in the CM films. The CM films exhibited random orientation, as indicated by an orientation parameter value of 1/3. CM films also showed higher crystallinity, longer d-spacing, larger lamellar thickness, and lower glass transition temperatures compared to Blown film (BF). Additionally, CM films had lower oxygen and carbon dioxide

permeabilities and water vapor transmission rates due to their larger d-spacing. PPeAT60 demonstrated lower permeabilities compared to PBAT and LLDPE, as well as a lower water vapor transmission rate than PBAT, attributed to differences in lamellar thickness. Overall, film-blown PPeAT60 showed promising potential as a drop-in replacement for LLDPE in flexible film packaging. Finally, a 100% biobased polyester was synthesized from 1,12-dodecanediol and 2,5-furandicarboxylic acid using direct esterification and polycondensation. PDDF is thermally stable up to 350°C. poly (dodecamethylene furandicarboxylate) (PDDF) features a similar T_m but a higher ΔH_m than PBAT, reflecting greater crystallinity and larger lamellar thickness. This increased crystallinity contributes to PDDF's higher Young's modulus and lower elongation at break compared to PBAT. PDDF exhibits shear-thinning behavior at high frequencies, but the Newtonian plateau is absent at low frequencies due to acid degradation. Both polymers show strain hardening, yet PDDF has lower elongational viscosity, likely due to its lower molecular weight. Additionally, PDDF has lower oxygen and carbon dioxide permeability than PBAT, positioning it as a promising candidate for flexible film packaging. However, the Biodegradation of PDDF is not as good as PBAT due to higher crystallinity and the presence of less ester groups per length of polymer chain.

8.2. Future work

This research presents results obtained under specific conditions; however, it did not investigate the effects of varying these conditions. While the findings offer valuable insights within the defined parameters, the lack of exploration into different conditions leaves room for future studies to assess how variations may impact the outcomes. This limitation suggests that additional research could enhance our understanding of the polyester properties under a broader range of conditions.

The film blower was operated at a constant blow-up ratio, draw ratio, extruder speed, air pressure and rolling speed. Varying these parameters can drastically impact the final properties of the blown film. For example, increasing the blow-up ratio will leads to thinner films with improved flexibility and transparency, while lower blow-up ratio can increase film thickness and mechanical strength. Moreover, increasing the draw ratio enhances the orientation of polymer chains, resulting in improved tensile strength, toughness, and barrier properties. Furthermore, increasing the extruder speed can lead to increased shear rates, resulting in better mixing and uniformity of the melt. While, faster rolling speeds can promote better alignment of polymer chains, enhancing the film's strength and barrier properties. Additionally, no processing aids were used in this work other than nucleating agent. In appendix D, a few proposed processing aids can be used to improve the film blowing process and improve the overall properties of the films.

In this work only ionomer nucleating agents were used to improve the crystallization rate of PPeAT. Future work could include other polymeric nucleating agents such as polycaprolactone and polyoxymethylene. The effect of different non ionomer nucleating agent on the crystallization temperature, melting temperature, glass transition temperature, crystallization kinetics, mechanical properties and rheological properties can also be studied.

Glycerol and hexane-1,2,5,6-tetrol were used as branching agents to induce branching and improve the mechanical and rheological properties of PPeAT60. Possible future work could be to use chain extender such as 4,4′-methylene diphenyl diisocyanate to improve the intrinsic viscosity, molecular weight and long-chain branching. Furthermore, investigate the impact of incorporating a chain extender on the mechanical, thermal, and rheological properties. Finally, prepare a film-blown sample of PPeAT60 with a chain extender and evaluate its mechanical and barrier properties.

PPeAT60 was depolymerized through methanolysis into its monomeric feedstock, which was later repolymerized. The original PPeAT60 and the repolymerized PPeAT60 need to be extensively characterize using DSC, TGA, NMR, SAXS, WAXS tensile testing and rheology in order to prove that the new grade of polyesters is not only 100 % biodegradable but also completely recyclable.

Only compression-molded films of PDDF polyester were characterized in this study. Future research could focus on producing film-blown PDDF and evaluating its various properties. Additionally, PDDF could be depolymerized via methanolysis, with the recovered monomeric feedstock used to synthesize a repolymerized version of the polyester. A comprehensive comparison of the properties between the original and repolymerized PDDF would help close the loop and assess material recyclability.

Appendix A: Supplementary material

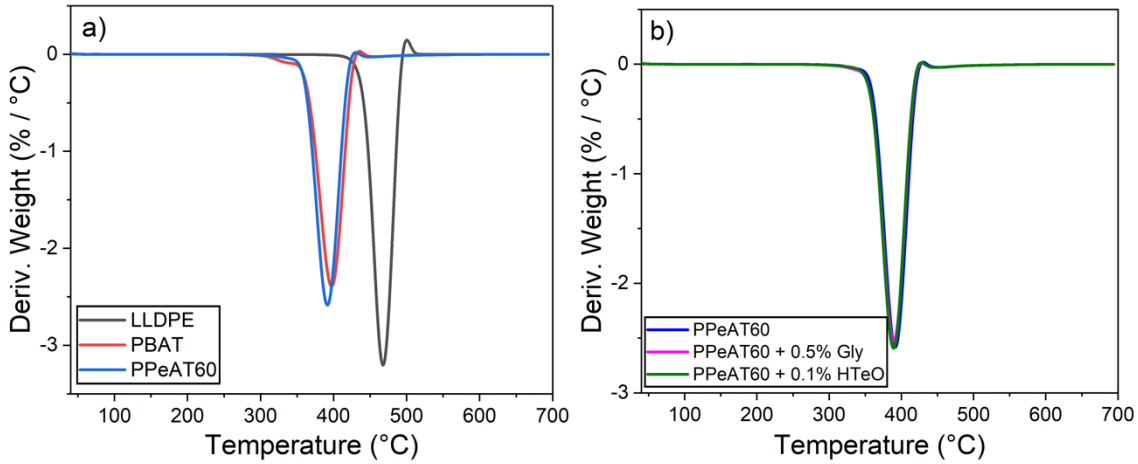

***Figure S1**: DTG results for a) LLDPE, PBAT, and PPeAT60 and b) PPeAT60, PPeAT60+0.1% HTeO and PPeAT60+0.5% Gly.*

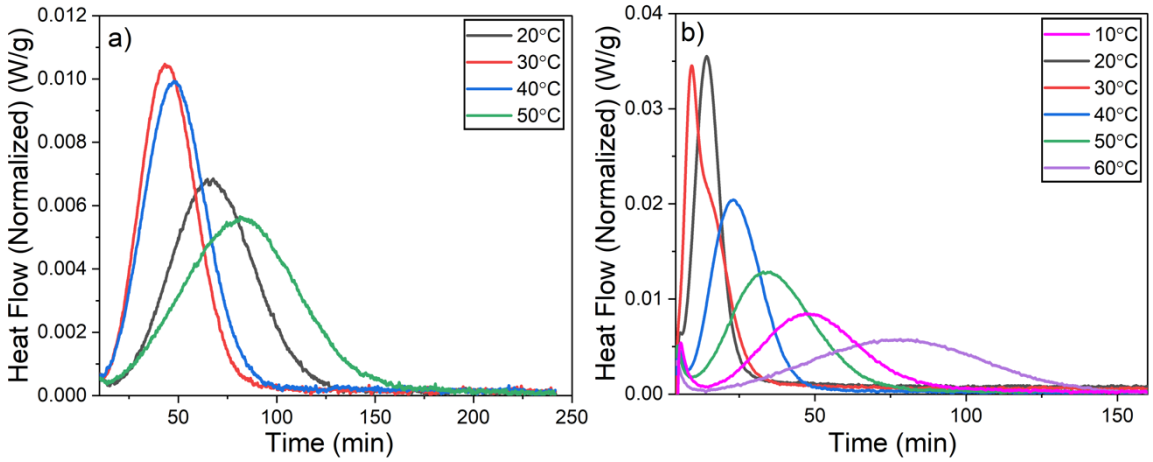

***Figure S2**: Isothermal crystallization results from DSC for PPeAT60+0.5% Gly and PPeAT60+0.1% HTeO.*

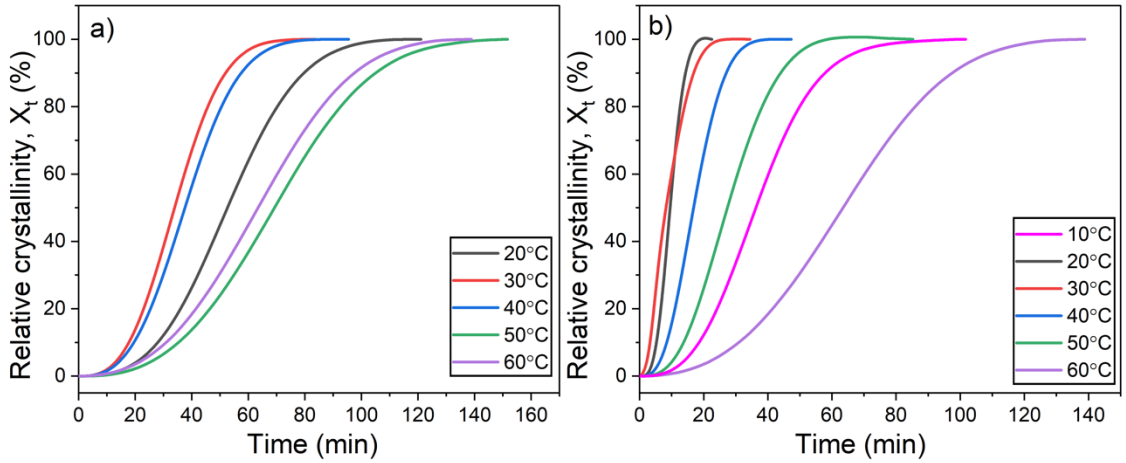

***Figure S3**: Avrami model results for PPeAT60+0.5% Gly and PPeAT60+0.1% HTeO*

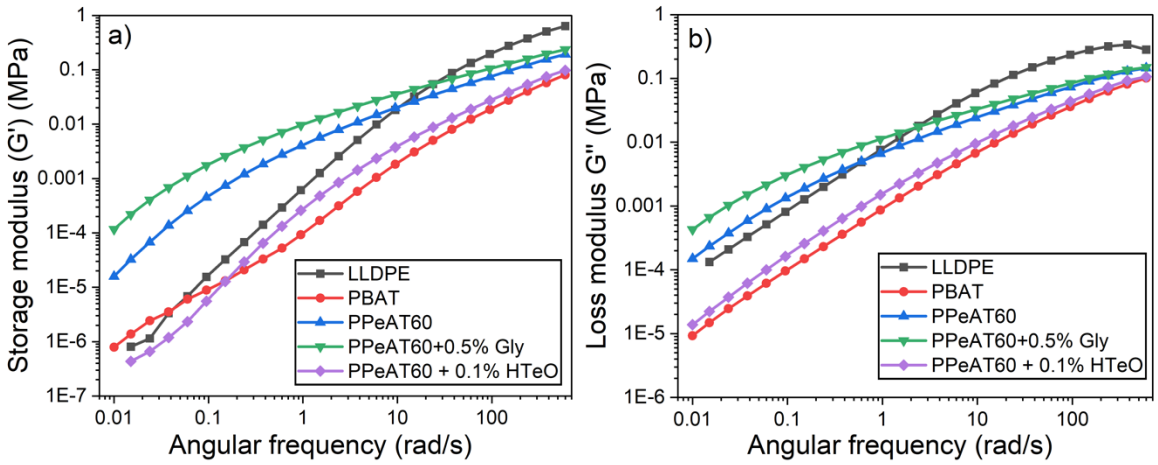

***Figure S4**: Storage modulus and loss modulus for LLDPE, PBAT, PPeAT60, PPeAT60+0.1% HTeO and PPeAT60+0.5% Gly.*

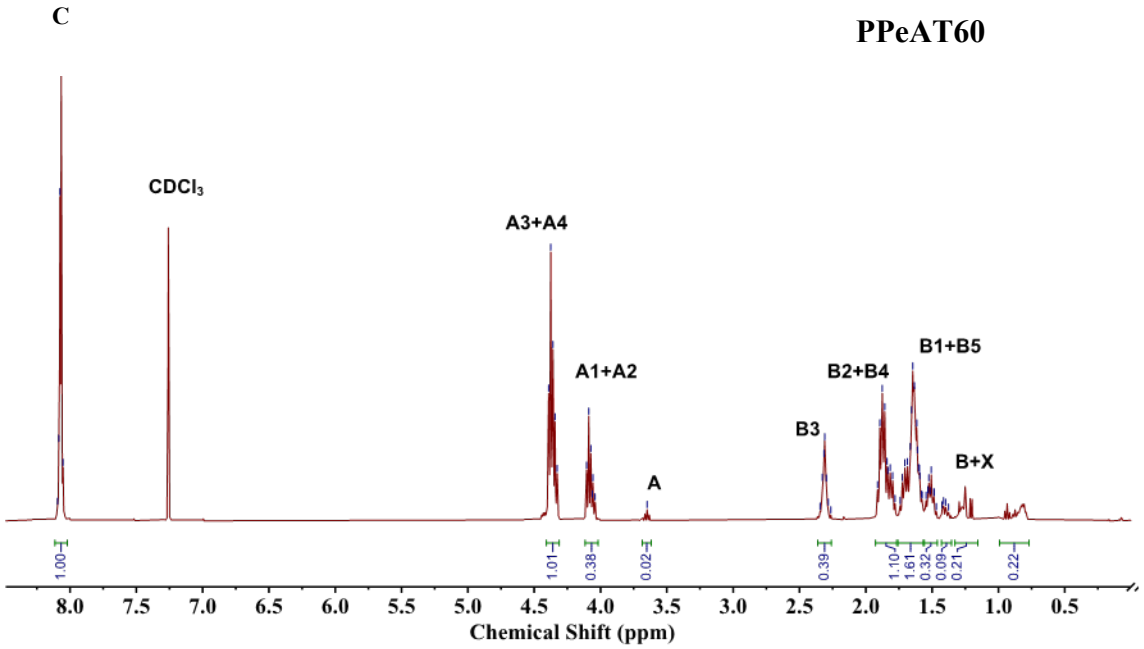

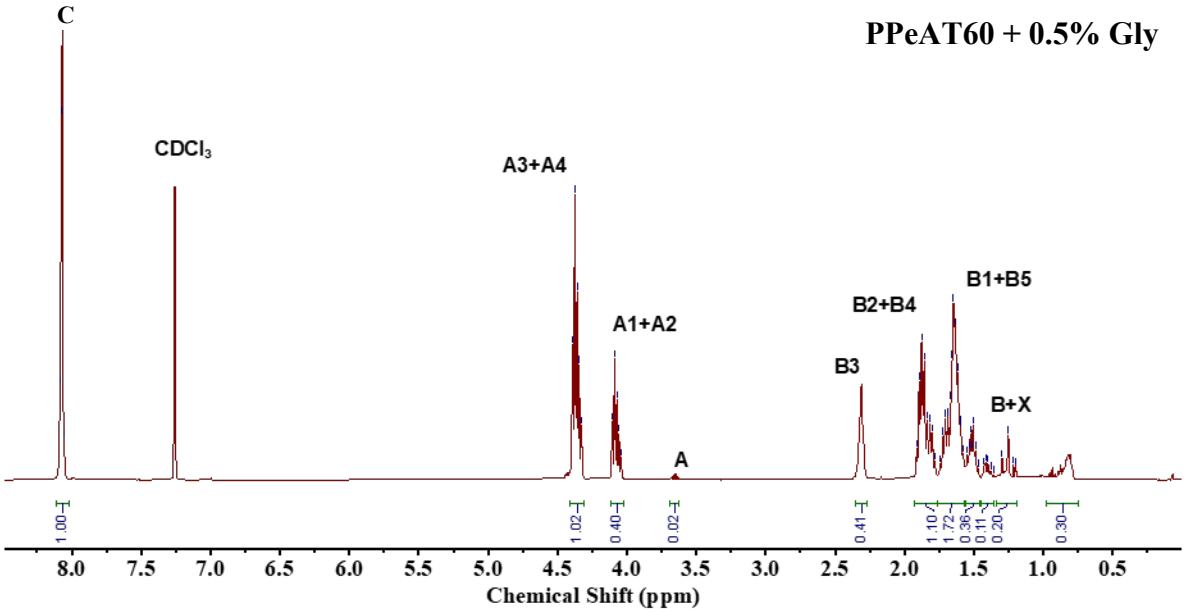
PPeAT60 + 0.5% Gly
C
CDCl3
A3+A4
A1+A2
A
B3
B2+B4
B1+B5
B+X
1.00
1.02
0.40
0.02
0.41
1.10
1.72
0.36
0.11
0.20
0.30
8.0 7.5 7.0 6.5 6.0 5.5 5.0 4.5 4.0 3.5 3.0 2.5 2.0 1.5 1.0 0.5
Chemical Shift (ppm)

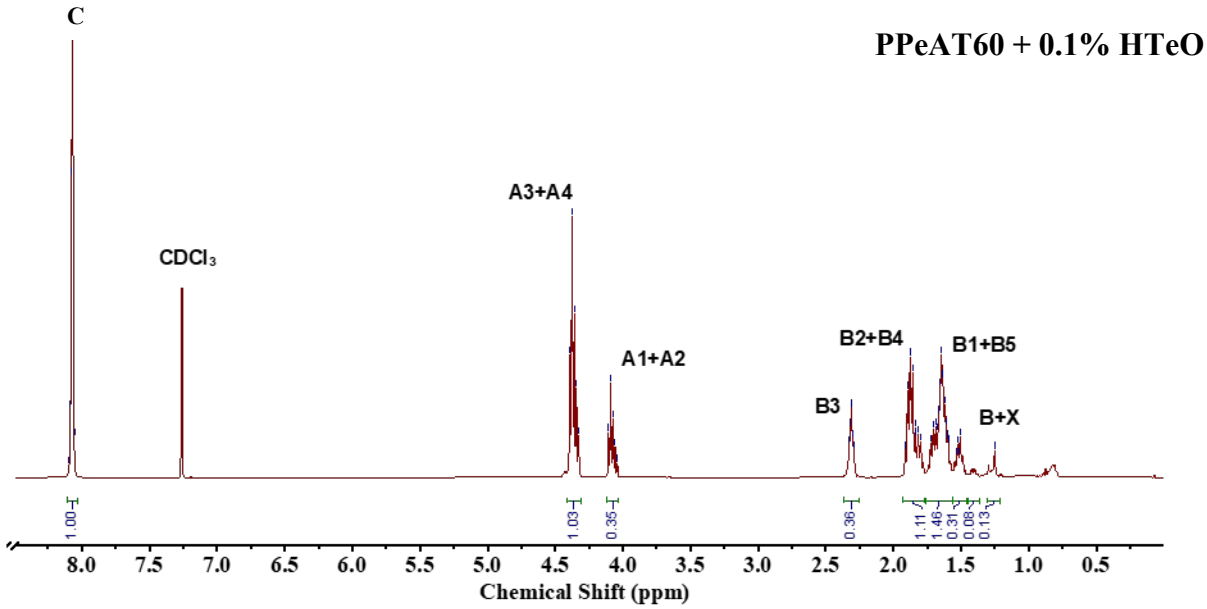
PPeAT60 + 0.1% HTeO
C
CDCl3
A3+A4
A1+A2
B3
B2+B4
B1+B5
B+X
1.00
1.03
0.35
0.36
1.11
1.46
0.31
0.08
0.13
8.0 7.5 7.0 6.5 6.0 5.5 5.0 4.5 4.0 3.5 3.0 2.5 2.0 1.5 1.0 0.5
Chemical Shift (ppm)

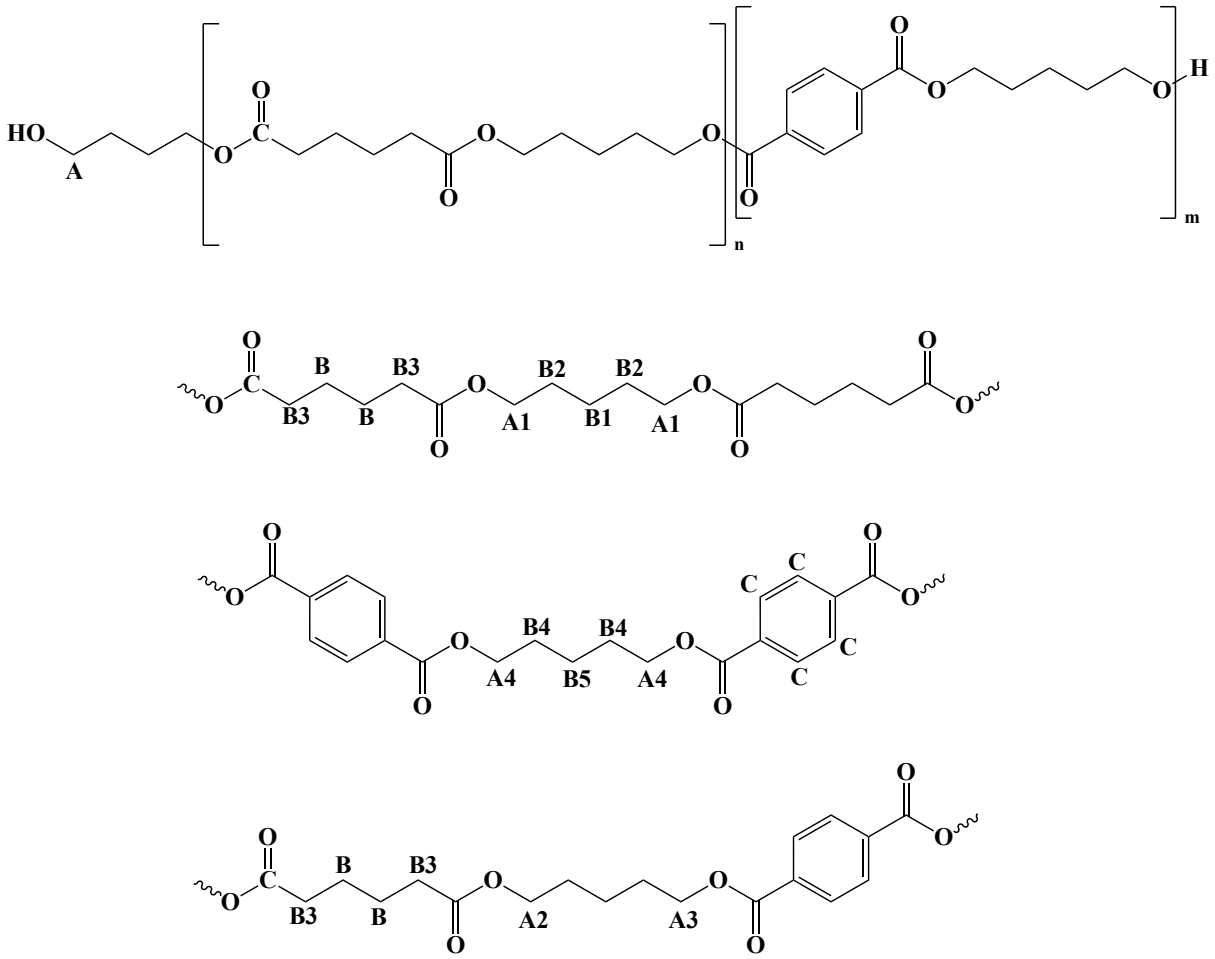

***Figure S5**: NMR Spectra for the PPeAT60 samples and triad assignments*

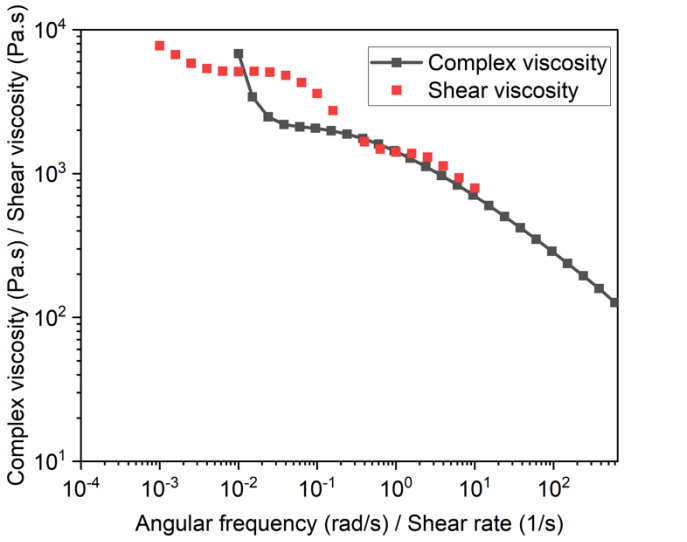

***Figure S6**: Validation of the Cox-Merz rule forPPeAT60 sample*

***Table S1**: List of ionomers used and thermal properties from DSC of PPeAT mixed with 0.05 wt% ionomer.*

Ion	Acid	Cation Neutralization Percentage of Ionomer	MI of Ionomer	T_g	T_c	ΔH_C	$T_{m,1}$	$\Delta H_{m,1}$	$T_{m,2}$
Li	E-MAA[1]	13.1	10.34	-15.3	31.3	15.2	91.1	29.5	91.9
	E-MAA[1]	20.0	5.09	-15.5	33.0	13.7	91.0	24.6	91.6
	E-MAA[2]	20.5	19.21	-16.4	35.0	15.1	90.3	27.4	91.1
	E-MAA[2]	26.2	9.53	-15.8	33.6	16.1	89.6	24.4	91.5
	E-MAA[2]	52.9	0.29	-16.3	32.3	14.3	92.0	27.1	91.7
	E-MAA[2]	57.5	0.2	-15.8	28.7	11.0	89.6	26.4	90.7
Na	E-MAA[1]	20.1	10.54	-16.2	35.7	14.3	89.6	27.1	91.3
	E-MAA[2]	20.6	36.65	-16.0	33.9	13.5	91.4	25.3	91.2
	E-MAA[2]	78.4	1.26	-15.3	30.0	9.3	90.9	28.3	91.5
	E-BA-AA[1]	20.2	23.5	-16.9	35.7	15.9	89.4	27.3	91.0
Mg	E-MAA[1]	20.9	13.81	-16.3	34.3	15.8	90.9	27.2	91.0
	E-MAA[2]	20.4	53.5	-15.7	34.3	14.1	90.1	26.0	92.2
	E-MAA[2]	72.9	0.88	-16.3	32.7	13.4	89.2	27.0	90.6

E-MAA[1] has an MI of 33, E-MAA[2] has an MI of 122. E-BA-AA[1] has an MI of 60.

***Table S2**: Student t-test results for non-isothermal properties (0.05 wt% addition except where noted). Lower numbers represent a greater probability that the samples are different.*

	1st melting temperature ($T_{m,1}$)					
	Li	**Na**	**Mg**	**Acid**	**Neat PPeAT**	**PPeAT + 0.5 wt% Na**
Na	0.70	-	-	-	-	-
Mg	0.45	0.73	-	-	-	-
Acid	0.00	0.00	0.00	-	-	-
Neat PPeAT	0.00	0.00	0.00	0.00	-	-
PPeAT + 0.5 wt% Na	0.00	0.00	0.00	0.01	0.00	-
PPeAT + 0.5 wt% Acid	0.00	0.00	0.00	0.47	0.00	0.02
	2nd melting temperature ($T_{m,2}$)					
	Li	**Na**	**Mg**	**Acid**	**Neat PPeAT**	**PPeAT + 0.5 wt% Na**
Na	0.44	-	-	-	-	-
Mg	0.80	0.96	-	-	-	-
Acid	0.00	0.00	0.00	-	-	-
Neat PPeAT	-	-	-	-	-	-
PPeAT + 0.5 wt% Na	0.00	0.00	0.00	0.03	-	-
PPeAT + 0.5 wt% Acid	0.00	0.00	0.00	0.29	-	0.01
	Crystallization temperature (T_c)					
	Li	**Na**	**Mg**	**Acid**	**Neat PPeAT**	**PPeAT + 0.5 wt% Na**
Na	0.40	-	-	-	-	-
Mg	0.20	1.00	-	-	-	-
Acid	0.00	0.00	0.00	-	-	-
Neat PPeAT	-	-	-	-	-	-
PPeAT + 0.5 wt% Na	0.00	0.00	0.00	0.00	-	-
PPeAT + 0.5 wt% Acid	0.00	0.00	0.00	0.00	-	0.00
	Glass Transition Temperature (T_g)					
	Li	**Na**	**Mg**	**Acid**	**Neat PPeAT**	**PPeAT + 0.5 wt% Na**
Na	0.47	-	-	-	-	-
Mg	0.34	0.95	-	-	-	-
Acid	0.00	0.00	0.00	-	-	-
Neat PPeAT	0.00	0.00	0.00	0.00	-	-
PPeAT + 0.5 wt% Na	0.00	0.00	0.00	0.00	0.00	-
PPeAT + 0.5 wt% Acid	0.00	0.00	0.00	0.40	0.00	0.01
	Enthalpy of Melting ($\Delta H_{m,1}$)					
	Li	**Na**	**Mg**	**Acid**	**Neat PPeAT**	**PPeAT + 0.5 wt% Na**
Na	0.64	-	-	-	-	-
Mg	0.82	0.71	-	-	-	-
Acid	0.00	0.01	0.00	-	-	-
Neat PPeAT	0.00	0.00	0.00	0.00	-	-
PPeAT + 0.5 wt% Na	0.00	0.00	0.00	0.02	0.28	-
PPeAT + 0.5 wt% Acid	0.19	0.34	0.08	0.00	0.00	0.00

	Enthalpy of crystallization (ΔH_c)					
	Li	**Na**	**Mg**	**Acid**	**Neat PPeAT**	**PPeAT + 0.5 wt% Na**
Na	0.56	-	-	-	-	-
Mg	0.87	0.5	-	-	-	-
Acid	0.00	0.03	0.02	-	-	-
Neat PPeAT	-	-	-	-	-	-
PPeAT + 0.5 wt% Na	0.02	0.09	0.07	0.00	-	-
PPeAT + 0.5 wt% Acid	0.01	0.07	0.06	0.00	-	0.17

Table S3*: Student t-test results for isothermal properties (0.05 wt% addition except where noted). Lower numbers represent a greater probability that the samples are different.*

	Half-time crystallization ($t_{1/2}$)			
	Li	**Na**	**Li**	**Acid**
Na	0.04	-	-	-
Mg	0.42	0.02	-	-
Acid	0.00	0.00	0.00	-
Neat PPeAT	0.00	0.00	0.00	0.00
	Rate constant (k)			
	Li	**Na**	**Mg**	**Acid**
Na	0.05	-	-	-
Mg	0.34	0.02	-	-
Acid	0.00	0.00	0.00	-
Neat PPeAT	0.00	0.00	0.02	0.00
	Avrami exponent (n)			
	Li	**Na**	**Mg**	**Acid**
Na	0.84	-	-	-
Mg	0.39	0.65	-	-
Acid	0.00	0.09	0.05	-
Neat PPeAT	0.00	0.01	0.01	0.00

Table S4*: Student t-test results for mechanical properties.*

	Young's modulus (E)		
	Li	**Na**	**Mg**
Na	0.49	-	-
Mg	0.81	0.39	-
	Yield stress (δ_y)		
	Li	**Na**	**Mg**
Na	0.92	-	-
Mg	0.24	0.49	-
	Yield strain (ε_y)		
	Li	**Na**	**Mg**
Na	0.93	-	-
Mg	0.15	0.46	-

	Stress at break (δ_b)		
	Li	**Na**	**Mg**
Na	0.19	-	-
Mg	0.57	0.48	-
	Elongation at break (ε_b)		
	Li	**Na**	**Mg**
Na	0.04	-	-
Mg	0.49	0.09	-
	Tensile toughness (U_t)		
	Li	**Na**	**Mg**
Na	0.09	-	-
Mg	0.35	0.35	-

Table S5*: Student t-test results for mechanical properties of PPeAT + Na ionomer.*

	Young's modulus (E)	
	Neat PPeAT	**PPeAT + 0.05 wt%**
PPeAT + 0.05 wt%	0.07	-
PPeAT + 0.5 wt%	0.05	0.14
	Yield stress (δ_y)	
	Neat PPeAT	**PPeAT + 0.05 wt%**
PPeAT + 0.05 wt%	0.33	-
PPeAT + 0.5 wt%	0.00	0.99
	Yield strain (ε_y)	
	Neat PPeAT	**PPeAT + 0.05 wt%**
PPeAT + 0.05 wt%	0.43	-
PPeAT + 0.5 wt%	0.07	0.13
	Stress at break (δ_b)	
	Neat PPeAT	**PPeAT + 0.05 wt%**
PPeAT + 0.05 wt%	0.00	-
PPeAT + 0.5 wt%	0.10	0.00
	Elongation at break (ε_b)	
	Neat PPeAT	**PPeAT + 0.05 wt%**
PPeAT + 0.05 wt%	0.00	-
PPeAT + 0.5 wt%	0.83	0.00

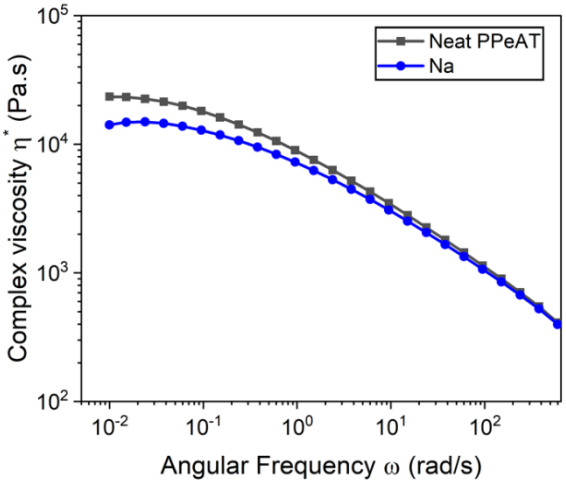

Figure S7*: Complex Viscosity results for neat PPeAT and PPeAT+0.5 wt% Na.*

Appendix B: Fundamentals, Effects, and Modifications of Permeability

Gas permeability in blown films is governed by the ability of gas molecules to diffuse through the polymer matrix, which depends on both the intrinsic properties of the polymer and the processing conditions used to produce the film. The permeability mechanism involves two key steps: the sorption of gas molecules onto the polymer surface, followed by diffusion through the film driven by a concentration gradient [173, 174]. In blown films, the degree of crystallinity, polymer chain packing, polymer chain orientation, and unoccupied volume created during processing significantly influence gas transport [175]. The level of orientation and cooling rate can vary across the film, leading to anisotropic permeability properties. Additionally, the type of polymer, processing conditions, and use of additives can further modulate these factors, allowing manufacturers to tailor permeability for specific applications [174].

Permeability plays a pivotal role in determining the success of materials used in gas barrier applications. High permeability can compromise the material's ability to restrict the diffusion of gases like oxygen or carbon dioxide, leading to potential failures in critical applications [176, 177]. For example, in food and beverage packaging, insufficient gas barrier performance can result in the loss of freshness, reduced shelf life, and compromised product safety. Hence a barrier material (a material with low permeability) is need for packaging applications [176, 177]. Moreover, performance trade-offs are a common challenge when designing films. Enhancing barrier properties often involves increasing the material's crystallinity or incorporating additives, which may compromise mechanical flexibility, transparency, or processability [178]. For instance, a high-barrier polymer may become brittle or difficult to process, limiting its application in flexible packaging [179]. On the other hand, having a low-barrier polymer could have balanced mechanical properties but a very high gas permeability Thus, optimizing permeability must account for the

intricate balance between barrier performance and other functional properties to meet the specific demands of an application [174].

For biodegradable polymers, moisture sensitivity adds another layer of complexity. These materials often exhibit higher permeability to water vapor compared to non-biodegradable alternatives, which can accelerate hydrolytic degradation [174, 175]. While this is advantageous for compostable products designed to degrade in controlled environments, excessive permeability can undermine the longevity of products that require moderate durability, such as agricultural mulch films or short-term food packaging. This highlights the necessity of carefully balancing permeability with the intended lifespan and environmental context of the material [174, 175].

The percent crystallinity and lamellar thickness play critical roles in determining the gas permeability and barrier properties of polymeric materials [180, 181]. Higher percent crystallinity typically enhances barrier properties by creating a more ordered structure that reduces unoccupied volume and the pathways available for gas molecules to diffuse [175]. Similarly, decreased lamellar thickness contributes to improved barrier performance. The finely dispersed thin lamellae within the amorphous matrix can lead to improved overall barrier properties due to optimized crystal distribution and enhanced chain packing in the amorphous regions [180]. Together, these factors reduce the gas permeability, making the material more effective as a barrier [175]. However, the extent of these effects depends on the degree of crystalline alignment, the polymer's chemical composition, and the interaction between the crystalline and amorphous phases [182].

Orientation in the thickness direction significantly enhances the barrier properties of polymeric materials by creating a more tortuous path for gas and moisture diffusion [183]. When polymer chains or crystalline domains are aligned perpendicular to the surface, they act as physical barriers that increase the distance and complexity of the diffusion pathway. This alignment reduces

the overall permeability by minimizing the rate at which molecules can pass through the material. The effect is particularly pronounced in semi-crystalline polymers, where the oriented crystalline regions contribute to denser, less permeable structures [183]. The degree of improvement in barrier performance depends on the level of orientation achieved and the interplay between the crystalline and amorphous phases, as the latter can still provide pathways for diffusion [175].

Additives are one of the most versatile tools for modifying permeability. Fillers, such as crosslinking agents, nano clay, cellulose, chitin, and lignin-based fillers, are widely used in polymer composites to reduce gas and moisture permeability [184-186]. These fillers act by creating a "tortuous path" for diffusing molecules. Instead of passing directly through the polymer, molecules must navigate around these layered or platelet-like structures, significantly increasing the effective diffusion path length [187]. This mechanism drastically reduces permeability, making such composites ideal for applications requiring high barrier properties, such as food packaging, where oxygen and moisture ingress can compromise shelf life [184]. Additionally, these fillers often could enhance mechanical and thermal properties, offering multifunctional benefits [187]. In contrast, the addition of plasticizers increases permeability by disrupting the polymer matrix and increasing unoccupied volume between chains [188]. Plasticizers are small, low-molecular-weight compounds that reduce intermolecular forces and enhance chain mobility [188]. This strategy is useful in applications like breathable membranes or agricultural films, where controlled diffusion of gases like oxygen and carbon dioxide is required. However, care must be taken to avoid excessive plasticization, which can compromise mechanical strength and other critical properties [188].

Processing conditions provide another powerful lever for tailoring and improving the polymer barrier properties. The cooling rate during polymer solidification significantly affects the

material's crystallinity [189]. Quenching, or rapid cooling, often results in an amorphous polymer structure due to the insufficient time for chains to organize into crystalline domains [190]. Amorphous regions are more permeable because they offer more unoccupied volume and less dense molecular packing [175]. This approach can be applied to create materials where permeability is desired, such as in gas-permeable membranes. Conversely, slow cooling allows the polymer chains more time to align and form crystalline regions, which are denser and less permeable [189]. Annealing further enhances this effect by exposing the polymer to controlled temperatures just below its melting point [191]. This thermal treatment reorganizes amorphous regions into crystalline domains, significantly improving barrier properties by reducing the unoccupied volume available for molecular diffusion [191]. Therefore, the compression-molded sheets exhibit lower gas permeability and water vapor transmission rates compared to blown films. This difference arises from the significantly slower cooling rate of compression-molded sheets, which occurs over hours, whereas blown films cool within minutes or even seconds [157].

The polydispersity index (PDI), which measures the distribution of molecular weights within a polymer, significantly affects gas permeability by influencing the polymer's structural characteristics [192]. A high PDI, indicating a broader molecular weight distribution, often leads to increased chain entanglements and varied packing densities within the polymer matrix. Longer polymer chains in a high-PDI system can enhance entanglements, reducing segmental mobility and decreasing the unoccupied volume available for gas diffusion [193]. This tighter packing hinders gas permeability [192]. Furthermore, in semi-crystalline polymers, a wide molecular weight distribution may promote the formation of denser or more heterogeneous crystalline regions, further extending the tortuous path for gas molecules and improving barrier properties [192]. Conversely, in some cases, a high PDI can create irregularities if low molecular weight

chains act as plasticizers, potentially increasing permeability [194]. Thus, the impact of PDI on gas permeability is complex and depends on the balance between these competing effects and the intrinsic properties of the polymer.

Given the aforementioned, the observed decrease in gas permeability and water vapor transmission rate of CM PPeAT60 compared to CM PBAT can be attributed to several factors. The first factor is lamellar thickness. While PBAT exhibits a percent crystallinity that is 16% higher than that of PPeAT60, the lamellar thickness of PPeAT60 is 41% lower. This reduced lamellar thickness contributes to a more compact structure, creating a more tortuous path for gas and moisture diffusion. The second factor is the use of a nucleating agent. Additives such as nucleating agents reduce crystal size while increasing the number of crystals, further enhancing the tortuous diffusion pathway. Specifically, the addition of nucleating agents reduced the lamellar thickness of PPeAT60 from 18.9 Å (neat) to 15.9 Å (nucleated), resulting in a decrease in oxygen and carbon dioxide permeability from 0.3 and 2.6 Barrer (neat) to 0.25 and 2.25 Barrer (nucleated), respectively. It's worth mentioning that PBAT does not have a nucleating agent. However, these factors alone cannot fully explain the four-fold reduction in oxygen and carbon dioxide permeability, suggesting additional mechanisms may be at play. This suggest that the improvement in barrier properties of PPeAT60 compared to PBAT is mainly due to PDI and orientation. The nucleated PPeAT60 is a combination of 15 different reaction yielding different molecular weights and hence different PDI. An average PDI was found to be 3.13 which is almost double the PDI of PBAT (1.6). That double in PDI could be a major factor in barrier properties improvement. Finally, orientation in the thickness direction plays a huge rule in barrier properties improvement. It was previously seen that increased orientation in the thickness direction could result in a reduction of barrier properties by as much as 50%. The reduction due to thickness orientation coupled with the

effect of lamellar thickness, nucleating agent and PDI could lead to the 4 folds improvement in barrier properties compared with PBAT.

Appendix C: Fundamentals, Effects, and Modifications of Orientation

Orientation in polymers refers to the alignment of polymer chains in a specific direction, which can occur in either the amorphous or crystalline regions of the material. In amorphous phases, orientation involves aligning polymer chains without forming a regular lattice, while in crystalline phases, it refers to the alignment of ordered crystallites [195]. This alignment significantly influences the material's macroscopic properties, as it changes the internal structure and alters the way the polymer interacts with external forces, light, and thermal energy [196, 197]. Orientation is a key factor in tailoring the performance of polymer-based products to meet specific application requirements.

Orientation is primarily developed during processing methods such as stretching, blowing, and extrusion. For instance, in processes like film blowing, the polymer is subjected to biaxial stretching, which aligns the chains in both the machine direction (MD) and transverse direction (TD). Similarly, during extrusion or fiber spinning, uniaxial stretching causes alignment in the machine direction. The degree of orientation depends on factors such as processing temperature, strain rate, and the intrinsic properties of the polymer [198, 199]. These methods effectively stretch the polymer chains, aligning them to enhance certain properties while compromising others.

Orientation plays a critical role in determining the mechanical properties of a polymer. Aligned crystalline regions, formed through processes like stretching or drawing, result in increased stiffness and tensile strength along the orientation direction. This occurs because the alignment enhances intermolecular interactions and restricts chain mobility, allowing the material to better resist deformation under stress. However, this improvement in strength often comes at the expense of elongation and flexibility [198]. Highly oriented polymers become brittle and are more prone to cracking or failure in directions perpendicular to the orientation. As such,

controlling the degree of orientation is crucial for applications that require a balance between strength and ductility, such as packaging films or fibers [200].

As previously mentioned**,** orientation also influences the barrier properties of polymers, particularly gas and moisture permeability. Increased orientation reduces permeability along the oriented direction by creating a more tortuous path for gas molecules, especially in semi-crystalline polymers where aligned crystalline domains act as impermeable barriers. However, in certain cases, excessive orientation may introduce defects or inconsistencies in the amorphous regions, which could slightly offset the improvements in barrier performance [183]. The effect of orientation on barrier properties is particularly critical for applications like food packaging, where maintaining low permeability is essential.

The optical properties of polymers, such as birefringence and haze, are also affected by orientation [201]. Birefringence arises when light travels through a material with different refractive indices along different axes, a phenomenon common in oriented films due to the alignment of polymer chains [201]. Orientation can reduce haze by aligning the polymer chains to minimize scattering at interfaces, enhancing clarity in films [202]. However, uneven orientation or excessive alignment may cause optical distortions, requiring careful control during processing [202].

One of the most effective ways to control orientation is by adjusting processing parameters during techniques like film blowing or extrusion. In film blowing, the blow-up ratio (BUR) and take-up ratio (TUR) directly influence the degree of biaxial stretching, allowing precise control over the alignment of polymer chains in both the MD and TD [203]. Similarly, in extrusion, optimizing drawing speeds ensures uniform orientation along the MD while minimizing defects or

uneven stress distributions. These adjustments can help achieve balanced mechanical strength, barrier properties, and optical clarity across the product [203].

Thermal treatments such as annealing are another strategy to modify orientation. By heating the polymer to a temperature below its melting point but above its glass transition temperature, oriented amorphous chains can relax, reducing internal stresses and balancing the alignment [204]. This process not only mitigates brittleness caused by excessive orientation but also enhances dimensional stability and barrier properties. Controlled annealing is particularly useful in semi-crystalline polymers where balancing crystalline and amorphous alignment is critical [204].

In summary, despite similar processing conditions and structures, subtle differences in crystallization behavior can result in significant variations in the degree of orientation. For example, while the addition of a nucleating agent to PPeAT60 improved its crystallization kinetics by five orders of magnitude, PBAT still exhibits a faster overall crystallization rate. The slower crystallization of PPeAT60 allows polymer chains more time to align under processing stresses, leading to a higher degree of orientation. In contrast, PBAT's rapid crystallization tends to lock the molecular structure into place more quickly, limiting the extent of chain alignment during processing. The degree of orientation for extruded sheets and blown films of PPeAT60 was observed to be higher than that of PBAT. Additionally, it was observed that PPeAT60 have a strong orientation in the MD compared with the TD. The percent of crystallinity in the MD was found to be 15% compared to only 5% in the TD. Hence, the polymer chains in the crystalline region are aligned in the MD rather than the TD. However, for PBAT, orientation in both the MD and in the TD can be observed. Both the MD and TD have a similar percent of crystallinity therefore the polymer chains in the crystalline region are aligned in both MD and TD. PBAT shows

a biaxial orientation while PPeAT60 tend more towards a uniaxial orientation. That could explain the small difference in permeability between CM PBAT and blown film PBAT compared with the larger difference in permeability between CM PPeAT60 and blown PPeAT60.

Appendix D: Processing Aids for Film Blowing

Processing aids are essential additives used in polymer film production to enhance manufacturability, improve efficiency, and achieve desired film properties. They optimize the performance of polymers during processing, such as extrusion or molding, by addressing issues like friction, blocking, melt flow and thermal degradation. Among the critical types of processing aids are slip agents, anti-blocking agents, lubricants, and antioxidants, each serving a unique function [205].

Slip agents are incorporated into polymer films to reduce the coefficient of friction (COF) between polymer layers or between the film and processing equipment. By lowering friction, these agents facilitate smoother film movement during handling and post-processing operations, such as printing or sealing. Fatty acid amides, such as erucamide and oleamide, are commonly used slip agents. They migrate to the film's surface, creating a lubricating layer that minimizes sticking and scratch, ensuring efficiency in high-speed production lines [206, 207].

Anti-blocking agents prevent adjacent layers of polymer film from adhering to each other after winding. Blocking occurs due to the smooth surfaces of polymer films creating a vacuum or adhesive force when in contact, particularly under pressure or high temperatures. Anti-blocking agents, such as silica, talc, or other fine inorganic particles, create microscopic surface roughness, reducing contact area and preventing sticking. This ensures easy unwinding and separation of films during subsequent operations [206, 207]. Additionally, organic waxes, amides, stearates, silicones, and polytetrafluoroethylene could be used as organic anti-blocking agents [207].

Lubricants improve the flow properties of polymer melts during extrusion by reducing viscosity and internal friction within the melt. These additives enable smoother processing, lower energy consumption, and reduced wear on equipment. Common examples include waxes,

stearates, and low-molecular-weight polyethylene. By enhancing melt flow, lubricants also help achieve uniform thickness and surface quality in polymer films, contributing to consistent product performance.

Antioxidants are vital processing aids in the film-blowing process, protecting polymers from thermal and oxidative degradation during high-temperature extrusion [208]. The intense heat and mechanical shear involved in film blowing can break down polymer chains, leading to discoloration, loss of mechanical properties, and reduced film quality. Antioxidants prevent these issues by neutralizing free radicals and decomposing peroxides formed during processing [209]. Primary antioxidants, such as hindered phenols, interrupt free-radical chain reactions, while secondary antioxidants, like phosphites and thioesters, decompose hydroperoxides into stable, non-reactive compounds [209]. By maintaining polymer stability, antioxidants enable smoother processing, enhance film durability, and extend the shelf life of finished products.

References

1. Wakefield, F., *Top 25 Recycling Facts and Statistics for 2022*, in *EcoWatch*. 2022.

2. Mikulec, V., et al., *Green Techniques for Detecting Microplastics in Marine with Emphasis on FTIR and NIR Spectroscopy—Short Review.* Processes, 2023. **11**(8). doi: 10.3390/pr11082360

3. MacKerron, C., K. McBee, and D. Shugar. *Waste and Opportunity 2020: Searching for Corporate Leadership*. 2020; Available from: https://www.asyousow.org/report-page/waste-and-opportunity-2020-searching-corporate-leadership.

4. Freitag, N., et al., *Waste Study on Flexible Food and Non-Food Packaging: Detailed Analysis of the Plastic Composition of European Polyethylene-Containing Waste Streams.* Materials (Basel), 2024. **17**(13). doi: 10.3390/ma17133202

5. Bauer, A.S., et al., *Recyclability and Redesign Challenges in Multilayer Flexible Food Packaging-A Review.* Foods, 2021. **10**(11). doi: 10.3390/foods10112702

6. Nanda, S., et al., *Innovations in applications and prospects of bioplastics and biopolymers: a review.* Environ Chem Lett, 2022. **20**(1): p. 379-395. doi: 10.1007/s10311-021-01334-4

7. Rosenboom, J.G., R. Langer, and G. Traverso, *Bioplastics for a circular economy.* Nat Rev Mater, 2022. **7**(2): p. 117-137. doi: 10.1038/s41578-021-00407-8

8. Babaremu, K., O.P. Oladijo, and E. Akinlabi, *Biopolymers: A suitable replacement for plastics in product packaging.* Advanced Industrial and Engineering Polymer Research, 2023. **6**(4): p. 333-340. doi: 10.1016/j.aiepr.2023.01.001

9. Onen Cinar, S., et al., *Bioplastic Production from Microalgae: A Review.* Int J Environ Res Public Health, 2020. **17**(11). doi: 10.3390/ijerph17113842

10. Gross, R.A. and B. Kalra, *Biodegradable Polymers for the Environment.* Science, 2002. **297**(5582): p. 3811-3818. doi: 10.1126/science.297.5582.803

11. Foujji, L.E., A.e.k. Qaiss, and R. Bouhfid, *Advanced biodegradable polymer nanocomposites for rechargeable lithium and sodium-ion battery applications*, in *Biodegradable and Biocompatible Polymer Nanocomposites*. 2023, Elsevier. p. 353-395.

12. Pires, J.R.A., et al., *Methodologies to Assess the Biodegradability of Bio-Based Polymers-Current Knowledge and Existing Gaps.* Polymers (Basel), 2022. **14**(7). doi: 10.3390/polym14071359

13. Shen, L., E. Worrell, and M. Patel, *Present and future development in plastics from biomass.* Biofuels, Bioproducts and Biorefining, 2010. **4**(1): p. 25-40. doi: 10.1002/bbb.189

14. Righetti, G.I.C., F. Faedi, and A. Famulari, *Embracing Sustainability: The World of Bio-Based Polymers in a Mini Review.* Polymers (Basel), 2024. **16**(7). doi: 10.3390/polym16070950

15. Wang, Y., et al., *Polyester biodegradability: importance and potential for optimisation.* Green Chem, 2024. **26**(7): p. 3698-3716. doi: 10.1039/d3gc04489k

16. Philp, J. and R. Atlas, *Microbial Resources for Global Sustainability*, in *Microbial Resources*, I. Kurtböke, Editor. 2017, Elsevier p. 77-101.

17. Ramlee, N.A. and Y. Tominaga, *Preparation and characterization of poly(ethylene carbonate)/poly(lactic acid) blends.* Journal of Polymer Research, 2018. **25**(2). doi: 10.1007/s10965-018-1451-4

18. Acemoglu, M., et al., *Poly(ethylene carbonate)s, part I: Syntheses and structural effects on biodegradation.* Journal of Controlled Release, 1997. **49**(2-3): p. 263-276. doi: 10.1016/S0168-3659(97)00097-7

19. Bhagia, S., et al., *Terephthalic Acid Copolyesters Containing Tetramethylcyclobutanediol for High-Performance Plastics.* ChemistryOpen, 2021. **10**(8): p. 830-841. doi: 10.1002/open.202100171

20. Singh, A.K., R. Bedi, and B.S. Kaith, *Composite materials based on recycled polyethylene terephthalate and their properties – A comprehensive review.* Composites Part B: Engineering, 2021. **219**. doi: 10.1016/j.compositesb.2021.108928

21. Turner, S.R. and Y. Liu, *Chemistry and Technology of Step-Growth Polyesters*, in *Polymer Science: A Comprehensive Reference*. 2012, Elsevier. p. 311-331.

22. Roy, S., et al., *Recent progress in PBAT-based films and food packaging applications: A mini-review.* Food Chemistry, 2024. **437**. 137822. doi: 10.1016/j.foodchem.2023.137822

23. Jian, J., Z. Xiangbin, and H. Xianbo, *An overview on synthesis, properties and applications of poly(butylene-adipate-co-terephthalate)–PBAT.* Advanced Industrial and Engineering Polymer Research, 2020. **3**(1): p. 19-26. doi: 10.1016/j.aiepr.2020.01.001

24. Sokolsky-Papkov, M., R. Langer, and A.J. Domb, *Synthesis of aliphatic polyesters by polycondensation using inorganic acid as catalyst.* Polym Adv Technol, 2011. **22**(5): p. 502-511. doi: 10.1002/pat.1541

25. Zorba, T., et al., *Synthesis, characterization and thermal degradation mechanism of three poly(alkylene adipate)s: Comparative study.* Polymer Degradation and Stability, 2007. **92**(2). doi: 10.1016/j.polymdegradstab.2006.11.009

26. Goldberg, I. and J.S. Rokem, *Organic and Fatty Acid Production, Microbial*, in *Encyclopedia of Microbiology*, M. Schaechter, Editor. 2009, Elsevier. p. 421-442.

27. Zhao, X., et al., *Sustainable bioplastics derived from renewable natural resources for food packaging.* Matter, 2023. **6**(1): p. 97-127. doi: 10.1016/j.matt.2022.11.006

28. Chen, G.Q. and M.K. Patel, *Plastics derived from biological sources: present and future: a technical and environmental review.* Chem Rev, 2012. **112**(4): p. 2082-99. doi: 10.1021/cr200162d

29. Swetha, T.A., et al., *A comprehensive review on polylactic acid (PLA) – Synthesis, processing and application in food packaging.* International Journal of Biological Macromolecules, 2023. **234**. 123715. doi: 10.1016/j.ijbiomac.2023.123715

30. Aliotta, L., et al., *A Brief Review of Poly (Butylene Succinate) (PBS) and Its Main Copolymers: Synthesis, Blends, Composites, Biodegradability, and Applications.* Polymers (Basel), 2022. **14**(4). 844. doi: 10.3390/polym14040844

31. Lu, J., et al., *Biobased 1,5-pentanediol derived aliphatic-aromatic copolyesters: Synthesis and thermo-mechanical properties of poly(pentylene succinate-co-terephthalate)s and poly(pentylene adipate-co-terephthalate)s.* Polymer Degradation and Stability, 2019. **163**: p. 68-75. doi: 10.1016/j.polymdegradstab.2019.02.010

32. Lu, J., L. Wu, and B.-G. Li, *High Molecular Weight Polyesters Derived from Biobased 1,5-Pentanediol and a Variety of Aliphatic Diacids: Synthesis, Characterization, and Thermo-Mechanical Properties.* ACS Sustainable Chemistry & Engineering, 2017. **5**(7): p. 6159-6166. doi: 10.1021/acssuschemeng.7b01050

33. Ali Hussain Motagamwala, W.W., Canan Sener, David Martin Alonso, Christos T. Maravelias, James A. Dumesic, *Toward biomass-derived renewable plastics: Productionof 2,5-furandicarboxylic acid from fructose.* Science Advances, 2018. **4**. doi: 10.1126/sciadv.aap9722

34. Pandey, S., et al., *Biobased 2,5-furandicarboxylic acid (FDCA) and its emerging copolyesters' properties for packaging applications.* European Polymer Journal, 2021. **160**. 110778. doi: 10.1016/j.eurpolymj.2021.110778

35. Terzopoulou, Z., et al., *Biobased poly(ethylene furanoate-co-ethylene succinate) copolyesters: solid state structure, melting point depression and biodegradability.* RSC Advances, 2016. **6**(87): p. 84003-84015. doi: 10.1039/c6ra15994j

36. Bianchi, E., et al., *Poly(butylene 2,4-furanoate), an Added Member to the Class of Smart Furan-Based Polyesters for Sustainable Packaging: Structural Isomerism as a Key to Tune the Final Properties.* ACS Sustain Chem Eng, 2021. **9**(35): p. 11937-11949. doi: 10.1021/acssuschemeng.1c04104

37. Wang, G. and J. Wang, *1,12-Dodecanediol-Based Polyesters Derived from Aliphatic Diacids with Even Carbons: Synthesis and Characterization.* Journal of Polymers and the Environment, 2023. **31**(11): p. 4770-4783. doi: 10.1007/s10924-023-02884-0

38. Shan-Chi Hsieh, J.-H.W., Yu-Chen Lai, Ching-Yeuh Su, Kung-Ta Lee, *Production of 1-Dodecanol, 1-Tetradecanol, and 1,12 Dodecanediol through whole-Cell Biotransformation in Escherichia coli.* Applied and Environmental Microbiology, 2018. **84**(4). doi: 10.1128/AEM

39. Wang, G., et al., *Bio-Based Poly(Butylene succinate-co-dodecylene succinate) Derived from 1,12-Dodecanediol: Synthesis and Characterization.* Journal of Polymers and the Environment, 2023. **31**(11): p. 4990-5002. doi: 10.1007/s10924-023-02916-9

40. Aouay, M., et al., *Biobased nucleation agents for poly-L-(lactic acid) - Effect on crystallization, rheological and mechanical properties.* Int J Biol Macromol, 2022. **218**: p. 588-600. doi: 10.1016/j.ijbiomac.2022.07.069

41. Cheng, Y., et al., *A new class of nucleating agents for poly(L-lactic acid): Environmentally-friendly metal salts with biomass-derived ligands and advanced nucleation ability.* Int J Biol Macromol, 2023. **225**: p. 1599-1606. doi: 10.1016/j.ijbiomac.2022.11.216

42. Saeidlou, S., et al., *Poly(lactic acid) crystallization.* Progress in Polymer Science, 2012. **37**(12): p. 1657-1677. doi: 10.1016/j.progpolymsci.2012.07.005

43. Agboola, O., E.R. Sadiku, and T. Mokrani, *Chapter 10 - Carbon Containing Nanostructured Polymer Blends*, in *Design and Applications of Nanostructured Polymer Blends and Nanocomposite Systems*, S. Thomas, R. Shanks, and S. Chandrasekharakurup, Editors. 2016, William Andrew Publishing: Boston. p. 187-213.

44. Jiang, X.L., et al., *Effect of nucleating agents on crystallization kinetics of PET.* Express Polymer Letters, 2007. **1**(4): p. 245-251. doi: 10.3144/expresspolymlett.2007.37

45. Haubruge, H.G., et al., *Epitaxial Nucleation of Poly(ethylene terephthalate) by Talc: Structure at the Lattice and Lamellar Scales.* Macromolecules, 2003. **36**(12): p. 4452-4456. doi: 10.1021/ma0341723

46. Furushima, Y., et al., *Crystallization kinetics of poly(butylene terephthalate) and its talc composites.* Journal of Applied Polymer Science, 2017. **134**(16). 44739. doi: 10.1002/app.44739

47. Aliotta, L., et al., *Improvement of the PLA Crystallinity and Heat Distortion Temperature Optimizing the Content of Nucleating Agents and the Injection Molding Cycle Time.* Polymers (Basel), 2022. **14**(5): p. 977-993. 977. doi: 10.3390/polym14050977

48. Hao, Y.P., et al., *Roles of physical filling and chemical crosslinking on the physico-mechanical properties of polylactic acid.* Journal of Applied Polymer Science, 2022. **139**(34). e52808. doi: 10.1002/app.52808

49. Helanto, K., R. Talja, and O.J. Rojas, *Effects of talc, kaolin and calcium carbonate as fillers in biopolymer packaging materials.* Journal of Polymer Engineering, 2021. **41**(9): p. 746-758. doi: 10.1515/polyeng-2021-0076

50. Raquez, J.M., et al., *Novel High-Performance Talc/Poly[(butylene adipate)-co-terephthalate] Hybrid Materials.* Macromolecular Materials and Engineering, 2008. **293**(4): p. 310-320. doi: 10.1002/mame.200700352

51. Zhou, Y., et al., *Preparation and Rheological and Mechanical Properties of Poly(butylene succinate)/Talc Composites for Material Extrusion Additive Manufacturing.* Macromolecular Materials and Engineering, 2019. **304**(7). 1900021. doi: 10.1002/mame.201900021

52. Sun, B., et al., *Effect of different amounts of modified talc on the mechanical, thermal, and crystallization properties of poly(butylene succinate).* Journal of Polymer Engineering, 2014. **34**(4): p. 379-385. doi: doi:10.1515/polyeng-2013-0229

53. Wu, W., et al., *Polylactide/halloysite nanotube nanocomposites: Thermal, mechanical properties, and foam processing.* Journal of Applied Polymer Science, 2013. **130**(1): p. 443-452. doi: 10.1002/app.39179

54. Li, X., et al., *Effect of surface property of halloysite on the crystallization behavior of PBAT.* Applied Clay Science, 2018. **157**: p. 218-226. doi: 10.1016/j.clay.2018.02.005

55. Kaseem, M., et al., *A Review on Synthesis, Properties, and Applications of Polylactic Acid/Silica Composites.* Polymers (Basel), 2021. **13**(18). 3036. doi: 10.3390/polym13183036

56. Yao, X., et al., *Non-Isothermal Crystallization Kinetics of Poly(Butylene Terephthalate)/Silica Nanocomposites.* Journal of Macromolecular Science, Part B, 2009. **48**(3): p. 537-549. doi: 10.1080/00222340902837642

57. Vassiliou, A.A., et al., *Effect of evolved interactions in poly(butylene succinate)/fumed silica biodegradablein situprepared nanocomposites on molecular weight, material properties, and biodegradability.* Journal of Applied Polymer Science, 2011. **119**(4): p. 2010-2024. doi: 10.1002/app.32887

58. Aslan, M., et al., *Physio-mechanical Characterization and Thermal Property Evaluation of Polylactic Acid/Waste Hazelnut Shell Flour Composite with Inorganic Additives.* Journal of Testing and Evaluation, 2023. **51**(5). 20220435. doi: 10.1520/jte20220435

59. Teamsinsungvon, A., C. Ruksakulpiwat, and Y. Ruksakulpiwat, *Effects of Titanium-Silica Oxide on Degradation Behavior and Antimicrobial Activity of Poly (Lactic Acid) Composites.* Polymers (Basel), 2022. **14**(16). 3310. doi: 10.3390/polym14163310

60. Petchwattana, N., S. Covavisaruch, and S. Petthai, *Influence of talc particle size and content on crystallization behavior, mechanical properties and morphology of poly(lactic acid).* Polymer Bulletin, 2014. **71**(8): p. 1947-1959. doi: 10.1007/s00289-014-1165-7

61. Lin, X., et al., *Non-isothermal crystallization kinetics of poly(ethylene terephthalate)/mica composites.* Polymer Bulletin, 2014. **71**(9): p. 2287-2301. doi: 10.1007/s00289-014-1187-1

62. Cayuela, D., et al., *Effect of different dispersing agents in the non-isothermal kinetics and thermomechanical behavior of PET/TiO2 composites.* Journal of Macromolecular Science, Part A, 2016. **53**(4): p. 237-244. doi: 10.1080/10601325.2016.1143321

63. M. L. Di Lorenzo, M.E.E., M. Avella *Thermal and morphological characterization of poly(ethylene terephthalate)/calcium carbonate nanocomposites.* Journal of Materials Science, 2002. **37**: p. 2351-2358. doi: https://doi.org/10.1023/A:1015358425449

64. Sperling, L.H. and L.W. Barrett. Nucleating agents for poly(ethylene terephthalate). 1994. 5,356,972. Istituto Guido Donegani S.p.A., Novara; Emichen S.p.A., Milan

65. Gilmer, J.W., et al., *The use of sodium salts as nucleation agents for polyethylene terephthalate with minimal molecular weight reduction.* Polymer Engineering & Science, 2004. **35**(17): p. 1407-1412. doi: 10.1002/pen.760351712

66. Gao, X., et al., *Crystallization and morphology of poly(ethylene-2,6-naphthalene dicarboxylate) in the presence of nucleating agents.* Journal of Polymer Science Part B: Polymer Physics, 2002. **40**(20): p. 2387-2394. doi: 10.1002/polb.10296

67. Ye, M., et al., *Fast Crystallization Of Poly(Ethylene Terephthalate).* Journal of Thermal Analysis, 1996. **46**: p. 905-920. doi: 10.1007/BF01983610

68. Garcia, D., *Heterogeneous nucleation of poly(ethylene terephthalate).* Journal of Polymer Science: Polymer Physics Edition, 1984. **22**(12): p. 2063-2072. doi: 10.1002/pol.1984.180221206

69. Zhao, X., et al., *Crystallization behaviors regulations and mechanical performances enhancement approaches of polylactic acid (PLA) biodegradable materials modified by organic nucleating agents.* International Journal of Biological Macromolecules, 2023. **233**. 123581. doi: 10.1016/j.ijbiomac.2023.123581

70. Najafi, N., M.C. Heuzey, and P.J. Carreau, *Crystallization behavior and morphology of polylactide and PLA/clay nanocomposites in the presence of chain extenders.* Polymer Engineering & Science, 2012. **53**(5): p. 1053-1064. doi: 10.1002/pen.23355

71. Tang, Z., et al., *The crystallization behavior and mechanical properties of polylactic acid in the presence of a crystal nucleating agent.* Journal of Applied Polymer Science, 2011. **125**(2): p. 1108-1115. doi: 10.1002/app.34799

72. Liu, S., Y. He, and J.-P. Qu, *Manufacturing High-Performance Polylactide by Constructing 3D Network Crystalline Structure with Adding Self-Assembly Nucleator.* Industrial & Engineering Chemistry Research, 2022. **61**(13): p. 4567-4578. doi: 10.1021/acs.iecr.2c00133

73. Nagarajan, V., A.K. Mohanty, and M. Misra, *Crystallization behavior and morphology of polylactic acid (PLA) with aromatic sulfonate derivative.* Journal of Applied Polymer Science, 2016. **133**(28). 43673. doi: 10.1002/app.43673

74. Jang, J., J.H. Oh, and S.I. Moon, *Crystallization Behavior of Poly(ethylene terephthalate) Blended with Hyperbranched Polymers: The Effect of Terminal Groups and Composition of Hyperbranched Polymers.* Macromolecules, 2000. **33**(5): p. 1864-1870. doi: 10.1021/ma991592c

75. Zhang, W., et al., *Poly(maleic acid-co-acrylic acid) ionomer as nucleating agent on the crystallization behavior and properties of poly(ethylene terephthalate).* Polymer Bulletin, 2021. **79**(6): p. 3803-3827. doi: 10.1007/s00289-021-03672-3

76. Ye, L., et al., *Nanohybrid Polymeric Nucleating Agents: In Situ Decorated Carbon Nanotubes and Serial Nucleation Behaviors in a Melt-Miscible Crystalline/Crystalline Blend.* Macromolecular Chemistry and Physics, 2015. **216**(17): p. 1801-1807. doi: 10.1002/macp.201500196

77. Yeh, J.-T., et al., *Study on the Crystallization Kinetic and Characterization of Poly(lactic acid) and Poly(vinyl alcohol) Blends.* Polymer-Plastics Technology and Engineering, 2008. **47**(12): p. 1289-1296. doi: 10.1080/03602550802497958

78. Yeh, J.-T., et al., *Study on the Crystallization, Miscibility, Morphology, Properties of Poly(lactic acid)/Poly(ε-caprolactone) Blends.* Polymer-Plastics Technology and Engineering, 2009. **48**(6): p. 571-578. doi: 10.1080/03602550902824390

79. Guo, X., et al., *Effects of Polyoxymethylene as a Polymeric Nucleating Agent on the Isothermal Crystallization and Visible Transmittance of Poly(lactic acid).* Industrial & Engineering Chemistry Research, 2014. **53**(43): p. 16754-16762. doi: 10.1021/ie502104y

80. Niyomsin, S., et al., *Synergistic effects of a novel multi-branched polylactide ionomer on polylactide film.* MRS Communications, 2022. **12**(2): p. 160-167. doi: 10.1557/s43579-022-00155-y

81. Ye, H.-M., et al., *Isomorphism in Poly(butylene succinate-co-butylene fumarate) and Its Application as Polymeric Nucleating Agent for Poly(butylene succinate).* Macromolecules, 2012. **45**(14): p. 5667-5675. doi: 10.1021/ma300685f

82. Yang, B., et al., *Effects of Poly(vinyl butyral) as a Macromolecular Nucleating Agent on the Nonisothermal Crystallization and Mechanical Properties of Biodegradable Poly(butylene succinate).* Macromolecules, 2013. **47**(1): p. 284-296. doi: 10.1021/ma4019894

83. Kim, H.-S., et al., *Cluster Formation in Plasticized Poly(phenylene oxide) Ionomers.* Polymer Journal, 1999. **31**(3): p. 306-308. doi: 10.1295/polymj.31.306

84. Lantman, C.W., W.J. MacKnight, and R.D. Lundberg, *25 - Ionomers*, in *Comprehensive Polymer Science and Supplements*, G. Allen and J.C. Bevington, Editors. 1989, Pergamon: Amsterdam. p. 755-773.

85. Rui, Y. and B.P. Grady, *Long-time crystallization kinetics in zinc-neutralized ethylene–methacrylic acid ionomers.* Thermochimica Acta, 2013. **565**: p. 183-193. doi: 10.1016/j.tca.2013.05.008

86. Morris, B.A., *2 - Converting Processes*. The Science and Technology of Flexible Packaging, ed. I.P.D. Library. 2017: William Andrew Publishing. 25-49. 978-0-323-24273-8. doi: 10.1016/B978-0-323-24273-8.00002-2

87. Rosato, D.V., *Blown film*. Extruding Plastics. 1998. 978-1-4615-5793-7. doi: 10.1007/978-1-4615-5793-7_7

88. Vlachopoulos, J., et al., *Chapter 5: Blown Film Dies*. Design of Extrusion Forming Tools. 2012: Smithers Rapra. 9781847355188.

89. Le Delliou, B., et al., *Development of extrusion blown films of poly(3-hydroxybutyrate-co-3-hydroxyvalerate) blends for flexible packaging.* Journal of Applied Polymer Science, 2024. **141**(16). doi: 10.1002/app.55240

90. Mistretta, M.C., et al., *Film Blowing of Biodegradable Polymer Nanocomposites for Agricultural Applications.* Macromolecular Materials and Engineering, 2021. **306**(9). doi: 10.1002/mame.202100177

91. Krishnaswamy, R.K. and A.M. Sukhadia, *Orientation characteristics of LLDPE blown films and their implications on Elmendorf tear performance.* Polymer, 2000. **41**(26): p. 9205–9217. doi: https://doi.org/10.1016/S0032-3861(00)00136-1

92. Bashirgonbadi, A., et al., *The interplay between macromolecular structure, rheology, processing condition, and morphology for (linear) low density polyethylenes in film blowing.* Polymer, 2024. **290**. doi: 10.1016/j.polymer.2023.126566

93. Gururajan, G. and A.A. Ogale, *Real-time crystalline orientation measurements during low-density polyethylene blown film extrusion using wide-angle X-ray diffraction.* Polymer Engineering & Science, 2012. **52**(7): p. 1532-1536. doi: 10.1002/pen.23100

94. Ge, C., et al., *Neat EVOH and EVOH/LDPE blend centered three-layer co-extruded blown film without tie layers.* Food Packaging and Shelf Life, 2016. **8**: p. 33-40. doi: 10.1016/j.fpsl.2016.03.001

95. Chau, C.C. and W.R. LaFollette, *Shear Yielding in Blown Oriented Polystyrene Films.* Advanced Materials, 2000. **12**(23): p. 1859-1864. doi: 10.1002/1521-4095(200012)12:23<1859::Aid-adma1859>3.0.Co;2-1

96. Harth, M. and A. Dornhofer, *Film Blowing of Linear and Long-Chain Branched Poly(ethylene terephthalate).* Polymers (Basel), 2020. **12**(7). 1605. doi: 10.3390/polym12071605

97. Itabana, B.E., et al., *Biodegradable blown film composite from poly (butylene adipate-co-terephthalate) and talc: Effect of uniaxial stretching on mechanical and barrier properties.* Food Packaging and Shelf Life, 2023. **39**. doi: 10.1016/j.fpsl.2023.101147

98. Jiang, Y., et al., *Super-Toughed PLA Blown Film with Enhanced Gas Barrier Property Available for Packaging and Agricultural Applications.* Materials (Basel), 2019. **12**(10). doi: 10.3390/ma12101663

99. Teixeira, P.F., et al., *Film Blowing of PHB-Based Systems for Home Compostable Food Packaging.* International Polymer Processing, 2020. **35**(5). doi: 10.1515/ipp-2020-350506

100. Rajabi, M., et al., *Keratinous materials: Structures and functions in biomedical applications.* Mater Sci Eng C Mater Biol Appl, 2020. **110**: p. 110612. doi: 10.1016/j.msec.2019.110612

101. Poh, L., et al., *Characterization of industrial low-density polyethylene: a thermal, dynamic mechanical, and rheological investigation.* Rheologica Acta, 2022. **61**(10): p. 701-720. doi: 10.1007/s00397-022-01360-1

102. Cardarelli, F., *Materials Handbook*. 3rd Edition ed. 2018: Springer Cham. 978-3-319-38923-3. doi: 10.1007/978-3-319-38925-7

103. Haynes, W.M., *CRC Handbook of Chemistry and Physics*. 97th Edition ed. 2016, CRC Press: Taylor & Francis Group. 9781315380476. doi: https://doi.org/10.1201/9781315380476

104. Liu, C., J. Wang, and J. He, *Rheological and thermal properties of m-LLDPE blends with m-HDPE and LDPE.* Polymer, 2002. **43**(13): p. 3811-3818. doi: 10.1016/S0032-3861(02)00201-X

105. McCaffrey, W.C., M.R. Kamal, and D.G. Cooper, *Thermolysis of polyethylene.* 1995. **47**(1): p. 133-139. doi: https://doi.org/10.1016/0141-3910(94)00096-Q

106. Krishnaswamy, R.K. and M.J. Lamborn, *Tensile properties of linear low density polyethylene (LLDPE) blown films.* Polymer Engineering and Science, 2000. **40**(11): p. 2385-2396. doi: 10.1002/pen.11370

107. Hussein, I.A., et al., *Miscibility of hexene-LLDPE and LDPE blends: influence of branch content and composition distribution.* Polymer, 2003. **44**(16): p. 4665-4672. doi: 10.1016/s0032-3861(03)00437-3

108. Bautista, M., et al., *Poly(butylene succinate) Ionomers with Enhanced Hydrodegradability.* Polymers, 2015. **7**(7): p. 1232-1247. doi: 10.3390/polym7071232

109. Yin, S., et al., *Mechanical and thermal properties of poly (butylene adipate-butylene terephthalate) modified with phenol hydroxyl terminated polysiloxane.* Polymer Engineering & Science, 2022. **62**(11): p. 3684-3694. doi: 10.1002/pen.26137

110. Sousa, F.M., et al., *Effect of composition on permeability, mechanical properties and biodegradation of PBAT/PCL blends films.* Polymer Bulletin, 2021. **79**(7): p. 5327-5338. doi: 10.1007/s00289-021-03745-3

111. Oksiuta, Z., et al., *Mechanical and Thermal Properties of Polylactide (PLA) Composites Modified with Mg, Fe, and Polyethylene (PE) Additives.* Polymers (Basel), 2020. **12**(12). doi: 10.3390/polym12122939

112. Barkhad, M.S., et al., *Thermal Insulation and Mechanical Properties of Polylactic Acid (PLA) at Different Processing Conditions.* Polymers (Basel), 2020. **12**(9). doi: 10.3390/polym12092091

113. Li, Z., J. Yang, and X.J. Loh, *Polyhydroxyalkanoates: opening doors for a sustainable future.* NPG Asia Materials, 2016. **8**(4): p. e265-e265. doi: 10.1038/am.2016.48

114. Panaitescu, D.M., et al., *Thermal and mechanical properties of poly(3-hydroxybutyrate) reinforced with cellulose fibers from wood waste.* Industrial Crops and Products, 2020. **145**. doi: 10.1016/j.indcrop.2019.112071

115. Innocentini-Mei, L.H., J.R. Bartoli, and R.C. Baltieri, *Mechanical and thermal properties of poly(3-hydroxybutyrate) blends with starch and starch derivatives.* Macromolecular Symposia, 2003. **197**(1): p. 77-88. doi: 10.1002/masy.200350708

116. Li, Z., et al., *Thermal and Mechanical Properties of the Biocomposites of Miscanthus Biocarbon and Poly(3-Hydroxybutyrate-co-3-Hydroxyvalerate) (PHBV).* Polymers, 2020. **12**(6). doi: 10.3390/polym12061300

117. T, S.M.K., et al., *Mechanical and thermal properties of spent coffee bean filler/poly(3-hydroxybutyrate-co-3-hydroxyvalerate) biocomposites: Effect of recycling.* Process Safety and Environmental Protection, 2019. **124**: p. 187-195. doi: 10.1016/j.psep.2019.02.008

118. Tripathi, L., et al., *Synthesis of Diblock copolymer poly-3-hydroxybutyrate -block-poly-3-hydroxyhexanoate [PHB-b-PHHx] by a β-oxidation weakened Pseudomonas putida KT2442.* Microbial Cell Factories, 2012. **11**. 44. doi: doi: 10.1186/1475-2859-11-44

119. Rai, R., et al., *Poly-3-hydroxyoctanoate P(3HO), a Medium Chain Length Polyhydroxyalkanoate Homopolymer from Pseudomonas mendocina.* Biomacromolecules, 2011. **12**(6): p. 2126-2136. doi: 10.1021/bm2001999

120. Krishna, S.H., et al., *Catalytic production of hexane-1,2,5,6-tetrol from bio-renewable levoglucosanol in water: effect of metal and acid sites on (stereo)-selectivity.* Green Chemistry, 2018. **20**(19): p. 4557-4565. doi: 10.1039/c8gc02455c

121. Cuello-Penaloza, P., et al., *Production of Hexane-1,2,5,6-tetrol from Biorenewable Levoglucosanol over Pt-WOx/TiO2.* ACS Sustainable Chemistry & Engineering, 2021. **9**(48): p. 16123-16132. doi: 10.1021/acssuschemeng.1c04759

122. Alidedeoglu, H.A. and G. Kannan. Color-stabilized biodegradable aliphatic-aromatic copolyesters, methods of manufacture, and articles thereof. 2015. 8,933,162 B2.

123. Micic, P. and S.N. Bhattacharya, *Rheology of LLDPE, LDPE and LLDPE/LDPE blends and its relevance to the film blowing process.* Polymer International, 2000. **49**(12): p. 1580-1589. doi: 10.1002/1097-0126(200012)49:12<1580::Aid-pi547>3.0.Co;2-q

124. Härth, M. and A. Dörnhöfer, *Film Blowing of Linear and Long-Chain Branched Poly(ethylene terephthalate).* Polymers, 2020. **12**(7): p. 1605. doi: 10.3390/polym12071605

125. International, A., *D5338 − 15: Standard Test Method for Determining Aerobic Biodegradation of Plastic Materials Under Controlled Composting Conditions, Incorporating Thermophilic Temperatures*. 2021, ASTM Standards. p. 1-7.

126. Brentzel, Z.J., et al., *Chemicals from Biomass: Combining Ring-Opening Tautomerization and Hydrogenation Reactions to Produce 1,5-Pentanediol from Furfural.* ChemSusChem, 2017. **10**(7): p. 1351-1355. doi: 10.1002/cssc.201700178

127. Prasad, S., et al., *Recent advances in the production of 2,5-furandicarboxylic acid from biorenewable resources.* Materials Science for Energy Technologies, 2023. **6**: p. 502-521. doi: 10.1016/j.mset.2023.04.005

128. Singh, O., et al., *Synthesis and characterization of biobased copolyesters based on pentanediol: (1) Poly(pentylene dodecanoate-co-furandicarboxylate).* Polymer Engineering & Science, 2024. **64**(10): p. 4935-4946. doi: 10.1002/pen.26892

129. Aboukeila, H., et al., *Synthesis and characterization of biobased copolyesters based on pentanediol: (2) Poly(pentylene adipate-co-terephthalate).* Polymer Engineering & Science, 2024. **64**(10): p. 4746-4759. doi: 10.1002/pen.26878

130. Herrera, R., et al., *Characterization and degradation behavior of poly(butylene adipate-co-terephthalate)s.* Journal of Polymer Science Part A: Polymer Chemistry, 2002. **40**(23): p. 4141-4157. doi: 10.1002/pola.10501

131. Pérez-Camargo, R.A., et al., *Even–Odd Effect in Aliphatic Polycarbonates with Different Chain Lengths: from Poly (Hexamethylene Carbonate) to Poly (Dodecamethylene Carbonate).* Macromolecules, 2020. **54**(1): p. 259-271. doi: 10.1021/acs.macromol.0c02374

132. Qiu, W., et al., *Effect of the Precise Branching of Polyethylene at Each 21st CH2 Group on Its Phase Transitions, Crystal Structure, and Morphology.* Macromolecules, 2006. **39**(1): p. 204-217. doi: 10.1021/ma052010w

133. Boyer, R.F., *The Relation of Transition Temperatures to Chemical Structure in High Polymers.* Rubber Chemistry and Technology, 1963. **36**(5): p. 1303-1418.

134. Sorrentino, L., et al., *Isothermal crystallization kinetics of chain-extended PET.* Journal of Polymer Science Part B: Polymer Physics, 2005. **43**(15): p. 1966-1972. doi: 10.1002/polb.20480

135. Pan, H., et al., *The effect of MDI on the structure and mechanical properties of poly(lactic acid) and poly(butylene adipate-co-butylene terephthalate) blends.* RSC Advances, 2018. **8**(9): p. 4610-4623. doi: 10.1039/c7ra10745e

136. Saleh, T.A., *Chapter 3 - Polymer science and polymerization methods toward hybrid materials*, in *Polymer Hybrid Materials and Nanocomposites*, T.A. Saleh, Editor. 2021, William Andrew Publishing. p. 59-103.

137. As'habi, L., et al., *Non-isothermal crystallization behavior of PLA/LLDPE/nanoclay hybrid: Synergistic role of LLDPE and clay.* Thermochimica Acta, 2013. **565**: p. 102-113. doi: 10.1016/j.tca.2013.04.016

138. Du, W., et al., *Different structure transitions and tensile property of LLDPE film deformed at slow and very fast speeds.* European Polymer Journal, 2018. **103**: p. 170-178. doi: 10.1016/j.eurpolymj.2018.04.003

139. Wang, L., et al., *Blends of Linear and Long-Chain Branched Poly(l-lactide)s with High Melt Strength and Fast Crystallization Rate.* Industrial & Engineering Chemistry Research, 2012. **51**(30): p. 10088-10099. doi: 10.1021/ie300526u

140. Yan, D., W.J. Wang, and S. Zhu, *Effect of long chain branching on rheological properties of metallocene polyethylene.* Polymer, 1999. **40**(7): p. 1737-1744. doi: 10.1016/S0032-3861(98)00318-8

141. Bourg, V., et al., *Shear and Extensional Rheology of Linear and Branched Polybutylene Succinate Blends.* Polymers, 2021. **13**(4): p. 652. doi: 10.3390/polym13040652

142. Micic, P., S.N. Bhattacharya, and G. Field, *Transient elongational viscosity of LLDPE/LDPE blends and its relevance to bubble stability in the film blowing process.* Polymer Engineering & Science, 1998. **38**(10): p. 1685-1693. doi: 10.1002/pen.10339

143. Münstedt, H., S. Kurzbeck, and J. Stange, *Importance of elongational properties of polymer melts for film blowing and thermoforming.* Polymer Engineering & Science, 2006. **46**(9): p. 1190-1195. doi: 10.1002/pen.20588

144. Yu, Y. and H. Bu, *Crystallization Behavior of Poly(ethylene terephthalate) Modified by Ionomers.* Macromolecular Chemistry and Physics, 2001. **202**(3): p. 421-425. doi: 10.1002/1521-3935(20010201)202:3<421::Aid-macp421>3.0.Co;2-v

145. Li, C. and Q. Dou, *Effect of Metallic Salts of Phenylmalonic Acid on the Crystallization of Poly(L-lactide).* Journal of Macromolecular Science, Part B, 2015. **55**(2): p. 128-137. doi: 10.1080/00222348.2015.1125050

146. Shokrollahi, M., B.T. Marouf, and R. Bagheri, *Controlling the rheological behavior of nucleated polypropylene via incorporating dimethylbenzylidene sorbitol (DMDBS) masterbatch.* Polyolefins Journal, 2023. **10**(1): p. 21-26. doi: 10.22063/POJ.2022.3189.1226

147. Wilsens, C., et al., *Effect of Thermal History and Shear on the Viscoelastic Response of iPP Containing an Oxalamide-Based Organic Compound.* Macromolecules, 2019. **52**(7): p. 2789-2802. doi: 10.1021/acs.macromol.8b02612

148. Mejia, E., et al., *Effect of Processing Techniques on the Microstructure and Mechanical Performance of High-Density Polyethylene.* Polymers (Basel), 2021. **13**(19). doi: 10.3390/polym13193346

149. Hedesiu, C., et al., *The effect of temperature and annealing on the phase composition, molecular mobility and the thickness of domains in high-density polyethylene.* Polymer, 2007. **48**(3): p. 763-777. doi: 10.1016/j.polymer.2006.12.019

150. Ren, Y., et al., *Different Dependence of Tear Strength on Film Orientation of LLDPE Made with Different Co-Monomer.* Polymers (Basel), 2019. **11**(3). doi: 10.3390/polym11030434

151. Alexander, L.E., *X-ray Diffraction Methods in Polymer Science*. 1969: Wiley-Interscience. 582. 9780471021834.

152. Bashir, Z. and S. Rastogi, *The Explanation of the Increase in Slope at the Tg in the Plot of d-Spacing Versus Temperature in Polyacrylonitrile.* Journal of Macromolecular Science, Part B, 2014. **44**(1): p. 55-78. doi: 10.1081/mb-200044588

153. Wojciechowski, P., *Thermotropic Mesomorphism of (2-Hydroxypropyl)cellulose Systems-the Role of Hydrophilic and Lipophilic Segments.* Molecular Crystals and Liquid Crystals Science and Technology. Section A. Molecular Crystals and Liquid Crystals, 2000. **354**(1): p. 309-317. doi: 10.1080/10587250008023623

154. Qin, P., et al., *Superior Gas Barrier Properties of Biodegradable PBST vs. PBAT Copolyesters: A Comparative Study.* Polymers (Basel), 2021. **13**(19). doi: 10.3390/polym13193449

155. Wang, Y., A.J. Easteal, and X.D. Chen, *Ethylene and oxygen permeability through polyethylene packaging films.* Packaging Technology and Science, 1998. **11**(4): p. 169-178. doi: 10.1002/(sici)1099-1522(199807/08)11:4<169::Aid-pts427>3.0.Co;2-q

156. Kamal, M.R., I.A. Jinnah, and L.A. Utracki, *Permeability of Oxygen and Water Vapor Through Polyethylene/Polyamide Films.* Polymer Engineering & Science, 1984. **24**(17): p. 1337-1347. doi: https://doi.org/10.1002/pen.760241711

157. Kim, K., et al., *Polyethylene Blends for Improved Oxygen Barrier: Processing-Dependent Microstructure and Gas Permeability.* ACS Applied Polymer Materials, 2023. **6**(1): p. 524-533. doi: 10.1021/acsapm.3c02211

158. Khanna, Y.P., et al., *Re-Examining the Oxygen Barrier of Nylon 6 Films. I. Role of Moisture and Processing Induced Variables.* Journal of Plastic Film & Sheeting, 1997. **13**(3). doi: 10.1177/875608799701300304

159. Bumbudsanpharoke, N., et al., *Morphology and permeability of bio-based poly(butylene adipate-co-terephthalate) (PBAT), poly(butylene succinate) (PBS) and linear low-density polyethylene (LLDPE) blend films control shelf-life of packaged bread.* Food Control, 2022. **132**. doi: 10.1016/j.foodcont.2021.108541

160. S Hemsri, K.P., K Saeaung and P Satung, *Low density polyethylene/poly(butylene adipate-co-terephthalate) films: Effect of a compatibilizer on morphology and properties.* International Conference on Engineering and Industrial Technology, 2020. **965**. doi: 10.1088/1757-899X/965/1/012020

161. Trifol, J., et al., *Effect of Crystallinity on Water Vapor Sorption, Diffusion, and Permeation of PLA-Based Nanocomposites.* ACS Omega, 2020. **5**(25): p. 15362-15369. doi: 10.1021/acsomega.0c01468

162. Tsanaktsis, V., G.Z. Papageorgiou, and D.N. Bikiaris, *A facile method to synthesize high-molecular-weight biobased polyesters from 2,5-furandicarboxylic acid and long-chain diols.* Journal of Polymer Science Part A: Polymer Chemistry, 2015. **53**(22): p. 2617-2632. doi: 10.1002/pola.27730

163. Papageorgiou, D.G., et al., *Fast Crystallization and Melting Behavior of a Long-Spaced Aliphatic Furandicarboxylate Biobased Polyester, Poly(dodecylene 2,5-furanoate).* Industrial & Engineering Chemistry Research, 2016. **55**(18): p. 5315-5326. doi: 10.1021/acs.iecr.6b00811

164. Fehrenbacher, U., et al., *Synthese und Charakterisierung von Polyestern und Polyamiden auf der Basis von Furan-2,5-dicarbonsäure.* Chemie Ingenieur Technik, 2009. **81**(11): p. 1829-1835. doi: 10.1002/cite.200900090

165. Zemenová, P., et al., *Calculations of Avrami exponent and applicability of Johnson–Mehl–Avrami model on crystallization in Er:LiY(PO3)4 phosphate glass.* Journal of Thermal Analysis and Calorimetry, 2019. **141**(3): p. 1091-1099. doi: 10.1007/s10973-019-09068-w

166. Rajendra K. Krishnaswamy, M.J.L., *Tensile Properties of Linear Low Density Polyethylene (LLDPE) Blown Films* Polymer Engineering & Science, 2000. **40**(11): p. 2385-2396. doi: https://doi.org/10.1002/pen.11370

167. Tsanaktsis, V., et al., *Thermal degradation kinetics and decomposition mechanism of polyesters based on 2,5-furandicarboxylic acid and low molecular weight aliphatic diols.* Journal of Analytical and Applied Pyrolysis, 2015. **112**: p. 369-378. doi: 10.1016/j.jaap.2014.12.016

168. Terzopoulou, Z., et al., *Thermal degradation of biobased polyesters: Kinetics and decomposition mechanism of polyesters from 2,5-furandicarboxylic acid and long-chain*

aliphatic diols. Journal of Analytical and Applied Pyrolysis, 2016. **117**: p. 162-175. doi: 10.1016/j.jaap.2015.11.016

169. Siracusa, V., et al., *Poly(butylene succinate) and poly(butylene succinate-co-adipate) for food packaging applications: Gas barrier properties after stressed treatments.* Polymer Degradation and Stability, 2015. **119**: p. 35-45. doi: 10.1016/j.polymdegradstab.2015.04.026

170. Zheng, L., et al., *Biodegradable High-Molecular-Weight Poly(pentylene adipate-co-terephthalate): Synthesis, Thermo-Mechanical Properties, Microstructures, and Biodegradation.* ACS Sustainable Chemistry & Engineering, 2023. **11**(38): p. 13885-13895. doi: 10.1021/acssuschemeng.3c01831

171. Tokiwa, Y. and B.P. Calabia, *Biodegradability and biodegradation of poly(lactide).* Appl Microbiol Biotechnol, 2006. **72**(2): p. 244-51. doi: 10.1007/s00253-006-0488-1

172. Lucas, N., et al., *Polymer biodegradation: mechanisms and estimation techniques.* Chemosphere, 2008. **73**(4): p. 429-42. doi: 10.1016/j.chemosphere.2008.06.064

173. Galizia, M., et al., *50th Anniversary Perspective: Polymers and Mixed Matrix Membranes for Gas and Vapor Separation: A Review and Prospective Opportunities.* Macromolecules, 2017. **50**(20): p. 7809-7843. doi: 10.1021/acs.macromol.7b01718

174. Yue, S., et al., *Recent Progress of Biodegradable Polymer Package Materials: Nanotechnology Improving Both Oxygen and Water Vapor Barrier Performance.* Nanomaterials (Basel), 2024. **14**(4). doi: 10.3390/nano14040338

175. Wu, F., M. Misra, and A.K. Mohanty, *Challenges and new opportunities on barrier performance of biodegradable polymers for sustainable packaging.* Progress in Polymer Science, 2021. **117**. doi: 10.1016/j.progpolymsci.2021.101395

176. Siracusa, V., *Food Packaging Permeability Behaviour: A Report.* International Journal of Polymer Science, 2012. **2012**: p. 1-11. doi: 10.1155/2012/302029

177. Souza, V.G.L., et al., *Permeation of Oxygen and Carbon Dioxide Through Food Packaging Materia*, in *Food Packaging Materials*. 2024. p. 219-232.

178. Murmu, U.K., et al., *Mechanical Properties of Crystalline and Semicrystalline Polymer Systems*, in *Encyclopedia of Materials: Plastics and Polymers*. 2022. p. 917-927.

179. Garcia-Garcia, D., et al., *Innovative solutions and challenges to increase the use of Poly(3-hydroxybutyrate) in food packaging and disposables.* European Polymer Journal, 2022. **178**. doi: 10.1016/j.eurpolymj.2022.111505

180. Sharafi Zamir, S., et al., *Crystallinity and Gas Permeability of Poly (Lactic Acid)/Starch Nanocrystal Nanocomposite.* Polymers (Basel), 2022. **14**(14). doi: 10.3390/polym14142802

181. Dai, Z., et al., *Nafion/PEG hybrid membrane for CO2 separation: Effect of PEG on membrane micro-structure and performance.* Separation and Purification Technology, 2019. **214**: p. 67-77. doi: 10.1016/j.seppur.2018.03.062

182. Wang, X., et al., *Advances on materials design and manufacture technology of plastic liner of type IV hydrogen storage vessel.* International Journal of Hydrogen Energy, 2022. **47**(13): p. 8382-8408. doi: 10.1016/j.ijhydene.2021.12.198

183. Marano, S., et al., *Tailoring the Barrier Properties of PLA: A State-of-the-Art Review for Food Packaging Applications.* Polymers (Basel), 2022. **14**(8). doi: 10.3390/polym14081626

184. Amenorfe, L.P., et al., *Innovative exploration of additive incorporated biopolymer-based composites.* Scientific African, 2022. **17**. doi: 10.1016/j.sciaf.2022.e01359

185. Lin, H., et al., *The Effect of Cross-Linking on Gas Permeability in Cross-LinkedPoly(Ethylene Glycol Diacrylate).* Macromolecules, 2005. **38**(20): p. 8381-8393. doi: https://doi.org/10.1021/ma0510136

186. Berean, K., et al., *The effect of crosslinking temperature on the permeability of PDMS membranes: Evidence of extraordinary CO2 and CH4 gas permeation.* Separation and Purification Technology, 2014. **122**: p. 96-104. doi: 10.1016/j.seppur.2013.11.006

187. Singha, S. and M.S. Hedenqvist, *A Review on Barrier Properties of Poly(Lactic Acid)/Clay Nanocomposites.* Polymers (Basel), 2020. **12**(5). doi: 10.3390/polym12051095

188. Eslami, Z., et al., *A Review of the Effect of Plasticizers on the Physical and Mechanical Properties of Alginate-Based Films.* Molecules, 2023. **28**(18). doi: 10.3390/molecules28186637

189. Yu, M., et al., *The Effect of Cooling Rates on Thermal, Crystallization, Mechanical and Barrier Properties of Rotational Molding Polyamide 11 as the Liner Material for High-Capacity High-Pressure Vessels.* Molecules, 2023. **28**(6). doi: 10.3390/molecules28062425

190. Shrivastava, A., *1 - Introduction to Plastics Engineering*, in *Introduction to Plastics Engineering*. 2018, William Andrew. p. 1-16.

191. Park, S., et al., *Annealing effect of thermotropic liquid crystalline copolyester fibers on thermo-mechanical properties and morphology.* Sci Rep, 2022. **12**(1): p. 13100. doi: 10.1038/s41598-022-17431-5

192. Wang, S., et al., *Insights into the relationship between structure and properties of Spirobichroman-based polyimides: Effects of substituents on molecular structure and gas separation.* Materials & Design, 2020. **194**. doi: 10.1016/j.matdes.2020.108933

193. Speight, J.G., *CHapter 14- Monomers, polymers and plastics*, in *Handbook of Industral Hydrocarbon processes*. 2020, Gulf Professional Publishing. p. 597-649.

194. Vieira, M.G.A., et al., *Natural-based plasticizers and biopolymer films: A review.* European Polymer Journal, 2011. **47**(3): p. 254-263. doi: 10.1016/j.eurpolymj.2010.12.011

195. Kawaguchi, D., et al., *Local orientation of chains at crystal/amorphous interfaces buried in isotactic polypropylene thin films.* Phys Chem Chem Phys, 2021. **23**(41): p. 23466-23472. doi: 10.1039/d1cp03959h

196. Distefano, G., et al., *Highly ordered alignment of a vinyl polymer by host-guest cross-polymerization.* Nat Chem, 2013. **5**(4): p. 335-41. doi: 10.1038/nchem.1576

197. Fulati, A., K. Uto, and M. Ebara, *Influences of Crystallinity and Crosslinking Density on the Shape Recovery Force in Poly(epsilon-Caprolactone)-Based Shape-Memory Polymer Blends.* Polymers (Basel), 2022. **14**(21). doi: 10.3390/polym14214740

198. Hashimoto, Y., et al., *Structural Formation of UHMWPE Film Tracked by Real-Time Retardation Measurements during Uniaxial/Biaxial Stretching.* Materials (Basel), 2018. **11**(11). doi: 10.3390/ma11112292

199. Tokuda, T., et al., *Planar or Biaxial Stretching of Poly(ethylene terephthalate) Fiber Webs Prepared by Laser-Electrospinning.* Materials (Basel), 2022. **15**(6). doi: 10.3390/ma15062209

200. Krevelen, D.W.V. and K.T. Nijenhuis, *Properties of Polymers: Their Correlation with Chemical Structure; Their Numerical Estimation and Prediction from Additive Group Contributions*. 4th ed. 2009: Elsevier Science. 1004. 978-0-08-054819-7.

201. Yu, W., et al., *Prediction of birefringence for polymer optical products based on a novel molecular chain orientation model.* Polymer, 2021. **233**. doi: 10.1016/j.polymer.2021.124230

202. Lin, Y., et al., *Transparent semi-crystalline polymeric materials and their nanocomposites: A review.* Polymer Engineering & Science, 2020. **60**(10): p. 2351-2376. doi: 10.1002/pen.25489

203. Cuesta, F., A.M. Camacho, and E.M. Rubio, *Influence of the Main Blown Film Extrusion Process Parameters on the Mechanical Properties of a High-Density Polyethylene Hexene Copolymer and Linear Low-Density Polyethylene Butene Copolymer Blend Used for Plastic Bags.* Applied Sciences, 2023. **13**(22). doi: 10.3390/app132212164

204. Ren, Y., et al., *Effect of annealing on microstructure and tensile properties of polypropylene cast film.* Colloid and Polymer Science, 2017. **296**(1): p. 41-51. doi: 10.1007/s00396-017-4220-8

205. Wiesinger, H., Z. Wang, and S. Hellweg, *Deep Dive into Plastic Monomers, Additives, and Processing Aids.* Environ Sci Technol, 2021. **55**(13): p. 9339-9351. doi: 10.1021/acs.est.1c00976

206. Patel, P. and N. Savargaonkar, *A Review of Additives for Plastics: Slips and Antiblocks.* Plastics Engineering, 2007. **63**(1): p. 48-51. doi: https://doi.org/10.1002/j.1941-9635.2007.tb00033.x

207. Markarian, J., *Slip and antiblock additives: surface medication for film and sheet.* Plastics, Additives and Compounding, 2007. **9**(6): p. 32-35. doi: 10.1016/s1464-391x(07)70156-3

208. Felgel-Farnholz, A., et al., *Comparative study on the degradation of HDPE, LLDPE and LDPE during multiple extrusions.* Polymer Degradation and Stability, 2023. **216**. doi: 10.1016/j.polymdegradstab.2023.110486

209. *Choosing an antioxidant: some of the basics.* Plastics, Additives and Compounding, 2005. **7**(1): p. 32-33. doi: 10.1016/S1464-391X(05)00332-6